A Framework for Numerical Simulations of Structure Formation

THÈSE N^{O} 4947 (2011)

PRÉSENTÉE LE 25 FÉVRIER 2011

À LA FACULTÉ SCIENCES DE BASE
LABORATOIRE DE PHYSIQUE DES PARTICULES ET DE COSMOLOGIE
PROGRAMME DOCTORAL EN PHYSIQUE

ÉCOLE POLYTECHNIQUE FÉDÉRALE DE LAUSANNE

POUR L'OBTENTION DU GRADE DE DOCTEUR ÈS SCIENCES

PAR

Claude BECKER

acceptée sur proposition du jury:

Prof. O. Schneider, président du jury
Prof. M. Shaposhnikov, directeur de thèse
Dr F. Courbin, rapporteur
Dr A. Maccio, rapporteur
Prof. J. Read, rapporteur

ÉCOLE POLYTECHNIQUE
FÉDÉRALE DE LAUSANNE

Suisse
2011

Abstract

In the absence of a full analytical treatment of nonlinear structure formation in the universe, numerical simulations provide the critical link between the properties of the underlying model and the features of the observed structures. Currently N-body simulations are the main tool to study structure growth. We explore an alternative framework for numerical simulations of structure formation. The underlying idea is to replace the long-range gravitational force in the Vlasov-Poisson system by a purely local interaction. To this end we trade the classical phase space distribution for its quantum mechanical counterpart, the Wigner distribution function. Its dynamical equation is equivalent to the Schrödinger equation and reduces to the Vlasov equation in the formal semi-classical limit. The proposed framework allows in principle to simulate systems with arbitrary phase space distributions and could for instance be beneficial for simulations of warm dark matter, where the velocity dispersion is important.

We discuss several methods to obtain a set of wavefunctions whose Wigner distribution is close to a given initial phase space distribution function. An auxiliary gauge field is introduced to mediate the gravitational interaction, thereby obtaining a local Schrödinger-Maxwell system. We also use the ideas of lattice gauge theories to obtain a fully gauge-invariant discretization of the equations of motion. Their iterative solution was implemented in a three-dimensional simulation code. We discuss its computational complexity and memory requirements. Several testbed simulations were performed with this method. We compared the gravitational collapse of a Gaussian wavefunction with an independent numerical solution of the spherically symmetric Schrödinger-Newton system. The results were found to be in good agreement. Finally, a simple example of the growth of cosmic perturbations is investigated within our framework. We conclude by outlining various possible directions to optimize and develop our method.

Keywords: Structure formation, N-body simulations, Wigner distribution function, Lattice gauge theory

Résumé

En l'absence d'une traitement analytique complet de la formation non-linéaire de structures dans l'univers, les simulations numériques fournissent le lien critique entre le modèle sous-jacent et les propriétés des structures observées. Actuellement les simulations à N corps sont le moyen principal pour étudier la croissance des structures. Nous explorons un cadre alternatif pour effectuer des simulations numériques de la formation de structures. L'idée de base est de remplacer la force gravitationnelle à longue portée dans le système de Vlasov-Poisson par une interaction purement locale. A cette fin, nous échangeons la fonction de distribution dans l'espace de phase classique contre son équivalent en mécanique quantique ; la distribution de Wigner. Son équation dynamique est équivalente à l'équation de Schrödinger et se réduit à l'équation de Vlasov dans la limite semi-classique formelle. Le cadre proposé permet, en principe, de faire des simulations de systèmes avec une distribution arbitraire dans l'espace de phase. Ceci pourrait par exemple être bénéfique pour des simulations de matière noire tiède, où la dispersion des vitesses est importante.

Nous discutons plusieurs méthodes pour obtenir un ensemble de fonctions d'onde ayant une distribution de Wigner proche d'une distribution initiale donnée. Nous introduisons un champ de jauge auxiliaire comme médiateur le l'interaction gravitationnelle et obtenons ainsi les équations locales de Schrödinger-Maxwell. Nous faisons aussi usage des idées de la théorie de jauge sur réseau pour obtenir une version discrétisée et entièrement invariante de jauge des équations du mouvement. Leur solution itérative a été implémentée dans un code de simulation tridimensionnel. Nous discutons sa complexité algorithmique et ses exigences en mémoire. Plusieurs simulations ont été faites pour prouver la validité de notre méthode. Nous avons comparé l'effondrement gravitationnel d'une fonction d'onde gaussienne avec une résolution numérique indépendante des équations de Schrödinger-Newton à symétrie sphérique. Les résultats obtenus sont en bon accord. Pour finir, nous examinons un cas simple de croissance de perturbations cosmiques. En conclusion, nous esquissons différentes directions pour optimiser et développer notre méthode.

Mots-clés : Formation de structures, Simulations N-corps, Distribution de Wigner, Théorie de jauge sur réseau

Contents

1. Introduction 1

2. Structure formation in the universe 7
- 2.1 Phase space formulation 8
  - 2.1.1 Cosmological Vlasov equation 9
- 2.2 N-body simulations 11
  - 2.2.1 Algorithms and complexity 11
  - 2.2.2 Millennium simulation 13
  - 2.2.3 Potential difficulties 13

3. Wigner distribution function 17
- 3.1 Phase space quantum mechanics 17
- 3.2 Wigner distribution function 18
- 3.3 Dynamical equation for the WDF 20
  - 3.3.1 Wigner equation from the Liouville equation 20
  - 3.3.2 Wigner equation from the Schrödinger equation 22
- 3.4 Semi-classical limit 23

4. WDF for a given phase space distribution 25
- 4.1 Minimization procedure 26
- 4.2 Eigenvalue problem for hermitian operator 27
  - 4.2.1 Generalization: weighted scalar product 28
- 4.3 Eigenvalue problem on the finite interval 29
- 4.4 Fourier series inspired decomposition 31
- 4.5 Cosmological initial conditions 32
- 4.6 Matrix formulation 33
- 4.7 Remarks concerning the number of wavefunctions 34

5. Local interaction framework 37
- 5.1 Introducing gauge fields 38
- 5.2 Lagrangian formulation 39
- 5.3 Dimensionless reformulation 41
- 5.4 Tachyonic instability 42

6. Lattice gauge theory formulation 45
6.1 Wilson's lattice gauge theory formulation 46
6.2 Lattice theory for our dimensionless formulation 50
6.3 Iterative solution of the equations of motion 51
6.4 Gauss constraint 52
6.5 Complexity and memory requirements 54

7. Discussion and Examples 57
7.1 Comparison with previous approaches 57
7.1.1 Coles et al. 57
7.1.2 Widrow et al. 57
7.2 Implementation 59
7.3 Numerical tests of the tachyonic instability 61
7.3.1 Stable mode 61
7.3.2 Unstable mode 62
7.3.3 Stable and unstable mode 64
7.4 Schrödinger-Newton system 67
7.4.1 Numerical solution of the spherically symmetric case . 67
7.4.2 Comparison with the 3D simulation 67
7.5 Growth of cosmic perturbations 69

8. Conclusion and Outlook 75

Acknowledgments 79

Appendix 81

A. Conventions 83

B. Numerical stability 85

C. Derivation of the lattice Schrödinger equation from the action 87

D. Unitarity of the discretized Schrödinger equation 89

E. Scalar field mediated gravitation 91

Curriculum Vitæ 93

Bibliography 95

1. Introduction

Standard Cosmology

Cosmology studies the properties and evolution of the universe as a whole. Physicists seek to investigate the characteristics of the universe from its earliest stage until now, and even its future fate. Modern cosmology started to develop at the beginning of the twentieth century. The equations governing the time evolution of the universe are derived within the framework of Einstein's theory of general relativity (1919). Alexander Friedmann's discovery (1922) of a non-static solution, together with Edwin Hubble's evidence (1924) that the observed galaxies are receding from earth, lead to the realization that we are living in an expanding universe. Georges Lemaître went one step further and suggested (1931) that this expansion required the universe to contract backwards in time, and it would continue to do so until contracted to a single point. George Gamow developed this idea of the big bang theory and used it to explain the origin of the chemical elements through a mechanism called big bang nucleosynthesis (1949). The direct observation by Arno Penzias and Robert Wilson (1965) of the predicted cosmic microwave background (CMB) gave strong experimental evidence for the big bang theory.

Modern satellites, like the Cosmic Background Explorer (COBE) or the Wilkinson Microwave Anisotropy Probe (WMAP) yield high precision measurements of the CMB. Combined with other cosmological observations like large-scale structure surveys, this allows for an accurate determination of many cosmological parameters (Komatsu et al. 2010). In particular it follows that ordinary baryonic matter makes up less than 5% of the content of today's universe but is still making up all the visible objects in the universe. Dark energy constitutes the largest fraction, almost 72%, whereas 23% are made of dark matter. Despite the many observational evidences for their existence (Albrecht et al. 2006; Roos 2010), not much is known about the fundamental nature of dark energy or dark matter. In its simplest form, dark energy can be modelled by a cosmological constant Λ in Einstein's equations (Peebles and Ratra 2003) and can account for the observed accelerated expansion of the universe (Riess et al. 1998). Although the nature of dark matter has not yet been identified, the candidates for DM particles are very light compared to the mass scales of typical galaxies (see for example Taoso, Bertone, and Masiero 2008). Given its large abundance, DM

is essential in the gravitational clustering. Current observations rule out the possibility that the dominant part of DM is made of hot dark matter (HDM), meaning particles that remained relativistic by the epoch of matter domination (see Hannestad et al. 2010, for a recent discussion). This leaves as possible candidates either cold dark matter (CDM) particles being created non-relativistically, or warm dark matter (WDM) particles becoming non-relativistic well before the matter domination epoch (Avila-Reese et al. 2001; Bode, Ostriker, and Turok 2001)(see also Boyarsky et al. 2009). From all these considerations emerged what is now known as the concordance model of cosmology or ΛCDM. It is incredibly successful in reproducing a large number of observations at various cosmic epochs.

Structure formation

Given the success of the concordance model, one can try to gain a deeper understanding of structure formation in the universe. The CMB is found to be very homogeneous with temperature fluctuations of the order of only 10^{-5}. On the other hand, different sky surveys provide a picture of today's large-scale structure in the universe. The problem of structure formation is to understand how the initially very small perturbations evolved into the galaxies and galaxy clusters we observe today.

According to the standard model of cosmology, a phase of exponential expansion, called inflation, brought the universe into an almost perfectly homogeneous and isotropic state with tiny, almost Gaussian perturbations, leading to the observed anisotropies of the CMB (more details can be found in many textbooks on cosmology, e.g. Dodelson 2003). These very small initial fluctuations are believed to be the seeds from which the structures we observe in today's universe have formed. The underlying picture is that, as time goes by, more and more matter is accumulated in the overdense regions, growing to the large structures we observe. The evolution of perturbations in the expanding universe is a highly non-linear problem, and a full analytical solution has so far proved intractable. Numerical simulations have therefore become an essential tool to study cosmological structure formation.

The details of how the small initial perturbations have been amplified through the gravitational interactions are closely related to the properties of the dark matter which dominates the gravitational clustering at large scales. Studying the formation of structure in the universe can therefore help us uncover the identity of the dark matter. Indeed, numerical simulations of structure formation played a decisive role in excluding standard massive neutrinos as a dark matter candidate (see for example White, Frenk, and Davis 1983).

Motivation and objectives

In the absence of a full analytical treatment of nonlinear structure growth, numerical simulations provide the critical link between the properties of the underlying model and the features of the finally observed structures. The formation of structures can be formulated in terms of the phase space evolution of a self-gravitating system described by the Vlasov-Poisson equations. Current simulations solve these equations via the method of characteristics and solve numerically the problem of the evolution of N self-gravitating bodies, where N is as large a number as computationally feasible. The state of the art N-body simulations – Aquarius (Navarro et al. 2010), Bolshoi (Klypin, Trujillo-Gomez, and Primack 2010), Millennium (Boylan-Kolchin et al. 2009), Via Lactea (Diemand et al. 2008) – are able to follow as many as a few billion particles and achieve impressive results. These simulations are however time-consuming and very expensive in computer power. One reason for this is that the gravitational force is long-ranged: at each time step, one has to sum over the contributions of all other particles, making the algorithm naively of $\mathcal{O}(N^2)$. Many ingenious techniques have been developed over the years (for a review, see for example Bertschinger 1998) to reduce the algorithmic complexity of the force integration to $\mathcal{O}(N \log N)$, or even $\mathcal{O}(N)$, as in the case of the Fast Multipole Method (Dehnen 2000; 2002).

Given the importance of numerical simulations of structure formation, we propose and try to explore an alternative approach. The main goal of this work is to investigate whether it is possible to replace the long-range gravitational interaction in the Vlasov-Poisson system by a purely local interaction. The inspiration is coming from gauge field theories, where spurious degrees of freedom are introduced in order to find a simpler description of the system. This local description is the starting point for a framework of numerical simulations using techniques of lattice gauge theory. Our objective is to describe this method in detail. We investigate its feasibility and study its conditions of validity and possible limitations.

Besides the hope that this could yield a faster algorithm for the simulations of cosmic structure formation, it will provide an alternative and independent approach to the existing N-body simulations.

Sketch of our approach

Let us briefly outline the major ingredients of our framework, which will be explained in more detail throughout this thesis. The figure 1.1 illustrates the main steps of our approach. On the top is the Vlasov-Poisson system governing the dynamics of structure formation. We want to model the long-range gravitational force by a local interaction with a gauge field. The classical phase space distribution function being a real quantity, it is

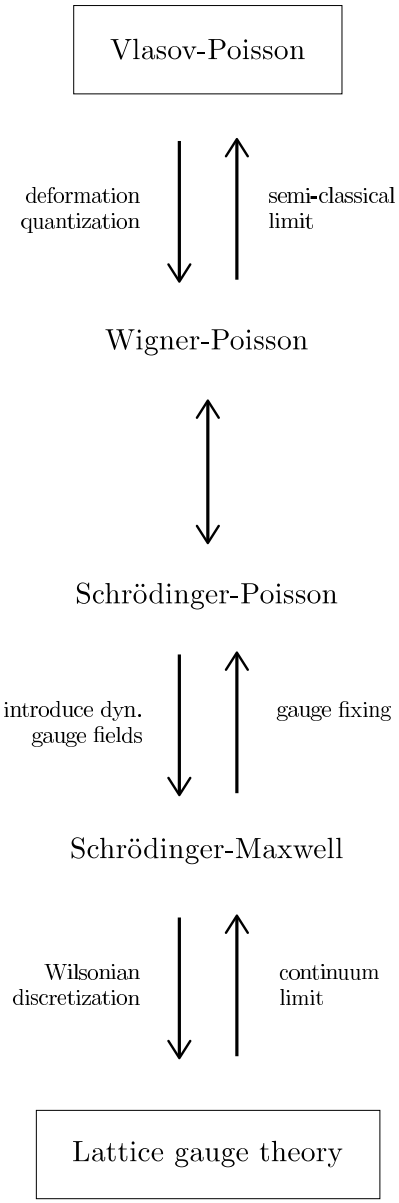

Fig. 1.1: Chart illustrating the main steps of our approach and how the different systems of equations are related. On the top is the Vlasov-Poisson system modelling the physics of structure formation, and on the bottom the related lattice gauge theory system, which we solve in the numerical simulations.

not obvious how one could make it transform under gauge transformations. To allow for the introduction of a gauge field, we will work with the corresponding quantum system described by the Wigner-Poisson equations. The Wigner equation is equivalent to the Schrödinger equation and, in the semi-classical limit, it reduces formally to the Vlasov equation.

The idea of trading the classical Vlasov-Poisson system for its quantum counterpart and solve the Schrödinger equation to study structure formation has already been considered before. In particular the works of Widrow and collaborators (Davies and Widrow 1997; Widrow and Kaiser 1993) investigated this method, and performed several testbed numerical simulations. They concluded that solving the Schrödinger-Poisson system can yield a promising alternative to existing N-body simulations. As we shall explain later in more detail, they evolved a single wavefunction, which didn't give a point-by-point correspondence with the classical phase space distribution. We suggest to improve this by allowing for several wavefunctions.

We also propose to take an additional step, and introduce a dynamical gauge field to get rid of the non-local Poisson equation to further reduce the complexity of the algorithm. At the level of the complex-valued wavefunction, we can introduce a gauge-transformation and an auxiliary Abelian gauge field and transform the Poisson equation into the set of Maxwell equations. The fiduciary gauge field mediates the gravitational force giving a completely local interaction. Moreover, having obtained a fully gauge-invariant theory, we can use the techniques of lattice gauge theories to obtain a framework well-adapted for numerical simulations.

Outline

The structure of this thesis is as follows: First, in chapter 2, we review the equations governing structure formation in the universe and describe briefly the algorithms and possible difficulties of N-body simulations. Next, in chapter 3, we discuss the properties of the Wigner distribution function, its dynamical equations, and how it is related to the Schrödinger and Vlasov equations. In chapter 4 we discuss the problem of initial conditions and investigate how to construct wavefunctions such that their Wigner distribution function is close to a given initial classical distribution function. Then we turn our full attention to describing the details of our local formulation. We describe how we introduce gauge fields to obtain a local interaction framework (chapter 5) and how we make use of Wilson's lattice gauge theory formulation to obtain an iterative solution of the equations of motion (chapter 6). In chapter 7 we compare our approach to similar methods that have been used before, and discuss some examples of testbed simulations we performed. Finally we present our conclusions and give an outlook on possible future work.

2. Structure formation in the universe

Standard cosmology assumes that the universe can be modelled by a perfect fluid of density ρ and pressure P in the isotropic and homogeneous Friedmann-Robertson-Walker spacetime. Under these assumptions, the Einstein equations reduce to the so-called Friedmann equations (Dodelson 2003)

$$\left(\frac{\dot{a}}{a}\right)^2 + \frac{kc^2}{a^2} - \frac{\Lambda c^2}{3} = \frac{8\pi G}{3}\rho, \tag{2.1a}$$

$$2\frac{\ddot{a}}{a} + \left(\frac{\dot{a}}{a}\right)^2 + \frac{kc^2}{a} - \Lambda c^2 = -8\pi G\frac{P}{c^2}, \tag{2.1b}$$

where a denotes the scale factor and $k = -1, 0, +1$ the curvature of the spacetime. Dots stand for derivatives with respect to the cosmological proper time t. For completeness we also introduced a cosmological constant Λ. To study the structure formation in the universe, one starts by writing the density ρ as the sum of an homogeneous background $\bar{\rho}$ plus small inhomogeneities $\delta\rho$. The background is assumed to evolve according to the Friedmann equations. In the case of a flat ($k = 0$) universe filled with non-relativistic matter ($P = 0$) and without cosmological constant ($\Lambda = 0$), sometimes called Einstein-de Sitter universe, the solution is found to be

$$a(t) = a_0\left(\frac{t}{t_0}\right)^{2/3}, \quad \bar{\rho}(t) = \frac{1}{6\pi G t^2}. \tag{2.2}$$

This corresponds to an expanding universe with a background density getting diluted by the expansion as $\bar{\rho} \propto a^{-3}(t)$.

Structure formation can be studied analytically within linear perturbation theory. We won't give an account of the details of this approach, but rather try to describe structure formation starting from a phase space picture. For a systematic treatment of the linear theory of gravitational perturbations the reader is invited to consult one of the reviews on the subject (Bernardeau et al. 2002; Ma and Bertschinger 1995; Mukhanov, Feldman, and Brandenberger 1992).

In the next section we briefly recall the phase space formulation and the related Vlasov equation. We then give the Vlasov equation for cosmological structure formation and show how it is equivalent to Newtonian cosmology. Finally we explain how N-body simulations solve the Vlasov equation

and shortly discuss the most important algorithms used. Some potential difficulties of N-body simulations are also outlined.

2.1 Phase space formulation

In classical mechanics, one may opt for a phase space formulation, to have a concise description of a dynamical system. For a given system of N particles, the phase space consists of the $6N$ dimensional space spanned by all possible values of positions x_i and momenta p_i of the particles. Every point in this multidimensional space defines a possible state of the system and a trajectory in phase space describes its time evolution.

If the number of particles is very large, one shouldn't try to keep track of the trajectories of all individual particles and try to find a statistical description instead. This allows to pass from the $6N$ to a 6 dimensional phase space[1]. The idea is to construct a distribution function $f(x, p, t)$ such that $f(x, p, t)dxdp$ gives the number of particles at position x with momentum p at a given time t. The normalization is chosen such that the integral over the whole phase space gives the total number of particles

$$\int dx \int dp\ f(x, p, t) = N. \tag{2.3}$$

When integrated over all momenta one obtains the particle number density $n(x, t)$, whereas the integral over all positions yields the momentum distribution $d_p(x, t)$

$$\int dp\ f(x, p, t) = n(x, t),\ \int dx\ f(x, p, t) = d_p(x, t). \tag{2.4}$$

Its time evolution is governed by Liouville's theorem which asserts that in case of dissipationless and collisionless dynamics (Binney and Tremaine 1987), the phase space distribution function is constant along the trajectories of the system

$$\frac{df}{dt} = \frac{\partial f}{\partial t} + \frac{\partial x}{\partial t}\frac{\partial f}{\partial x} + \frac{\partial p}{\partial t}\frac{\partial f}{\partial p} = 0. \tag{2.5}$$

Using the definition of the momentum $p = m\dot{x}$ and Newton's law $\dot{p} = F = -\nabla U$ for a force F derived from a potential U, this can be rewritten as

$$\frac{\partial f}{\partial t} + \frac{p}{m}\frac{\partial f}{\partial x} - \frac{\partial U}{\partial x}\frac{\partial f}{\partial p} = 0, \tag{2.6}$$

which is known as *Vlasov equation*.

[1] See for instance (Bertschinger 1995, section 3.2) for a derivation of the Vlasov equation from the BBGKY hierarchy of the Klimontovich density of a collisionless system of N self-gravitating particles.

A common way to look for solutions of the Vlasov equation is to use the method of characteristics (Zwillinger 1997). Given a partial differential equation of the form $\sum_{i=1}^{n} a_i(x_1, \ldots, x_n, u) \frac{\partial u}{\partial x_i} = c(x_1, \ldots, x_n, u)$, a solution is obtained through the characteristics given parametrically by $(x_1, \ldots, x_n, u) = (x_1(s), \ldots, x_n(s), u(s))$ such that the following system of ordinary differential equations holds

$$\begin{aligned} \frac{dx_i}{ds} &= a_i(x_1, \ldots, x_n, u), \\ \frac{du}{ds} &= c(x_1, \ldots, x_n, u). \end{aligned} \tag{2.7}$$

In the case of Vlasov's equation (2.6), the characteristics correspond to Newton's law and the definition of the canonical momentum

$$\frac{dp}{dt} = F, \tag{2.8a}$$

$$\frac{dx}{dt} = \frac{p}{m}\,. \tag{2.8b}$$

2.1.1 Cosmological Vlasov equation

We now turn to describing the phase space formulation of cosmic structure formation. Let us work in comoving coordinates and conformal time

$$x_{\mathrm{com}} = \frac{x_{\mathrm{phys}}}{a(t)}, \quad d\tau = \frac{dt}{a(t)}. \tag{2.9}$$

From now on x always refers to comoving coordinates and dots represent derivatives with respect to conformal time. The Vlasov-Poisson system reads (Bernardeau et al. 2002; Bertschinger 1995)

$$\frac{\partial f}{\partial \tau} + \frac{p}{am}\frac{\partial f}{\partial x} - am\frac{\partial U}{\partial x}\frac{\partial f}{\partial p} = 0, \tag{2.10a}$$

$$\nabla^2 U = 4\pi G a^2 \delta\rho. \tag{2.10b}$$

Note that only the density contrast $\delta\rho = \rho - \bar{\rho}$ sources the Poisson equation. We still need to define the relationship between the mass density ρ and the phase space distribution f. The common choice (2.3) is to normalize f to the total number of particles N. Since Vlasov's equation is linear in f, this normalization is defined up to an overall constant. If all particles have the same mass m, we may instead choose to normalize the phase space distribution to the total mass $M_{\mathrm{tot}} := mN$

$$\int dx \int dp\; f(x, p, \tau) = M_{\mathrm{tot}}. \tag{2.11}$$

We adopt this convention because structure formation is driven by the mass density and not the particle density. The physical mass density and peculiar velocity fields can then be defined by

$$\rho(x,p,\tau) = \frac{1}{a^3(\tau)} \int d^3p \; f(x,p,\tau), \tag{2.12}$$

$$\rho u(x,p,\tau) = \frac{1}{m\, a^4(\tau)} \int d^3p \; p \, f(x,p,\tau). \tag{2.13}$$

The density contrast is therefore given by

$$\begin{aligned} \delta\rho &= \rho - \langle\rho\rangle_V = \rho - \frac{1}{V}\int d^3x \; \rho \\ &= \frac{1}{a^3(\tau)} \left(\int d^3p \; f(x,p,\tau) - \frac{M_{\text{tot}}}{V} \right), \end{aligned} \tag{2.14}$$

where V denotes the total comoving volume over which we average.

As a cross-check, it can be shown that the characteristics of the Vlasov equation (2.10a) correspond to the equations of motion in Newtonian cosmology and the definition of the canonical momentum

$$\frac{d^2x}{d\tau^2} + \frac{\dot{a}}{a}\frac{dx}{d\tau} = -\nabla U(x), \tag{2.15a}$$

$$p = am\frac{dx}{d\tau}. \tag{2.15b}$$

The term proportional to $\frac{\dot{a}}{a}$ can be seen as a viscous force: the expansion of the universe opposes gravitational infall and as a result the growth of perturbations is slower in an expanding universe.

If we integrate the Vlasov equation (2.10a) over all momenta, we obtain

$$\partial_\tau \left(a^3\rho\right) + a^3\nabla(\rho u) = 0. \tag{2.16}$$

Expressed in terms of the cosmological time t and Hubble's parameter $H = \partial_t a/a$, the above equals

$$\partial_t\rho + 3H\rho + \frac{1}{a}\nabla(\rho u) = 0, \tag{2.17}$$

which is nothing but the continuity equation in an expanding universe. Further integrating over all comoving coordinates, we get the usual mass conservation

$$\partial_\tau M_{\text{tot}} = 0. \tag{2.18}$$

Assuming the dark matter be single-streaming (i.e. having a vanishing stress tensor, meaning that the velocity dispersion is negligible), the Vlasov equation leads to the Euler equation

$$\partial_\tau u + aHu + (u\cdot\nabla)u + \nabla U = 0, \tag{2.19}$$

which describes momentum conservation.

Linearizing and combining the continuity equation (2.17), Euler's equation (2.19) and Poisson's equation (2.10b) one can derive (see for instance Bernardeau et al. 2002) an equation for the evolution of the density contrast $\delta = \frac{\delta\rho}{\bar{\rho}}$:

$$\partial_t^2 \delta + 2H\partial_t \delta - 4\pi G\bar{\rho}\,\delta = 0. \tag{2.20}$$

For a matter dominated universe this equation admits two linearly independent power-law solutions $D_\pm(t)\delta(x, t_0)$, where $D_+(t) \propto a(t) \propto t^{2/3}$ is a growing mode and $D_-(t) \propto t^{-1}$ a decaying mode. $D_+(t)$ is called the linear growth factor. The quick dominance of the growing mode shows that the initial overdensities will be amplified and grow proportionally to the scale factor. This growth is the origin of the structure formation in the universe.

2.2 N-body simulations

In the absence of a full analytical understanding of nonlinear structure growth, numerical simulations provide the main tool to study structure formation in the universe. Instead of solving the underlying Vlasov-Poisson system (2.10) directly, current simulations solve numerically the problem of the evolution of N self-gravitating bodies, hence the name N-body simulations. Each body is evolved according to Newton's law (2.15a) under the influence of the gravitational potential created by all the others given by Poisson's equation (2.10b). In other words, N-body simulations solve the Vlasov equation via its characteristics by sampling the initial phase space distribution with a discrete number of particles. The number of bodies is typically chosen as large as computationally feasible. The advent of large supercomputers combined with the development of more efficient numerical algorithms has enabled the field of cosmological simulations to make considerable progress over the last decades. The state of the art simulations (Millennium; Aquarius; Via Lactea; Bolshoi) are able to follow as many as a few billion particles. Besides allowing to study the details of structure formation for a given model, N-body simulations are also used for testing approximate solutions for the growth of density perturbations. Comparison with numerical simulations allows to validate approximations and gain a better understanding under which conditions they can be used. For a review of the topic of N-body simulations, refer for instance to (Bagla 2005; Bertschinger 1998) or the textbook (Hockney and Eastwood 1988).

2.2.1 Algorithms and complexity

The art of N-body simulations lies chiefly in the computational algorithm used to obtain the gravitational force. Many ingenious techniques have been

developed over the years to reduce the algorithmic complexity of the force integration.

Particle-Particle (PP) algorithm

Computing the long-ranged force by direct summation over the contributions from all other bodies – called Particle-Particle method – is prohibitive for many particles, as $\mathcal{O}(N^2)$ operations are required to evaluate the gravitational force on all N bodies.

Tree algorithm

The Barnes-Hut tree algorithm divides the space recursively into a hierarchy of cells, which can contain several particles. The force of a distance group of particles is then approximated by the force due to a single body in the center of the cell, with mass equal to the total mass of the particles in that cell. This algorithm reduces the number of operations to $\mathcal{O}(N \log N)$, but the approximation introduces errors on the force which need to be kept under control.

Particle-Mesh (PM) algorithm

The Particle-Mesh algorithm relies on solving Poisson's equation on a Cartesian mesh using the Fast Fourier Transform (FFT). Since N-body simulations use discrete particles to represent the density field, one must first define a procedure to obtain the mass density on the grid. Moreover the gravity field obtained as a solution of Poisson's equation on the mesh must be interpolated back to the particles. The complexity of the PM algorithm is $\mathcal{O}(N_g \log N_g) + \mathcal{O}(N)$, where N_g is the number of grid cells used for the FFT. The drawback of this method is that the force poorly approximates Newton's inverse square law for separations less than several grid spacings. The force resolution of PM codes can be improved by using an adaptive mesh refinement, rather than a static grid to solve Poisson's equation.

Particle-Particle/Particle-Mesh (P^3M) & Tree-PM algorithms

The P^3M method is a hybrid of the PP and PM algorithms. The force computation via the PM method is supplemented by a direct particle-particle calculation for the pairs separated by only a few grid spacings. Combining this with an adaptive grid, the computational complexity is claimed to be $\mathcal{O}(N \log N)$. Another option is to resort to a tree code for the short-range force evaluation leading to a Tree-PM algorithm.

Fast Multipole Method (FFM)

The Fast Multipole Method is a variant of the tree algorithm and also relies on a hierarchical approximation of the force (Dehnen 2000; 2002). The complexity of this algorithm is $\mathcal{O}(N)$ making it the fastest force integration technique known today. This method was for instance implemented in the cosmological code `PkdGRAV` and among others used to study the galactic mass dark matter halo (Stadel et al. 2008).

2.2.2 Millennium simulation

Let us give a quantitative idea of some features of N-body simulations by looking at the example of the Millennium simulation (Springel et al. 2005). It tracks a total of $N = 2160^3 \sim 10^{10}$ particles and uses the `Gadget-2` code (Springel 2005) implementing a Tree-PM algorithm to evaluate the gravitational forces. In particular the FFT was done on a grid of 2560^3 cells. The simulation box corresponds to a cubic region of $500\,\mathrm{h}^{-1}$Mpc per side, while the spatial resolution is given to be of the order of $5\,\mathrm{h}^{-1}$kpc. The individual bodies had a mass of $8.6 \cdot 10^8 M_\odot \mathrm{h}^{-1}$. The cosmological parameters were chosen to be consistent with the first-year WMAP data.

The simulation started at redshift $z = 127$ and was evolved to the present using about 11 000 timesteps. The initial power spectrum was generated using the Boltzmann code `CMBFAST` (Seljak and Zaldarriaga 1996). The initial conditions were set up in two steps. The first is to construct a homogeneous particle distribution representing the uniform, unperturbed background density. The second step is to use Zel'dovich approximation (Zeldovich 1970) to generate a displacement field on the uniform particle distribution to obtain a density fluctuation with the desired statistical properties.

The computational complexity of the simulation can be illustrated by the fact that it required 350 000 hours of CPU time on a cluster with 512 processors, which is the equivalent of 28 days of wall-clock time. In total, about $5 \cdot 10^{17}$ floating point operations were performed. The simulation required a total of 1TB of memory and generated an output of about 20TB of data.

2.2.3 Potential difficulties

Even though cosmological N-body simulations have provided a most valuable tool to investigate the non-linear structure formation in our Universe, it is fair to say, that they also contain a number of difficulties. Gaining a quantitative understanding of these issues would allow to better define the limits of validity of current simulations and open the doors to include new physics, such as warm or hot dark matter. We will briefly list some of these limitations of N-body simulations.

Coarse-graining

In spite of the number of particles being of order of 10^{11} in recent simulations, it is still many orders of magnitude away from the actual number of DM particles in the universe. In other words, simulations follow the motion of unphysical macro-particles with masses of several solar masses and hence made up of huge lumps of elementary DM particles. This coarse-graining influences the validity of the simulations.

Velocity dispersion

N-body simulation attribute a certain velocity to the coarse-grained macro-particles. They are not able to track the velocities of the individual DM particles, but only the average velocity of the huge lumps of particles. This procedure is especially hard to justify in the case of warm or hot dark matter where the velocity dispersion of the particles is relevant.

To some extent, these first difficulties not only apply to N-body techniques. Other methods, like mesh codes, which are based on the discretization on a lattice, also present coarse-graining, as they contain minimal length and velocity scales that can be resolved, which typically correspond to the lattice spacing. In N-body simulations, however, the situation is more subtle, and it appears to me, that one should seek a deeper understanding of how the finite number of bodies affects the validity of the results, in particular for simulations in presence of warm and hot dark matter.

Discreteness effects

The "problem of discreteness" is that of the relation between the results of the N-body simulations and the solutions to the theoretical Vlasov-Poisson system they attempt to model. It has to be stressed that this does not refer to the errors arising in any numerical simulation because of the discretization of the equations of motion. Despite its obvious relevance, it seems that the question of the precise quantitative importance of the discreteness effects is still not settled (Joyce 2008). Wang and White (2007) have shown that discreteness errors might be even more important in simulations of HDM or WDM.

Force softening

Since the dark matter fluid is supposed to be collisionless, one has to manually suppress artificial two-body collisions arising between the pseudo-particles introduced to sample the phase space distribution. This is usually done by introducing an ad-hoc softening length and suppressing the gravitational force at scales below it (Dehnen 2001). N-body simulations are run

under the assumption that for a suitable choice of the smoothing, the evolution of the N pseudo-particles under the softened force should be the same as the gravitational evolution of the elementary DM particles.

Only game in town

As a matter of fact, there are no alternative tools to study the cosmic structure formation with the same resolution as N-body simulations. This is of course not a limitation of the N-body method itself, but makes it more complicated to evaluate the possible errors of N-body simulations quantitatively, as there are basically no independent results to compare with.

3. Wigner distribution function

We have seen that cosmic structure formation can be described by the Vlasov-Poisson equations in classical phase space. I this chapter we would like to put the problem of structure formation aside for the moment, and begin a new line of development, one that will lead to a new method of analysing the Vlasov-Poisson system. We now want to investigate the possibility of a phase space formulation of quantum mechanics and discuss the properties of the corresponding distribution function, called the *Wigner distribution function*. The equation governing its time evolution will be derived, and we will examine its relationship with the classical Vlasov equation.

3.1 Phase space quantum mechanics

Quantum mechanics is often presented as stemming from the Hamiltonian formulation of classical mechanics through "canonical quantization". This rather heuristic procedure consists in promoting the classical variables to hermitian operators and replacing the classical Poisson brackets by commutators.

Alternatively one can start from the phase space formulation of classical mechanics and try to find the quantum equivalent of the classical phase space distribution function (Ercolessi et al. 2007; Hillery et al. 1984). In other words one has to find a correspondence between classical functions in phase space, called symbols, and quantum operators in Hilbert space:

$$\text{operators in Hilbert space} \leftrightarrow \text{symbols in phase space} \tag{3.1}$$

Since the position and momentum do not commute, there is a priori no unambiguously defined mapping. Different operator orderings can give different functions. Hermann Weyl proposed a systematic way of associating quantum operators to classical distribution functions, referred to as Weyl quantization. Its inverse, the Wigner transform, associates to every quantum operator $\hat{A}$ a real phase space function A via

$$\text{sym}(\hat{A}) := \int dy\, e^{\frac{i}{\hbar}py} \langle q - \frac{y}{2}|\hat{A}|q + \frac{y}{2}\rangle = A(q,p). \tag{3.2}$$

To the product of two operators $\hat{A}\hat{B}$ is associated the Moyal star product of the corresponding symbols:

$$\text{sym}(\hat{A}\hat{B}) = \text{sym}(\hat{A}) * \text{sym}(\hat{B}), \tag{3.3}$$

where

$$f(q,p) * g(q,p) := f(q,p) \exp\left[\frac{i\hbar}{2}\left(\overleftarrow{\partial_q}\overrightarrow{\partial_p} - \overleftarrow{\partial_p}\overrightarrow{\partial_q}\right)\right] g(q,p). \tag{3.4}$$

Defining the Moyal bracket (Moyal 1949) by

$$\{f,g\}_M := f * g - g * f, \tag{3.5}$$

the commutator of operators is associated to the Moyal bracket of symbols

$$\mathrm{sym}([\hat{A},\hat{B}]) = \{\mathrm{sym}(\hat{A}), \mathrm{sym}(\hat{B})\}_M. \tag{3.6}$$

In the phase space formulation of quantum mechanics, the dynamical equations are expressed in terms of the Moyal bracket:

$$i\hbar\,\partial_t f = \{H,f\}_M, \tag{3.7}$$

which in the semiclassical limit $\hbar \to 0$ reduces to the classical equation in terms of the Poisson bracket

$$\partial_t f = \{H,f\}_P = H\left(\overleftarrow{\partial_q}\overrightarrow{\partial_p} - \overleftarrow{\partial_p}\overrightarrow{\partial_q}\right) f. \tag{3.8}$$

This illustrates how the algebraic structures of classical and quantum mechanics are related through the continuous changing of the parameter $\hbar$. This is the reason why such an approach to quantum mechanics is known as *deformation quantization* (Hirshfeld and Henselder 2002).

3.2 Wigner distribution function

The Wigner transform (3.2) maps a quantum operator $\hat{A}$ to a classical function in phase space. Wigner used this to associate to a quantum system a real phase space function, now called Wigner distribution function (WDF) (Wigner 1932). It is defined to be the symbol associated to the density operator $\hat{\rho}$ describing the quantum system

$$P_W(x,p) := \int d^3y\; e^{\frac{i}{\hbar}py}\; \langle x - \frac{y}{2}|\hat{\rho}|x + \frac{y}{2}\rangle. \tag{3.9}$$

In the case of a mixed state, the density operator can be written as convex combination of the pure state wavefunctions ψ_n

$$\hat{\rho} = \sum_n \lambda_n |\psi_n\rangle\langle\psi_n|, \quad \lambda_n \geq 0, \quad \sum_n \lambda_n = 1. \tag{3.10}$$

For mixed states the WDF thus reads

$$P_W(x,p) = \int d^3y\; e^{\frac{i}{\hbar}py} \sum_n \lambda_n \psi_n^*(x + \frac{y}{2})\psi_n(x - \frac{y}{2}), \tag{3.11}$$

while for a pure state it reduces to

$$P_W(x,p) = \int d^3y \; e^{\frac{i}{\hbar}py} \, \psi^*(x+\frac{y}{2})\psi(x-\frac{y}{2}). \tag{3.12}$$

The WDF has many similarities to the classical distribution function: $P_W(x,p)$ is a real function, as follows by taking the complex conjugate and changing variables $y \mapsto -y$. It is normalized to 1 in the following sense

$$\int d^3x \int \frac{d^3p}{(2\pi\hbar)^3} \; P_W(x,p) = 1. \tag{3.13}$$

When integrated over all momenta, it gives the probability density:

$$\begin{aligned} \int \frac{d^3p}{(2\pi\hbar)^3} P_W &= \int d^3y \; \delta^3(y) \sum_n \lambda_n \psi_n^*(x+\frac{y}{2})\psi_n(x-\frac{y}{2}) \\ &= \sum_n \lambda_n |\psi_n(x)|^2, \end{aligned} \tag{3.14}$$

whereas when integrated over all positions, it yields the momentum distribution

$$\begin{aligned} \int d^3x \; P_W &= \sum_n \lambda_n \int d^3x_- \int d^3x_+ \; e^{\frac{i}{\hbar}px_+} e^{-\frac{i}{\hbar}px_-} \psi_{n+}^* \psi_{n-} \\ &= \sum_n \lambda_n \left| \tilde{\psi}_n\Big(\frac{p}{\hbar}\Big) \right|^2, \end{aligned} \tag{3.15}$$

where the subscripts $\pm$ denote the dependence on $x_\pm := x \pm \frac{y}{2}$. The WDF thus has the attractive property that the marginal distributions, obtained by integrating over either the position or momentum variables, do reproduce the correct non-negative position and momentum probability distributions respectively, as specified by quantum mechanics.

Compared to the classical distribution function, the Wigner distribution function has the peculiar property that it may assume negative values. For this reason it is usually called a *quasi-probability distribution* and cannot be interpreted as a phase space probability density in the sense of classical mechanics. The non-positivity of the WDF can be seen from the property

$$\int dx \int dp \; P_W[\psi](x,p) P_W[\phi](x,p) \propto |\langle\psi|\phi\rangle|^2. \tag{3.16}$$

The right-hand side vanishes for any two orthogonal states ψ, ϕ; which implies that the WDF cannot be everywhere positive. According to the Hudson theorem (Hudson 1974), the WDF of a pure state is pointwise non-negative if and only if the state is Gaussian.

If $\hat{\rho}$ is not a pure state, it can be represented as a convex combination of pure state operators, $\hat{\rho} = \sum_n \lambda_n |\psi_n\rangle\langle\psi_n|$, in infinitely many ways. The

WDF satisfies the so-called mixture property (Ballentine 2000), which is the requirement that the phase space distribution should depend only on the density operator $\hat{\rho}$, and not on the particular way it is represented as a mixture of some set of pure states $\{|\psi_n\rangle\}$.

To summarize, the Wigner distribution function has many properties similar to the classical phase space distribution. Nevertheless it has been realized from the early days, that the concept of a joint probability at a phase space point is limited in quantum mechanics because the Heisenberg uncertainty principle makes it impossible to simultaneously specify the position and momentum of a particle. Therefore, the best one can hope to do is to define a function that has a maximum of properties analogous to those of the classical distribution function. Many different variants of distribution functions – Husimi, Kirkwood-Rihaczek, Glauber – have been studied over the decades, all with their own advantages and shortcomings (Lee 1995, and references therein). The WDF is despite it's non-positivity considered to be a useful calculational tool and finds applications in various domains outside of quantum physics, like signal processing or optics (Bastiaans 1997).

Given that there is no unique way to define a probability distribution in quantum mechanics, we choose to work with the Wigner distribution function, because it satisfies a number of properties, which are helpful for our approach. In particular it has the correct marginal distributions and, as we will show in the next paragraph, its dynamical equation is closely related to the classical Vlasov equation. The downside of the WDF is its nonpositivity[1]. Let us stress that our goal is not to interpret the Wigner distribution function as a fully-fledged phase space distribution, but rather as a convenient mathematical tool.

3.3 Dynamical equation for the WDF

We now want to derive the dynamical equation satisfied by the WDF. We shall do it in two different ways, first starting from Liouville's equation for the density matrix (Ballentine 2000), and secondly from Schrödinger's equation for the wavefunction.

3.3.1 Wigner equation from the Liouville equation

The Wigner distribution being the symbol of the density matrix $\hat{\rho}$, we can derive an equation of motion for it starting from the time evolution of $\hat{\rho}$

$$i\hbar\frac{d}{dt}\hat{\rho} = 0 \Rightarrow i\hbar\,\partial_t\hat{\rho} = [\hat{H},\hat{\rho}] \qquad \text{(Liouville equation)}. \tag{3.17}$$

[1] See also section 7.1.2 discussing the work of Widrow et al. They opted for the Husimi distribution, which is positive-definite, but does not have the correct marginal distributions and a more complicated dynamical equation.

Consider a Hamiltonian of the form $\hat{H} = \frac{\hat{P}^2}{2m} + \hat{V}$. Then we get

$$\partial_t \hat{\rho} = \frac{1}{i\hbar}\frac{1}{2m}\left(\hat{P}^2\hat{\rho} - \hat{\rho}\hat{P}^2\right) + \frac{1}{i\hbar}\left(\hat{V}\hat{\rho} - \hat{\rho}\hat{V}\right). \tag{3.18}$$

We shall separately compute the two terms of the right hand side. The first term is most easily evaluated in the momentum representation

$$\partial_t \langle p|\hat{\rho}|p'\rangle = \frac{1}{i\hbar}\frac{1}{2m}\left(p^2 - p'^2\right)\langle p|\hat{\rho}|p'\rangle. \tag{3.19}$$

Using the expression for the Wigner distribution in momentum space

$$P_W(x,p) = \int dk\; e^{-\frac{i}{\hbar}xk}\langle p - \frac{k}{2}|\hat{\rho}|p + \frac{k}{2}\rangle, \tag{3.20}$$

one finds

$$\partial_t P_W = -\frac{p}{m}\partial_x P_W, \tag{3.21}$$

which is nothing but the free Vlasov equation.

The second term can be computed in position representation

$$\partial_t \langle x|\hat{\rho}|x'\rangle = \frac{1}{i\hbar}\left(V(x) - V(x')\right)\langle x|\hat{\rho}|x'\rangle, \tag{3.22}$$

yielding

$$\partial_t P_W = \frac{1}{i\hbar}\int dy\; e^{\frac{i}{\hbar}py}\left(V(x - \frac{y}{2}) - V(x + \frac{y}{2})\right)\langle x - \frac{y}{2}|\hat{\rho}|x + \frac{y}{2}\rangle. \tag{3.23}$$

Let us for simplicity consider a pure state described by a single wavefunction. The dynamical equation for the Wigner distribution function becomes

$$\partial_t P_W + \frac{p}{m}\frac{\partial}{\partial x}P_W - \frac{1}{i\hbar}\int dy\; e^{\frac{i}{\hbar}py}\left(V_+ - V_-\right)\psi_+^*\psi_- = 0, \tag{3.24}$$

which we shall refer to as *Wigner equation*.

Note that, written in this form, the Wigner equation does not only involve the WDF but also the wavefunction. So it seems that we would have to define initial conditions for both. Now we show that the Wigner equation can be rewritten in terms of P_W only. Expanding the potential in a Taylor series

$$V(x + \frac{y}{2}) - V(x - \frac{y}{2}) = y\frac{\partial}{\partial x}V(x) + 2\sum_{\substack{n\geq 3\\ n\text{ odd}}}\frac{1}{n!}V^{(n)}(x)\left(\frac{y}{2}\right)^n, \tag{3.25}$$

we can write the dynamical equation for the WDF as follows

$$\partial_t P_W + \frac{p}{m}\frac{\partial}{\partial x}P_W - \frac{\partial V}{\partial x}\frac{\partial}{\partial p}P_W + \sum_{\substack{n\geq 3\\ n\text{ odd}}}\frac{1}{n!}\left(\frac{\hbar}{2i}\right)^{n-1}\partial_x^n V\,\partial_p^n P_W = 0. \tag{3.26}$$

One can notice that the first three terms correspond to the classical Vlasov equation. In three cases, the Wigner equation exactly coincides with the classical Vlasov equation: for a free particle ($V = 0$), for a uniform field ($V \propto x$) and for the harmonic oscillator ($V \propto x^2$). In general, there are additional terms that can be interpreted as quantum corrections.

It sounds surprising that the equation for the harmonic oscillator reduces exactly to the classical Vlasov equation, even though we know that the quantum mechanical treatment introduces discrete energy levels. In this case the quantum information is encoded purely in the initial conditions.

3.3.2 Wigner equation from the Schrödinger equation

The same dynamical equation can be derived by simply taking the time derivative of the Wigner distribution function for pure states, and using the fact that the wave function satisfies Schrödinger equation. Conversely, when inserting the expression of the Wigner distribution function into the above equation of motion, one finds the Schrödinger equation for the wave function.

To be slightly more generic, let us now consider the case of a WDF for a mixed state

$$P_W(x,p,t) \equiv \int d^3y \; e^{\frac{i}{\hbar}py} \sum_n \lambda_n \psi_n^*(x+\frac{y}{2},t)\psi_n(x-\frac{y}{2},t). \tag{3.27}$$

Suppose each of the wavefunctions satisfies Schrödinger equation

$$i\hbar\partial_t\psi_n = -\frac{\hbar^2}{2m}\nabla^2\psi_n + V\psi_n, \tag{3.28}$$

then the time-derivative of the WDF becomes

$$\begin{aligned}\partial_t P_W = \int d^3y \; e^{\frac{i}{\hbar}py} \sum_n \lambda_n \Big[\; & \frac{1}{i\hbar}\frac{\hbar^2}{2m}\left(\nabla_+^2\psi_{n+}^*\psi_{n-} - \psi_{n+}^*\nabla_-^2\psi_{n-}\right) \\ & - \frac{1}{i\hbar}\left(V_+ - V_-\right)\psi_{n+}^*\psi_{n-}\Big],\end{aligned} \tag{3.29}$$

where the subscripts $+,-$ denote the dependence on $x_\pm = x \pm \frac{y}{2}$. The term with the Laplacians can be rewritten as follows:

$$\begin{aligned}\partial_t P_W &\supset \int d^3y \; \sum_n \lambda_n \frac{2i\hbar}{m}\left[\vec{\nabla}_y\psi_{n+}^* \cdot \vec{\nabla}_y\left(e^{\frac{i}{\hbar}py}\psi_{n-}\right) - \vec{\nabla}_y\left(e^{\frac{i}{\hbar}py}\psi_{n+}^*\right)\cdot\vec{\nabla}_y\psi_{n-}\right] \\ &= \int d^3y \; \sum_n \lambda_n e^{\frac{i}{\hbar}py}\left(-\frac{2\vec{p}}{m}\right)\left(\vec{\nabla}_y\psi_{n+}^*\psi_{n-} - \psi_{n+}^*\vec{\nabla}_y\psi_{n-}\right) \\ &= -\frac{\vec{p}}{m}\int d^3y \; e^{\frac{i}{\hbar}py}\sum_n \lambda_n\left(\vec{\nabla}_x\psi_{n+}^*\psi_{n-} + \psi_{n+}^*\vec{\nabla}_x\psi_{n-}\right) \\ &= -\frac{\vec{p}}{m}\cdot\vec{\nabla}_x P_W.\end{aligned}$$

We thus obtained the same dynamical equation as before, now generalized to several wavefunctions

$$\partial_t P_W + \frac{\vec{p}}{m} \cdot \vec{\nabla}_x P_W - \frac{1}{i\hbar} \int d^3y \, e^{\frac{i}{\hbar} py} \, (V_+ - V_-) \sum_n \lambda_n \psi^*_{n+} \psi_{n-} = 0. \quad (3.30)$$

Note that in this derivation, the only assumption made on λ_n is that it be constant. In principle any value is acceptable and it can even be negative or complex. In our subsequent development (see chapter 4) we will make use of this freedom. As a consequence, the set of wavefunctions ψ_n and weights λ_n can no longer be given the interpretation of a mixed state in quantum mechanics, as the condition (3.10) is no longer satisfied. They are only seen as a convenient tool to encode the phase space information and do not correspond to any physical quantum mechanical system.

3.4 Semi-classical limit

The Wigner equation (3.26) describing the dynamics of the WDF reduces to the classical Vlasov equation in the naive $\hbar \to 0$ limit. Even though the quantum correction is formally $\mathcal{O}(\hbar^2)$, the derivatives of P_W could generate additional inverse powers of $\hbar$, making the semiclassical limit more involved[2].

The properties of the semi-classical limit depend of course on the potential $V(x)$. In this paragraph we present some results concerning the case of interest to us, where the potential satisfies Poisson's equation. In particular, different authors investigated the semi-classical limit of the Wigner-Poisson (W-P) system to the Vlasov-Poisson (V-P) system for the Coulomb potential.

The mathematically rigorous classical limit from W-P to V-P has been solved first in 1993 independently by (Lions and Paul 1993) and (Markowich and Mauser 1993). Both references consider a so-called completely mixed state; i.e. an infinite number of pure states with a strong additional constraint on the occupation probabilities

$$\mathrm{Tr}\rho^2 = \sum_{n=1}^{\infty} (\lambda_n)^2 \leq \hbar^3 \text{ Const.} \quad (3.31)$$

Under this assumption, the classical limit of the solution to the 3D W-P system converges to the solution of the V-P system. Note that the Wigner distribution function can also have negative values, whereas the semi-classical limit is a true, nonnegative distribution function. In both references, this was overcome by using a Gaussian-smoothed Wigner function.

[2] This formulation of the statement is not fully satisfying, as the true semi-classical limit is also a statement about the properties of the wavefunction, and not identical to sending $\hbar \to 0$; which is anyway a dimensionful parameter.

The situation for a pure state is completely different (Zhang, Zheng, and Mauser 2002). According to the authors, it appears that a density operator which has the above property that the trace of its square tends to zero with the third power of the Planck constant seems to be closer to classical mechanics than a pure state. For a pure state in 1D, the semi-classical limit is not unique: examples have been constructed where different regularization schemes give different limits (Majda, Majda, and Zheng 1994). The question whether there exists a selection principle to pick the correct classical solution has also been investigated but is not yet settled (Jin, Liao, and Yang 2007). No proof of the semi-classical limit from W-P to V-P is known for the pure state case in 2D or 3D.

For more details the reader is referred to the original papers or the review (Mauser 2002). See also (Fröhlich, Graffi, and Schwarz 2007) for an alternative approach of the semi-classical limit.

4. WDF for a given phase space distribution

We would like to trade the Vlasov equation for the phase space distribution function for Schrödinger's equation for the wavefunctions, as this allows for the introduction of a gauge field as the mediator of the gravitational force. Or course we don't require the wavefunctions to have any intrinsic physical interpretation. We rather consider them, just like the WDF, as a mathematical tool and not as fundamental entities. Still we are faced with the problem of how to determine a set of wavefunctions such that their WDF corresponds to the initial classical phase space distribution.

From the outset it is clear that, since the wavefunctions encode both, the position and momentum information, a single wavefunction (pure state) cannot be sufficient to describe a generic $f(x,p)$. One should rather look for a set of wavefunctions (mixed state). The more wavefunctions we allow for, the more freedom we have and the more accurately the WDF should represent any given distribution. At the same time the total number of wavefunctions should be as small as possible because this will reduce the computational complexity of our numerical simulations.

Given the classical distribution function $f(x,p)$, we want to expand it using the WDF Ansatz

$$f(x,p) \equiv \sum_{n=1}^{N_\psi} \lambda_n \int d^3y \; e^{\frac{i}{\hbar}py} \, \psi_n^*(x+\frac{y}{2}) \, \psi_n(x-\frac{y}{2}). \tag{4.1}$$

Fourier transforming from p-space to η-space we get

$$f(x,\eta) \equiv \sum_{n=1}^{N_\psi} \lambda_n \psi_n^*(x-\frac{\eta}{2}) \, \psi_n(x+\frac{\eta}{2}). \tag{4.2}$$

We will discuss different approaches to tackle this problem of determining the set of wavefunctions ψ_n and weights λ_n representing a given initial phase space distribution $f(x,p)$. Let us stress from the outset that these procedures need only to be used once at the beginning of a numerical simulation, to set up the initial conditions.

4.1 Minimization procedure

The first method we present to choose the initial wavefunctions is a brute-force minimization. The underlying idea is to define a functional measuring the total absolute error made by approximating the phase space distribution by the WDF Ansatz

$$\Phi[\psi_n, \lambda_n, N_\psi] := \int d^3x \int d^3\eta \left| f(x,\eta) - \sum_{n=1}^{N_\psi} \lambda_n \psi_n^*(x - \frac{\eta}{2}) \psi_n(x + \frac{\eta}{2}) \right|^2 , \quad (4.3)$$

and determine a set of wavefunctions that minimizes this error. In practice, the minimization is most easily done via discretization on a lattice. The problem is then cast into a minimization of the scalar error function with a large number of variables corresponding to the values of the wavefunctions at the lattice points. For different fixed $N_\psi = 1, 2, \ldots$, we can determine the set of wavefunctions ψ_n and corresponding weights λ_n which minimizes the error. One can then compare the results for different N_ψ to find an optimal approximation with a high enough accuracy and a minimal number of wavefunctions.

Since we are not seeking a true quantum mechanical interpretation, let's consider the most general case of complex-valued weights. A naive minimization will not yield wavefunctions normalized to unity. Instead of adding this normalization as a constraint to the minimization, we remove the module of the complex weights λ_n, and only keep their phases $e^{i\varphi_n}$. The modules of the weights are taken to be the norm of the wavefunctions, thereby normalizing them to unity.

Splitting the wavefunctions into real and imaginary parts $\psi_n(x) \equiv \alpha_n(x) + i\beta_n(x)$ and introducing the notation $x_\pm = x \pm \frac{\eta}{2}$, we get

$$\begin{aligned} e^{i\varphi_n} \psi_{n-}^* \psi_{n+} = &\left[\cos\varphi_n \left(\alpha_{n-}\alpha_{n+} + \beta_{n-}\beta_{n+}\right) - \sin\varphi_n \left(\alpha_{n-}\beta_{n+} - \alpha_{n+}\beta_{n-}\right)\right] \\ &+ i\left[\cos\varphi_n \left(\alpha_{n-}\beta_{n+} - \alpha_{n+}\beta_{n-}\right) + \sin\varphi_n \left(\alpha_{n-}\alpha_{n+} + \beta_{n-}\beta_{n+}\right)\right] . \end{aligned}$$

The real and imaginary parts of the error are therefore

$$\mathscr{E}_{\mathrm{Re}} := \mathrm{Re} f - \sum_{n=1}^{N_\psi} \left[\cos\varphi_n \left(\alpha_{n-}\alpha_{n+} + \beta_{n-}\beta_{n+}\right) - \sin\varphi_n \left(\alpha_{n-}\beta_{n+} - \alpha_{n+}\beta_{n-}\right)\right] ,$$

$$\mathscr{E}_{\mathrm{Im}} := \mathrm{Im} f - \sum_{n=1}^{N_\psi} \left[\cos\varphi_n \left(\alpha_{n-}\beta_{n+} - \alpha_{n+}\beta_{n-}\right) + \sin\varphi_n \left(\alpha_{n-}\alpha_{n+} + \beta_{n-}\beta_{n+}\right)\right] .$$

If we simply minimize the error functional, we will in general obtain wavefunctions that are not smooth enough on the lattice to be evolved numerically. For this purpose it is useful to add a sort of kinetic term to the functional that will allow us to enforce a certain degree of smoothness. We

construct the kinetic term from the square of the discretized derivatives with a certain overall factor $\varkappa$ to tune the smoothness:

$$\mathcal{K} := \varkappa \sum_x \sum_{n=1}^{N_\psi} |\alpha_n(x+1) - \alpha_n(x)|^2 + |\beta_n(x+1) - \beta_n(x)|^2 \,. \tag{4.5}$$

Finally, we minimize this kinetic term with the total error summed over all lattice points

$$\mathscr{E}_{\text{total}} := \mathcal{K} + \sum_x \sum_\eta \left(|\mathscr{E}_{\text{Re}}|^2 + |\mathscr{E}_{\text{Im}}|^2 \right). \tag{4.6}$$

The minimization procedure was implemented in MATHEMATICA and independently in C++ using the minimization routines of the `Gnu Scientific Libraries`. Both methods were applied to cosmic initial conditions of cold dark matter in the Zel'dovich approximation, for simplicity in a one-dimensional case. The results confirm the expectation that, increasing the number of wavefunctions, the total error is reduced. In the case we studied, it turned out that already a relatively small number of wavefunctions (compared for instance to the number of lattice points) was enough to achieve a reasonable accuracy.

As usual with minimization procedures, there is no guarantee that the algorithm converges to a global minimum. This would for instance mean that one has to repeat the minimization with different initial random seeds and compare their outcomes. Also, even though this minimization was shown to work for a given phase space distribution $f(x,p)$, in practice it becomes computationally challenging even for rather small 3D lattice sizes, as the number of variables in the minimization procedure grows too quickly. Despite its applicability to any distribution function, the brute-force minimization might not be the best method to determine the initial wavefunctions.

4.2 Eigenvalue problem for hermitian operator

We now turn our attention to obtaining an analytic solution to the problem of determining the initial wavefunctions. More precisely we will show how the Wigner Ansatz can be reformulated as an eigenvalue problem, which we then solve analytically in the special case of a phase space distribution function in the form $f(x,p) = \rho(x)\delta(p)$, meaning the product of a generic distribution in x with a delta function in momentum. This choice corresponds to the case of CDM at early times, when the velocities are negligible.

Since $f(x,\eta)$ is the Fourier transform of a real function $f(x,p)$, it satisfies the condition $f^*(x,-\eta) = f(x,\eta)$. In the coordinates $x_\pm := x \pm \frac{\eta}{2}$ we can define

$$\hat{f}(x_-, x_+) := f\left(\frac{x_+ + x_-}{2}, x_+ - x_-\right), \tag{4.7}$$

which is then hermitian

$$\hat{f}^*(x_+, x_-) = \hat{f}(x_-, x_+). \tag{4.8}$$

Any square-integrable hermitian kernel can be expressed in terms of its spectral decomposition (Hilbert-Schmidt theorem)

$$\hat{f}(x_-, x_+) \equiv \sum_n \lambda_n \psi_n^*(x_-)\psi_n(x_+), \tag{4.9}$$

where the λ_n are the real eigenvalues and $\{\psi_n\}_n$ the set of orthonormal eigenfunctions with respect to the standard scalar product on $L^2(\mathbb{C}^3)$

$$\langle \psi_n | \psi_m \rangle := \int d^3x \; \psi_n^*(x)\psi_m(x) = \delta_{nm}. \tag{4.10}$$

The WDF Ansatz (4.2) has exactly the same form as the spectral decomposition (4.9). Therefore we conclude that *any* given phase space distribution function $f(x, p)$ can be written exactly as WDF, if need be with an infinite number of wavefunctions. The wavefunctions are the eigenfunctions of the hermitian operator $\hat{f}(x_-, x_+)$ and its real eigenvalues correspond to the weights of the wavefunctions in the mixed state. Notice though, that they can in general take negative values, implying that we cannot give a full quantum-mechanical interpretation to the mixed state, as the corresponding density operator is not positive-definite. Let us emphasize once more that we consider the wavefunctions as a mere mathematical tool.

Multiplying both sides of (4.9) by $\psi_\alpha(x_-)$ and integrating over x_-, the orthonormality of the eigenfunctions implies the following integral equation

$$\int d^3x_- \; \hat{f}(x_-, x_+)\psi_\alpha(x_-) = \lambda_\alpha \psi_\alpha(x_+). \tag{4.11}$$

This equation shows that the determination of the wavefunctions reduces to finding the eigenfunctions of the hermitian kernel $\hat{f}$. Unfortunately, for a completely general phase space distribution function, the above equation might not allow for an analytic solution.

4.2.1 Generalization: weighted scalar product

Above we discussed the eigenvalue problem for the standard scalar product 4.10. We now ask the question whether we could generalize the analysis by allowing for a non-trivial weight function $w(x)$ in the scalar product:

$$\langle \phi | \psi \rangle_w := \int d^3x \; \phi^*(x)\psi(x)w(x). \tag{4.12}$$

It must first be noted that the hermitian kernel $\hat{f}^*(x_+, x_-) = \hat{f}(x_-, x_+)$ still allows to define an integral operator

$$(\hat{f}\phi)(x) := \int d^3y \; \hat{f}(y, x)\phi(y)w(y), \tag{4.13}$$

that is self-adjoint with respect to the weighted scalar product

$$\langle \hat{f}\phi|\psi\rangle_w = \langle \phi|\hat{f}\psi\rangle_w \; . \tag{4.14}$$

This ensures us that the spectral decomposition 4.9 exists, but now the eigenfunctions are orthonormal with respect to the weighted scalar product $\langle\psi_n|\psi_m\rangle_w = \delta_{nm}$, and the eigenvalue problem reads

$$\int d^3y \; \hat{f}(y, x)\psi_\alpha(y)w(y) = \lambda_\alpha\psi_\alpha(x). \tag{4.15}$$

Let us emphasize that the weighted scalar product is only used to determine the wavefunctions whose WDF equals the classical distribution function. The choice of $w(x)$ is completely arbitrary and does not affect the properties of the WDF or the Schrödinger evolution of the wavefunctions. Clearly the spectrum will depend on the choice of weight function. The additional freedom of choosing $w(x)$ could allow to reduce the number of wavefunctions needed in the Wigner Ansatz. Furthermore the arbitrariness of the weight function also reflects the freedom we have to choose wavefunctions representing the initial state.

4.3 Eigenvalue problem on the finite interval

Let us study the eigenvalue problem for a phase space distribution of the form[1] $f(x, p) = \rho(x)\delta(p)$, for which the integral operator $\hat{f}$ becomes real and symmetric

$$\hat{f}(x_-, x_+) = \rho\left(\frac{x_+ + x_-}{2}\right). \tag{4.16}$$

We choose the trivial weight function $w(x) = 1$, which might not be the optimal choice for a minimal number of wavefunctions, but yields a working example of the method. Consider a density distribution that is periodic $\rho(x + L) = \rho(x)$ and expand it as a Fourier series

$$\rho(x) = \sum_{n=1}^{\infty}\left[a_n \cos\left(\frac{2\pi n}{L}x\right) + b_n \sin\left(\frac{2\pi n}{L}x\right)\right]. \tag{4.17}$$

[1] For the sake of simplicity we restrict the analysis of this section to the one dimensional case, but the generalization to the 3D case is straightforward.

We omit the spatially constant mode ρ_0 which we can trivially represent as a WDF using a constant wavefunction.

It's easiest to solve the eigenfunction problem on the doubled interval $[0, 2L]$. We consider real, square-integrable functions on $[0, 2L]$ extending them periodically beyond. Using the scalar product defined by

$$\langle\phi|\psi\rangle := \frac{1}{L}\int_0^{2L} dx\ \phi(x)\psi(x)\,, \tag{4.18}$$

the eigenvalue problem reads

$$\frac{1}{L}\int_0^{2L} dy\ \rho\left(\frac{x+y}{2}\right)\psi(y) = \lambda\psi(x). \tag{4.19}$$

Let's expand ψ on the Fourier basis on $[0, 2L]$

$$\psi(x) = \sum_{n=1}^{\infty}\left[\alpha_n \cos\left(\frac{\pi n}{L}x\right) + \beta_n \sin\left(\frac{\pi n}{L}x\right)\right]. \tag{4.20}$$

Since moreover

$$\rho\left(\frac{x+y}{2}\right) = \sum_{n=1}^{\infty}\left[a_n \cos\left(\frac{2\pi n}{L}\frac{x+y}{2}\right) + b_n \sin\left(\frac{2\pi n}{L}\frac{x+y}{2}\right)\right], \tag{4.21}$$

we may use the trigonometric identities

$$\begin{aligned}\cos(\alpha \pm \beta) &= \cos\alpha\cos\beta \mp \sin\alpha\sin\beta\,,\\ \sin(\alpha \pm \beta) &= \sin\alpha\cos\beta \pm \cos\alpha\sin\beta\,,\end{aligned}$$

and the orthonormality relations

$$\begin{aligned}&\frac{1}{L}\int_0^{2L} dx\ \cos\left(\frac{\pi n}{L}x\right)\cos\left(\frac{\pi m}{L}x\right) = \delta_{nm} = \frac{1}{L}\int_0^{2L} dx\ \sin\left(\frac{\pi n}{L}x\right)\sin\left(\frac{\pi m}{L}x\right),\\ &\frac{1}{L}\int_0^{2L} dx\ \cos\left(\frac{\pi n}{L}x\right)\sin\left(\frac{\pi m}{L}x\right) = 0\,,\end{aligned}$$

to rewrite the eigenvalue problem (4.19) as

$$\begin{aligned}\sum_{n=1}^{\infty}\Big[(a_n\alpha_n + b_n\beta_n)\cos\left(\frac{\pi n}{L}x\right) + (b_n\alpha_n - a_n\beta_n)\sin\left(\frac{\pi n}{L}x\right)\Big]&\\ = \lambda\sum_{n=1}^{\infty}\left[\alpha_n\cos\left(\frac{\pi n}{L}x\right) + \beta_n\sin\left(\frac{\pi n}{L}x\right)\right].&\end{aligned} \tag{4.22}$$

This is equivalent to an eigenvalue problem for the Fourier coefficients

$$\begin{pmatrix} a_n & b_n \\ b_n & -a_n\end{pmatrix}\begin{pmatrix}\alpha_n\\ \beta_n\end{pmatrix} = \lambda\begin{pmatrix}\alpha_n\\ \beta_n\end{pmatrix}. \tag{4.23}$$

Therefore the normalized eigenfunctions and corresponding eigenvalues of our symmetric integral operator are finally given by

$$\psi_n^{\pm}(x) = \mathcal{N}^{-1/2}\left[\left(a_n \pm \sqrt{a_n^2+b_n^2}\right)\cos\left(\frac{\pi n}{L}x\right) + b_n \sin\left(\frac{\pi n}{L}x\right)\right], \quad (4.24a)$$

$$\lambda_n^{\pm} = \pm\sqrt{a_n^2+b_n^2}, \quad (4.24b)$$

where $\mathcal{N} := \left(a_n \pm \sqrt{a_n^2+b_n^2}\right)^2 + b_n^2$ normalizes the eigenfunctions to unity . It can be checked explicitly that these eigenvectors satisfy the condition of orthonormality

$$\langle\psi_n^+|\psi_n^+\rangle = \langle\psi_n^-|\psi_n^-\rangle = 1,\ \langle\psi_n^+|\psi_n^-\rangle = 0\,, \quad (4.25)$$

and yield the correct spectral representation

$$\rho\left(\frac{x+y}{2}\right) = \sum_{n=1}^{\infty}\left[\lambda_n^+\psi_n^+(x)\psi_n^+(y) + \lambda_n^-\psi_n^-(x)\psi_n^-(y)\right]. \quad (4.26)$$

As a conclusion we have been able to solve the eigenvalue problem on the finite interval and use it to find the wavefunctions for the WDF Ansatz. This applies for a generic density profile $\rho(x)$ periodic on $[0, L]$ and a phase space distribution of the form $f(x,p) = \rho(x)\delta(p)$. The wavefunctions are harmonic functions with increasing momenta. In general we would need an infinite number of wavefunctions. For many applications a finite or even small number of wavefunctions may be sufficient.

4.4 Fourier series inspired decomposition

Inspired by the above results, we can actually write down a different choice of wavefunctions, which are even closer to the Fourier basis. Let us again start by decomposing the density profile on a finite interval $[0, L]$ as Fourier series:

$$\rho(x) = \sum_{n=1}^{\infty} a_n \cos\left(\frac{2\pi n}{L}x\right) + \sum_{n=1}^{\infty} b_n \sin\left(\frac{2\pi n}{L}x\right) \equiv \rho^c(x) + \rho^s(x). \quad (4.27)$$

We can expand the first term in cosine on the following set of wavefunctions:

$$\begin{cases} \psi_n^{c1}(x) & = \cos\left(\frac{\pi n}{L}x\right) \quad @\ \lambda_n = a_n\,, \\ \psi_n^{c2}(x) & = \sin\left(\frac{\pi n}{L}x\right) \quad @\ \lambda_n = -a_n\,. \end{cases} \quad (4.28)$$

Indeed

$$\begin{aligned}\sum_n \lambda_n\psi_n^*(x)\psi_n(y) &= \sum_{n\geq 1} a_n \cos\left(\frac{\pi n}{L}x\right)\cos\left(\frac{\pi n}{L}y\right) + \sum_{n\geq 1}(-a_n)\sin\left(\frac{\pi n}{L}x\right)\sin\left(\frac{\pi n}{L}y\right) \\ &= \sum_{n\geq 1} a_n \cos\left(\frac{\pi n}{L}(x+y)\right) = \rho^c\left(\frac{x+y}{2}\right).\end{aligned}$$

The sine part on the other hand, can be expanded on

$$\begin{cases} \psi_n^{s1}(x) &= \frac{1}{\sqrt{2}}\left[\cos\left(\frac{\pi n}{L}x\right) + \sin\left(\frac{\pi n}{L}x\right)\right] \quad @\ \lambda_n = b_n\,, \\ \psi_n^{s2}(x) &= \frac{1}{\sqrt{2}}\left[\cos\left(\frac{\pi n}{L}x\right) - \sin\left(\frac{\pi n}{L}x\right)\right] \quad @\ \lambda_n = -b_n\,, \end{cases} \tag{4.29}$$

as can be checked as follows

$$\begin{aligned} \sum_n \lambda_n \psi_n^*(x)\psi_n(y) &= \sum_{n\geq 1} b_n \frac{1}{2}\left[\cos\left(\frac{\pi n}{L}x\right) + \sin\left(\frac{\pi n}{L}x\right)\right]\left[\cos\left(\frac{\pi n}{L}y\right) + \sin\left(\frac{\pi n}{L}y\right)\right] \\ &\quad + \sum_{n\geq 1}(-b_n)\frac{1}{2}\left[\cos\left(\frac{\pi n}{L}x\right) - \sin\left(\frac{\pi n}{L}x\right)\right]\left[\cos\left(\frac{\pi n}{L}y\right) - \sin\left(\frac{\pi n}{L}y\right)\right] \\ &= \sum_{n\geq 1} b_n \left[\cos\left(\frac{\pi n}{L}x\right)\sin\left(\frac{\pi n}{L}y\right) + \sin\left(\frac{\pi n}{L}x\right)\cos\left(\frac{\pi n}{L}y\right)\right] \\ &= \sum_{n\geq 1} b_n \sin\left(\frac{\pi n}{L}(x+y)\right) = \rho^s\left(\frac{x+y}{2}\right). \end{aligned}$$

This illustrates once more that the wavefunctions may be taken to be harmonic functions. The number of wavefunctions needed for an exact representation is proportional to the number of significant Fourier modes in the density $\rho(x)$. Note however that in this case the wavefunctions are not eigenfunctions of the integral operator $\hat{f}$ and are not orthogonal on the interval $[0, L]$ but only normalized. Depending on the even or odd nature of n, the wavefunctions are either periodic or anti-periodic on $[0, L]$. It can be checked that the Schrödinger Hamiltonian is still hermitian for this mixed choice of boundary conditions. Working with these functions comes at the price of having to introduce two different types of boundary conditions in the numerical simulation. For the purpose of our exploratory work we decided instead to work with the previous solution on the doubled interval $[0, 2L]$, where all functions are periodic.

4.5 Cosmological initial conditions

Observations of structure in the universe are perfectly compatible with the simplest possible statistical description, namely a Gaussian distribution. More precisely, each Fourier mode of the density contrast $\delta(\vec{k})$ (not to be confused with the Dirac delta distribution) satisfies an isotropic Gaussian distribution, entirely described by the power spectrum $P(k) := \langle|\delta(\vec{k})|^2\rangle$, which is a function of the modulus k only, not of the direction (for details, refer for instance to the textbook Weinberg 2008). From the knowledge of the power spectrum one can then generate a realization with the desired statistical properties

$$\delta(\vec{x}) = \sum_{\vec{k}} \left[\sqrt{P(k)}\mathcal{N}(0,1)\cos(\vec{k}\cdot\vec{x}) + \sqrt{P(k)}\mathcal{N}(0,1)\sin(\vec{k}\cdot\vec{x})\right], \tag{4.30}$$

where $\mathcal{N}(0,1)$ denotes a Gaussian random number with zero mean and unit dispersion. This shows that the density contrast for cosmological initial conditions is in a form for which we know how to construct the WDF, provided that we start our simulation at times, when the Zel'dovich velocities of the particles are negligible. Compared to N-body simulations we don't need to first perform a FFT to compute $\delta(\vec{x})$ but can find the initial wavefunctions directly from the power spectrum. Additionally we don't need any glassy pre-initial conditions to model the constant background. On the other hand, we would in principle need as many wavefunctions as Fourier modes are important in the power spectrum.

4.6 Matrix formulation

Given that the WDF Ansatz can be thought of as spectral decomposition of an hermitian operator, we can now analyze the solution in the discrete case, where the problem reduces to a matrix problem. Let's again restrict the analysis to one dimension. Working on a lattice $(x_1, x_2, \dots x_N)$, we can think of any function $f(x)$ as a vector $(f(x_1), \dots, f(x_N))^T$ and of any function of two variables as a matrix. We can thus reinterpret the functional relationship

$$\hat{f}(x_-, x_+) := f\left(\frac{x_+ + x_-}{2}, x_+ - x_-\right) = \sum_{n=1}^{N_\psi} \lambda_n \psi_n^*(x_-)\psi_n(x_+), \tag{4.31}$$

in terms of matrices:

$$\hat{F}_{ij} \equiv \sum_{n=1}^{N_\psi} \lambda_n \Psi_{jn}^* \Psi_{in} = \sum_{n=1}^{N_\psi}\sum_{k=1}^{N_\psi} \Psi_{in}\lambda_n \delta_{nk} \Psi_{kj}^\dagger \,. \tag{4.32}$$

The property $\hat{f}(x_+, x_-) = \hat{f}^*(x_-, x_+)$ then translates into the fact that $\hat{F}$ is a hermitian matrix $\hat{F}^\dagger = \hat{F}$, which we can diagonalize by means of a unitary transformation

$$\hat{F}_{ij} \equiv \left(\Psi \cdot \Lambda \cdot \Psi^\dagger\right)_{ij} \,, \tag{4.33}$$

where

$$\hat{F} \in \mathbb{C}^{N\times N}, \quad \Psi \in \mathbb{C}^{N\times N_\psi}, \quad \Lambda = \mathrm{diag}(\lambda_1, \dots \lambda_{N_\psi}) \in \mathbb{R}^{N_\psi \times N_\psi}.$$

The columns of Ψ are the wavefunctions ψ_n sampled on the lattice. The property that Ψ is unitary $\Psi^\dagger\Psi = \mathbb{I}$ implies the normalization of the wavefunctions on the lattice. This matrix formulation has the advantage, that it's straightforward to compute the spectrum of any given hermitian matrix. The shortcomings of this approach are two-fold: firstly we would need as many wavefunctions as lattice points, which comes at a big computational

cost, and secondly the eigenvectors have no a priori reason to be smooth enough to be used as initial conditions for our numerical scheme. Moreover it has to be noted that we would need to compute the eigenvectors for a matrix containing the full 3D lattice. Computing the eigenvectors of a $n \times n$ matrix is in general a problem of complexity $\mathcal{O}(n^3)$ (Numerical Recipes 2007). Since the size of the matrix is related to the number of lattice points N^3, one quickly reaches lattice sizes making the solution of the eigenvalue problem impossible.

4.7 Remarks concerning the number of wavefunctions

For numerical simulations in a finite box with periodic boundary conditions, the spatial lattice resolution also dictates the resolution in momentum space. The size of the box is related to the lattice size in k-space since the wavevectors take discrete values $\vec{k} = \frac{2\pi}{L}\vec{n}$. The maximal wavevector is linked to the lattice spacing in real space. This illustrates the relationship between the number of wavefunctions and the spatial resolution of the simulation. If we keep all the modes, we need $\mathcal{O}(N_x^3)$ wavefunctions, where N_x is the number of lattice points in one direction. Note that this corresponds, in order of magnitude, to the number of particles in N-body simulations. So even if we keep the maximal number of wavefunctions needed to accurately represent the initial conditions, the complexity of our numerical scheme will still be comparable to the naive $\mathcal{O}(N^2)$ complexity of N-body simulations.

The other advantage of working with harmonic wavefunctions to represent the initial conditions is that we have an intuitive picture of what happens if we remove some modes. In analogy with the Fourier series, the density will not be represented exactly at every point, but the approximation becomes closer and closer as we include more and more modes. Knowing some of the properties of the system we want to model may help to get a deeper insight into which modes are really needed.

In many simulations one does not necessarily need the same resolution on all scales. Instead one could work with an adaptive grid (Plewa, Linde, and Weirs 2005) and have higher resolution in the scales of interest. This would allow to reach better precisions while keeping the number of wavefunctions constant.

In the special case of simulations of cosmic structure formation, the concept of cosmic variance could help to further reduce the number of wavefunctions required. Indeed, given that we can only observe one universe, the statistical fluctuation in large angular patches is high, as not many statistically independent patches are available in our sky. This is a well-known fact when studying the CMB radiation. This means that the statistical error is anyway large on these scales, so we don't need to work with a very high

precision. The cosmic variance could provide a tool to estimate how many wavefunctions are really needed in a given range of scales.

Let us also recall that the freedom of choosing the weight function in the scalar product (4.12) of the eigenvalue problem may help to considerably reduce the number of wavefunctions. Even though this seems to be a promising route to take, we didn't investigate it any further in this work.

Last but not least, we need to emphasize that the number of wavefunctions is preserved by the quantum mechanical evolution. Only their shapes will change. This shows that it is the complexity of the initial conditions that dictates the number of wavefunctions required. In a setup where only a restricted number of harmonics are present in the initial density distribution, already relatively few wavefunctions would be sufficient to represent the system and its time evolution.

5. Local interaction framework

In Newtonian gravity, much like in classical electrodynamics, each body moves in the potential generated by all the other. As both forces are long-ranged, the total force acting on each of the N particles will be given by the sum of the contributions from *all* the other particles, no matter how far away. In gravitational N-body simulation this picture yields the naive $\mathcal{O}(N^2)$ estimate for the force calculation at each timestep. But it is well-known that this long-ranged interaction through the potential can be replaced by a purely local interaction with a gauge boson. In this approach, each particle only interacts locally with the gauge field.

We propose to reformulate the cosmological Vlasov-Poisson system we presented in section 2.1.1

$$\begin{aligned}&\frac{\partial f}{\partial \tau}+\frac{p}{am}\frac{\partial f}{\partial x}-am\frac{\partial U}{\partial x}\frac{\partial f}{\partial p}=0,\\&\nabla^2 U=4\pi G a^2\delta\rho,\end{aligned}$$

as a purely local problem, by introducing an auxiliary $U(1)$ gauge field. To achieve local gauge invariance, we shall trade the real-valued phase space distribution function $f(x,p)$ for a finite set of complex-valued wavefunctions $\{\psi_n(x)\}_n$. For this we shall assume that the classical distribution function can be approximated by the Wigner distribution function of some auxiliary mixed state

$$f(x,p)\simeq P_W(x,p)=\int dy\; e^{\frac{i}{\hbar}py}\sum_n \lambda_n\psi_n^*(x+\frac{y}{2})\psi_n(x-\frac{y}{2}). \tag{5.1}$$

The details of how this approximation is to be understood, and how we construct in practice the set of wavefunctions $\{\psi_n\}_n$ for any given $f(x,p)$ have been discussed in the chapter 4. For the time being, let us assume that we have determined a set of wavefunctions such that the above approximation holds.

The dynamical evolution of the WDF is given by the quantum-corrected Vlasov equation (3.26), or equivalently, by the Schrödinger equations (3.28) of the wavefunctions interacting in a self-consistent way with a potential obeying the Poisson equation. The cosmological Vlasov equation is very similar to the classical one, up to the replacements

$$m\mapsto a(\tau)m,\quad V\mapsto a(\tau)mU. \tag{5.2}$$

Therefore the Schrödinger-Poisson system in the expanding universe becomes

$$i\hbar\partial_\tau\psi_n(\tau,\vec{x}) = -\frac{\hbar^2}{2ma(\tau)}\nabla_x^2\psi_n(\tau,\vec{x}) + ma(\tau)U(\tau,\vec{x})\psi_n(\tau,\vec{x}), \tag{5.3a}$$

$$\nabla_x^2 U(\tau,\vec{x}) = 4\pi G a^2(\tau)\delta\rho(\tau,\vec{x}), \tag{5.3b}$$

where ρ is the mass density [kg m^{-3}] related to the wavefunctions [kg$^{1/2}$m$^{-3/2}$] by

$$\rho = \frac{1}{a^3}\int\frac{d^3\vec{p}}{(2\pi)^3}f(\tau,\vec{x},\vec{p}) = \frac{1}{a^3}\sum_n \lambda_n|\psi_n|^2. \tag{5.4}$$

The normalization is chosen such that the phase space density integrates to the total mass

$$\int d^3\vec{x}\int\frac{d^3\vec{p}}{(2\pi)^3}f(\tau,\vec{x},\vec{p}) = \int d^3\vec{x}\sum_n \lambda_n|\psi_n|^2 = M_{\rm tot}, \tag{5.5}$$

implying for the background density

$$\bar{\rho} = \langle\rho\rangle = \frac{1}{V}\frac{1}{a^3}\int d^3\vec{x}\sum_n \lambda_n|\psi_n|^2 = \frac{1}{a^3}\frac{M_{\rm tot}}{V}, \tag{5.6}$$

where V denotes the total comoving volume. Therefore the density contrast $\delta\rho := \rho - \bar{\rho}$ reads

$$\delta\rho = \frac{1}{a^3}\left(\sum_n \lambda_n|\psi_n|^2 - \frac{M_{\rm tot}}{V}\right). \tag{5.7}$$

In the semi-classical limit, the Schrödinger-Poisson system (5.3) formally reduces to the original Vlasov-Poisson system describing gravitational structure formation.

5.1 Introducing gauge fields

The reformulation in terms of the complex-valued wavefunction has the advantage that it allows for the introduction of a gauge symmetry. In analogy with the gauge-invariant variables of electrodynamics (Vlasov et al. 1987), we can introduce new fields defined by[1]:

$$\Psi_n(\tau,\vec{x}) := e^{\frac{im}{\hbar c}\varkappa\alpha(\tau,\vec{x})}\psi_n(\tau,\vec{x}), \tag{5.8a}$$

$$\vec{A}(\tau,\vec{x}) := \frac{1}{c}\vec{\nabla}\alpha(\tau,\vec{x}), \tag{5.8b}$$

$$\alpha(\tau,\vec{x}) := \frac{c}{\varkappa}\int_{\tau_0}^{\tau}d\tau' a(\tau')U(\tau',\vec{x}). \tag{5.8c}$$

[1] Dimensions: $\alpha : \frac{\rm J\,m}{\rm kg}$ $\vec{A} : \frac{\rm J\,s}{\rm m\,kg}$ $U : \frac{\rm J}{\rm kg}$, $G : \frac{\rm J\,m}{\rm kg^2}$, $a, \varkappa$: dimensionless

In terms of the transformed fields, the Schrödinger and Poisson equations become

$$i\frac{\hbar}{m}\partial_\tau \Psi_n = \frac{1}{2a}\left(-i\frac{\hbar}{m}\vec{\nabla} - \varkappa\vec{A}\right)^2 \Psi_n\,,$$
$$\vec{\nabla}\cdot\partial_\tau\vec{A} = \frac{4\pi G}{\varkappa}\left(\sum_n \lambda_n|\Psi_n|^2 - \frac{M_{\rm tot}}{V}\right).$$

The mass m only appears together with $\hbar$ in the combination $\zeta := \frac{\hbar}{m}$. The dimensionless constant $\varkappa$ has no physical meaning as it can trivially be reabsorbed into $\vec{A}$. Henceforth we will adopt the canonical choice $\varkappa = 1$:

$$i\zeta\partial_\tau \Psi_n = \frac{1}{2a}\left(i\zeta\vec{\nabla} + \vec{A}\right)^2 \Psi_n\,, \tag{5.9a}$$
$$\vec{\nabla}\cdot\partial_\tau\vec{A} = 4\pi G\left(\sum_n \lambda_n|\Psi_n|^2 - \frac{M_{\rm tot}}{V}\right). \tag{5.9b}$$

5.2 Lagrangian formulation

So far the field $\vec{A}$ is non-dynamical and there are no propagating waves associated to it. It is an artifact of the field redefinition. In order to obtain a local formulation of the Poisson equation (5.9b), we want to render the gauge fields dynamical and add their propagating waves. We promote $\vec{A}$ to a dynamical gauge field by adding a temporal component A_0 and a kinetic term. For this purpose it is most transparent to work with a Lagrangian formulation using the standard toolbox of field theory.

Consider the non-relativistic, gauge-invariant theory of an Abelian gauge field interacting with a set of complex scalar fields ϕ_n described by the Lagrangian

$$\begin{aligned}\mathscr{L} = {}& \alpha\frac{1}{2}F_{0i}F_{0i} - \beta\frac{1}{4}F_{ij}F_{ij} \\ & + 4\pi G\sum_n \lambda_n\left[\frac{1}{2}\left(\phi_n^* D_0\phi_n + D_0\phi_n^*\phi_n\right) - \frac{1}{2a}\vec{D}\phi_n^*\cdot\vec{D}\phi_n\right] + 4\pi G\bar{\rho}A_0,\end{aligned} \tag{5.10}$$

where α, β are dimensionless parameters introduced for later convenience. $D_0\phi := (i\zeta\partial_\tau - A_0)\phi$ and $\vec{D}\phi := (i\zeta\vec{\nabla} + \vec{A})\phi$ denote the covariant derivatives. For $\alpha = \beta = 1$ the first two terms of the Lagrangian reduce to the usual Maxwell Lagrangian $\mathscr{L}_{\rm Maxwell} = -\frac{1}{4}F_{\mu\nu}^2$ describing the theory of a free $U(1)$ gauge field.

The last term $4\pi G\bar{\rho}A_0$ was added to ensure that Poisson's equation is sourced by the density contrast $\delta\rho$ instead of the full mass density. This additional term preserves the gauge-invariance of the action, as the comoving background density $\bar{\rho} = \frac{M_{\rm tot}}{V}$ is time-independent and it does not affect the other equations of motion.

The equations of motion obtained from the Lagrangian (5.10) read:

$$(i\zeta\partial_\tau - A_0)\phi_n = \frac{1}{2a}(i\zeta\vec{\nabla} + \vec{A})^2\phi_n\,, \tag{5.11a}$$

$$\alpha\partial_i F_{0i} = 4\pi G\left(\sum_n \lambda_n|\phi_n|^2 - \frac{M_{\text{tot}}}{V}\right), \tag{5.11b}$$

$$-\alpha\partial_0 F_{0i} + \beta\partial_j F_{ji} = 4\pi G\frac{-1}{2ac}\sum_n \lambda_n\left(\phi_n^*\vec{D}^i\phi_n + \vec{D}^i\phi_n^*\phi_n\right), \tag{5.11c}$$

and are invariant under the gauge transformations:

$$\phi_n \mapsto e^{\frac{i\vartheta}{\zeta c}}\phi_n, \quad A_0 \mapsto A_0 - \frac{1}{c}\partial_\tau\vartheta, \quad \vec{A} \mapsto \vec{A} + \frac{1}{c}\vec{\nabla}\vartheta. \tag{5.12}$$

We can make use of the gauge freedom to fix the gauge and work in the temporal gauge $A_0 = 0$:

$$i\zeta\partial_\tau\phi_n = \frac{1}{2a}(i\zeta\vec{\nabla} + \vec{A})^2\phi_n\,, \tag{5.13a}$$

$$-\alpha\,\vec{\nabla}\cdot\partial_\tau\vec{A} = 4\pi G\left(\sum_n \lambda_n|\phi_n|^2 - \frac{M_{\text{tot}}}{V}\right), \tag{5.13b}$$

$$\alpha\ddot{\vec{A}} + \beta c^2\,\vec{\nabla}\times\left(\vec{\nabla}\times\vec{A}\right) = 4\pi G\frac{-1}{2a}\sum_n \lambda_n\left(\phi_n^*\vec{D}\phi_n + \vec{D}\phi_n^*\phi_n\right). \tag{5.13c}$$

The first two equations (5.13a) and (5.13b) correspond to what we had in (5.9) before promoting the gauge fields to dynamical fields. The third equation (5.13c) is new and encodes the dynamics and interaction of waves. We also see that the Poisson equation has the correct sign for the attractive gravitational force only if we take $\alpha = -1$, thus changing the sign in front of the first term in the Maxwell Lagrangian. We will discuss the implications of this change of sign in more detail in section 5.4.

It also has to be stressed that the speed of propagation of the waves, c, is a purely fiducial number, which is in general different from the physical speed of light $c_{\text{phys}} = 299\,792\,458$ m/s. We are free to choose this parameter in a way that is convenient for our simulations (see section 5.4), as long as we remain in the non-relativistic limit, meaning that the waves propagate much faster than the matter. An additional condition of validity of the method is that the effects due to the dynamical waves are small. In particular we don't want that a particle can lose its momentum by emitting radiation. In practice we can require that the total energy in the waves is small compared to the potential energy. This can also be controlled by the choice of the parameter c.

5.3 Dimensionless reformulation

A standard technique for numerical simulations is to rescale all quantities to obtain a dimensionless reformulation.

Introducing typical time- and lengthscales of the problem T, L, we can define dimensionless coordinates, fields and parameters:

$$\begin{aligned} \theta &:= \frac{\tau}{T}, \qquad y := \frac{x}{L}, \\ b_0 &:= \frac{T^2}{L^2} A_0, \qquad \vec{b} := \frac{T}{L}\vec{A}, \qquad \chi_n := \sqrt{\frac{L^3}{M_{\text{tot}}}}\Psi_n, \\ \lambda &:= \zeta \frac{T}{L^2}, \qquad \Lambda := 4\pi G T^2 \frac{M_{\text{tot}}}{L^3}, \qquad C := c\frac{T}{L}, \end{aligned} \tag{5.14}$$

with the normalization of the wavefunctions chosen as

$$\int\limits_{[0,L]^3} d^3x \sum_n \lambda_n |\Psi_n|^2 = M_{\text{tot}}, \qquad \int\limits_{[0,1]^3} d^3y \sum_n \lambda_n |\chi_n|^2 = 1. \tag{5.15}$$

In this dimensionless reformulation the Lagrangian (5.10) becomes (ignoring overall coefficients, since they don't affect the equations of motion)

$$\begin{aligned} \mathscr{L} \propto\ & \alpha \frac{1}{2}\left(\dot{\vec{b}} + \vec{\nabla} b_0\right)^2 - \beta \frac{1}{2} C^2 \left(\vec{\nabla} \times \vec{b}\right)^2 \\ & + \Lambda \sum_n \lambda_n \left[\frac{1}{2}\left(\chi_n^* D_0 \chi_n + D_0 \chi_n^* \chi_n\right) - \frac{1}{2a}\vec{D}\chi_n^* \cdot \vec{D}\chi_n\right] + \Lambda b^0, \end{aligned} \tag{5.16}$$

where $D_0\chi = (i\lambda\partial_\theta - b_0)\chi$ and $\vec{D}\chi = (i\lambda\vec{\nabla} + \vec{b})\chi$. The dots and gradients are understood with respect to the dimensionless coordinates θ and y. The gauge transformations for the dimensionless fields are:

$$\chi \mapsto e^{\frac{i\Theta}{\lambda}}\chi, \quad b_0 \mapsto b_0 - \dot{\Theta}, \quad \vec{b} \mapsto \vec{b} + \vec{\nabla}\Theta. \tag{5.17}$$

In the temporal gauge $b_0 = 0$, the Schrödinger-Maxwell equations read

$$i\lambda\dot{\chi_n} = \frac{1}{2a}\left(i\lambda\vec{\nabla} + \vec{b}\right)^2 \chi_n\,, \tag{5.18a}$$

$$-\alpha\vec{\nabla}\cdot\dot{\vec{b}} = \Lambda\left(\sum_n \lambda_n |\chi_n|^2 - 1\right), \tag{5.18b}$$

$$\alpha\ddot{\vec{b}} + \beta C^2 \vec{\nabla}\times\left(\vec{\nabla}\times\vec{b}\right) = \Lambda\frac{-1}{2a}\sum_n \lambda_n\left[\chi_n^*\vec{D}\chi_n + \vec{D}\chi_n^*\chi_n\right]. \tag{5.18c}$$

To summarize we have shown how the cosmological Vlasov-Poisson system was transformed into the Schrödinger-Maxwell system (5.18). In the chapter 6 we will explain how the dynamical evolution of the above system of equations is done using the tools of lattice gauge theories.

5.4 Tachyonic instability

We try to model the purely attractive gravitational force by means of an Abelian vector field A_μ. This is of course not meant to be a fundamental description of gravity, which is described by a helicity 2 field. Instead we seek the simplest model yielding the correct gravitational force in the context of our numerical simulations. In order to use a vector field as a mediator, we need to change the sign in the Poisson equation to make it correspond to a purely attractive force. As we will see, this comes at the price of having a negative coefficient in front of the kinetic energy. The system can thus lower its energy by increasing the amplitude of the gauge field. This growth is exponential and is what we call the *tachyonic instability*. In our simulations, we have to keep this tachyonic mode under control. The time for this exponentially growing mode to develop should be small compared to the typical timescale we are interested in. This requirement will impose some restrictions on the parameters of the Lagrangian, which we want to study in this section.

Consider a Lorentz-violating Lagrangian of the type

$$\mathscr{L} = \alpha\frac{1}{2}F_{0i}F_{0i} - \beta\frac{1}{4}F_{ij}F_{ij} - \frac{1}{c\epsilon_0}A_\mu J^\mu, \tag{5.19}$$

where α and β are real parameters. For $\alpha = \beta = 1$ we recover the usual Maxwell Lagrangian. The equations of motion are

$$\begin{cases} \alpha\partial_i F^{i0} = J^0\frac{1}{c\epsilon_0} = \frac{1}{\epsilon_0}\rho, \\ \alpha\partial_0 F^{0i} + \beta\partial_j F^{ji} = \frac{1}{c\epsilon_0}J^i, \end{cases} \tag{5.20}$$

The first equation shows that the sign of α fixes the sign in Poisson's law.

In order to study the stability of the solutions, let's first remove the unphysical degrees of freedom. We work in the temporal gauge $A^0 \equiv 0$. Let's also decompose the gauge field into its longitudinal and transverse parts: $\vec{A} \equiv \vec{A}_T - \vec{\nabla}f$, with $\vec{\nabla}\cdot\vec{A}_T = 0$. Then the equations of motion read

$$\begin{cases} \alpha\nabla^2\dot{f} = \frac{1}{\epsilon_0}\rho, \\ \alpha(\ddot{\vec{A}}_T - \vec{\nabla}\ddot{f}) - \beta c^2\nabla^2\vec{A}_T = \frac{1}{\epsilon_0}\vec{J}, \end{cases} \tag{5.21}$$

We can use the Poisson equation[2] to solve for the longitudinal component

$$\dot{f} = -\frac{1}{4\pi}\frac{1}{\alpha\epsilon_0}\int d^3y\frac{\rho(y)}{|x-y|}, \tag{5.22}$$

and then, using current conservation $\dot{\rho} = -\vec{\nabla}\cdot\vec{J}$, integrate it out in the second equation

$$\alpha\ddot{\vec{A}}_T - \beta c^2\nabla^2\vec{A}_T = \frac{1}{\epsilon_0}\vec{J} + \frac{1}{4\pi\epsilon_0}\vec{\nabla}_x\int d^3y\frac{\vec{\nabla}_y\cdot\vec{J}(y)}{|x-y|} =: \frac{1}{\epsilon_0}\vec{J}_T. \tag{5.23}$$

[2] Note that this argument goes through whether the source is ρ or $\delta\rho$, since $\dot{\rho} = \delta\dot{\rho}$.

Let's use the dimensionless form of this equation to study the stability. In the case of a linear differential equation, we would apply a Fourier transform to obtain the dispersion relation. Our equation is unfortunately non-linear in the fields. To study the stability of the gauge mode, we may assume that the scalar field is constant, and drop the gradient terms. We can then Fourier transform the spatial coordinates in the equation of motion:

$$\alpha\ddot{\vec{b}}_T(\theta,\vec{k}) + \beta C^2\vec{k}^2\vec{b}_T(\theta,\vec{k}) = -\Lambda\frac{1}{a(\theta)}\overline{\chi^*\chi}\,\vec{b}_T(\theta,\vec{k})\,, \tag{5.24}$$

where the notation $\overline{\chi^*\chi} := \sum_n \lambda_n\chi_n^*\chi_n$ emphasizes that the wavefunctions χ_n are assumed to be constant. Note that it is always the full density entering, not the density contrast as in Poisson's equation.

The source term is still proportional to the time-dependent scale factor. In order to be able to also Fourier transform with respect to the time coordinate, we assume that this time-dependence can be neglected. Hence

$$(-\omega^2\alpha + \beta C^2\vec{k}^2)\vec{b}_T = -\frac{\Lambda}{\bar{a}}\overline{\chi^*\chi}\,\vec{b}_T, \tag{5.25}$$

implying the dispersion relation

$$\omega^2 = \frac{\beta}{\alpha}C^2\vec{k}^2 + \frac{1}{\alpha}\frac{\Lambda}{\bar{a}}\overline{\chi^*\chi}. \tag{5.26}$$

As long as the right-hand side is positive, ω is real, and the solution is oscillating in time. If, however, it becomes negative, ω becomes imaginary, and the solution contains an exponentially growing mode $\propto e^{|\omega|\theta}$. The system exhibits an instability. Hence the condition for the absence of instabilities:

$$\frac{\beta}{\alpha}C^2\vec{k}^2 + \frac{1}{\alpha}\frac{\Lambda}{\bar{a}}\overline{\chi^*\chi} \geq 0. \tag{5.27}$$

For the attractive Poisson equation, $\alpha = -1$, we get $-\beta C^2\vec{k}^2 \geq \frac{\Lambda}{\bar{a}}\overline{\chi^*\chi} \geq 0$. For this equation to have a solution for real $\vec{k}$ (no exponentially growing mode in space), we need to choose β negative.

Let's choose $\alpha = -1, \beta = -1$. The dispersion relation is then

$$\omega^2 = C^2\vec{k}^2 - \frac{\Lambda}{\bar{a}}\overline{\chi^*\chi}. \tag{5.28}$$

In the absence of matter we have $\omega^2 = C^2\vec{k}^2$. This shows that the propagation velocity of the waves in vacuum is C. For the non-relativistic limit we are interested in, this should be large compared to the typical velocities of the particles.

The stability condition for the gravitational case is:

$$C^2\vec{k}^2 \geq \frac{\Lambda}{\bar{a}}\overline{\chi^*\chi}. \tag{5.29}$$

For large enough values of $\vec{k}^2$ there are no instabilities. Choosing C large, we can decrease the minimal value of $\vec{k}^2$. Also note that, for zero sources, the condition reduces to $\vec{k}^2 \geq 0$. This translates the fact that it is only through the coupling to matter that the negative kinetic term for the gauge field can produce instabilities. In the absence of any sources, we can simply redefine the sign of the energy.

Let's use the stability condition to deduce a bound on C. The strongest bound on C comes from the smallest value of k, i.e. $k = 2\pi/L_{\text{box}}$ and the smallest scale factor. In our simulations the scale factor is normalized to 1 at the initial time and is then increasing. Therefore the strongest bound is

$$C^2 \geq \Lambda\overline{\chi^*\chi}\frac{L_{\text{box}}^2}{(2\pi)^2}\,. \tag{5.30}$$

Moreover, for our choice of adimensional units, $L_{\text{box}} = 1$. Let us write $C = \frac{1}{s}\frac{\Delta y}{\Delta\theta}$, meaning that the wave advances by 1 lattice spacing every s timesteps. Now the constraint becomes in terms of s

$$s \leq \frac{\Delta y}{\Delta\theta}\frac{2\pi}{\sqrt{\Lambda\overline{\overline{\chi^*\chi}}}}\,. \tag{5.31}$$

We can combine this condition for the absence of the tachyonic mode with the Courant condition for the numerical stability (see appendix B), which essentially requires that the waves should not propagate more than one lattice spacing each timestep:

$$1 \lesssim s \leq \frac{\Delta y}{\Delta\theta}\frac{2\pi}{\sqrt{\Lambda\overline{\overline{\chi^*\chi}}}}\,. \tag{5.32}$$

In our numerical simulations, we have to choose the speed of propagation of the fiducial gauge fields such that the above relation is satisfied. This ensures the absence of the tachyonic mode, and the stability of the numerical scheme.

To summarize we can say that our wish to model the gravitational interaction by an Abelian gauge field introduces an exponentially growing mode in our theory. Let us emphasize that the presence of this tachyon has nothing to do with how we decide to numerically solve the equations. Its existence was shown in the continuum theory. By an appropriate choice of parameters, the growth of the unstable mode can be avoided. In the upcoming section 7.3 we will perform some testbed numerical simulations to check if our estimates for the stability condition can be trusted and to show that the tachyonic mode can indeed be kept under control.

6. Lattice gauge theory formulation

We have mapped the cosmological Vlasov-Poisson system to the Schrödinger evolution of a set of wavefunctions interacting with a dynamical gauge field. Our next step is to describe how to solve these equations numerically. The standard procedure would be to discretize the equations on a lattice using finite-differences, and then solve these iteratively. Having added the auxiliary Abelian gauge field to model the long-range gravitational interaction, we propose to use a numerical scheme that is gauge-invariant. This will be done along the lines of lattice gauge theories.

Insisting on a manifestly gauge-invariant numerical scheme has several practical advantages. One possible consequence of breaking the gauge invariance can be that the numerical scheme becomes unstable and leads to diverging solutions (Grigoriev, Rubakov, and Shaposhnikov 1989). Additionally, in a gauge-invariant theory, Poisson's equation plays a special role, as it only corresponds to a constraint on the initial data. Put in a nutshell this means that we have one less equation to solve in the simulation (refer to section 6.4 for more details).

In preparation for the numerical simulation of the Maxwell-Schrödinger system on a lattice, we first explain the Wilson approach (Wilson 1974) to lattice gauge theories and apply it to the special case of an Abelian gauge field interacting with a non-relativistic scalar field. Textbooks on lattice field theory (Montvay and Münster 1994; Rothe 2005; Smit 2002) present the construction of the gauge-invariant action using the Wilson lines. Following the same approach, we derive the action for the Maxwell-Schrödinger theory on a lattice. By varying the action, we deduce the classical equations of motion. They are gauge invariant and yield the usual Maxwell-Schrödinger equations in the continuum limit. Finally, we show how the equations of motion can give an explicit scheme to numerically compute the time evolution of the fields from their initial configuration. We explain the special role played by Gauss' constraint, and describe how we construct initial conditions that satisfy it.

Notations

In this part, no summation is understood for repeated lower indices, and will be written explicitly when present. The lattice spacing is denoted by a_μ: $\Delta t = \frac{1}{c} a_0$ is the time spacing and $a_i = \Delta x$ is the spatial grid size (assumed

to be the same for all three directions). $\sum_x$ denotes the sum over all lattice points. The lattice neighbour of the point x in the direction $\hat{\mu}$ is denoted by $x + a\hat{\mu}$. Forward finite differences are denoted by Δ

$$\Delta_\mu f(x) := \frac{1}{a_\mu} \left(f(x + a\hat{\mu}) - f(x) \right), \tag{6.1}$$

and overlined operators correspond to backward finite differences

$$\overline{\Delta}_\mu f(x) := \frac{1}{a_\mu} \left(f(x) - f(x - a\hat{\mu}) \right). \tag{6.2}$$

When a field appears without an explicit argument, it is understood to be taken at x (resp y for the adimensional coordinates):

$$U_i \phi(x + a\hat{i}) + D_i \phi \equiv U_i(x) \phi(x + a\hat{i}) + D_i \phi(x). \tag{6.3}$$

6.1 Wilson's lattice gauge theory formulation

In order to do numerical simulations, we need to discretize the field theory on a lattice. According to the standard discretization procedure one would replace all derivatives by finite differences. The details of the discretization are not unique, but all ambiguities should disappear in the continuum limit where the lattice spacing is sent to zero. The problem with the standard discretization is however that it breaks gauge invariance. We will follow Wilson's approach to make the lattice theory gauge-invariant.

Let the action of an element of the gauge group $G \in U(1)$ on the scalar field ϕ be

$$\phi(x) \mapsto G(x)\phi(x), \quad \phi^*(x) \mapsto \phi^*(x) G^\dagger(x). \tag{6.4}$$

Introduce the *parallel transporter*, or *Wilson line*

$$U_\mu(x) := e^{\frac{ie}{\hbar c} a_\mu A_\mu(x)}, \tag{6.5}$$

transforming as

$$U_\mu(x) \mapsto G(x) U_\mu(x) G^\dagger(x + a\hat{\mu}). \tag{6.6}$$

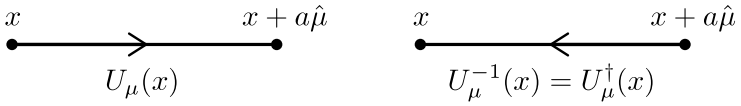

Fig. 6.1.1: Wilson line, or link variable, between two lattice sites.

As opposed to the matter field $\phi(x)$, which takes values on each lattice site, the Wilson line $U_\mu(x)$ links two neighbouring lattice points (see figure 6.1.1) and is therefore often referred to as *link variable*.

In order to make the action manifestly gauge-invariant, one has to insert Wilson lines between any two field operators taken at different lattice points, e.g. $\phi^*(x)U_\mu(x)\phi(x+a\hat{\mu})$. Alternatively, the substitution to be made can be written for the discretized derivative

$$\frac{1}{a_\mu}\left(\phi(x+a\hat{\mu})-\phi(x)\right) \longrightarrow \frac{1}{a_\mu}\left(\phi(x+a\hat{\mu})-U_\mu^\dagger(x)\phi(x)\right). \tag{6.7}$$

This is the lattice equivalent of the covariant derivative as can be seen from its gauge transformation law:

$$\frac{1}{a_\mu}\left(\phi(x+a\hat{\mu})-U_\mu^\dagger(x)\phi(x)\right) \mapsto G(x+a\hat{\mu})\frac{1}{a_\mu}\left(\phi(x+a\hat{\mu})-U_\mu^\dagger(x)\phi(x)\right).$$

To complete the construction of the lattice action, we need to find a gauge-invariant term corresponding to the kinetic term $F_{\mu\nu}^2$ in the continuum limit. First, we can obtain a gauge-invariant object of link variables by building a loop or *plaquette*

$$P_{\mu\nu}(x) := U_\mu(x)U_\nu(x+a\hat{\mu})U_\mu^\dagger(x+a\hat{\nu})U_\nu^\dagger(x). \tag{6.8}$$

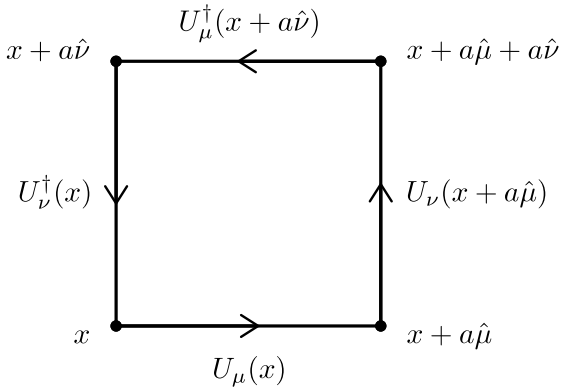

Fig. 6.1.2: Gauge-invariant plaquette of Wilson lines.

Its gauge transformation is

$$P_{\mu\nu}(x) \mapsto G(x)P_{\mu\nu}(x)G^\dagger(x). \tag{6.9}$$

In the Abelian case, the plaquette operator is itself gauge-invariant since the fields commute. In the non-Abelian case, its trace is a gauge-invariant quantity.

Using the expression of the Wilson line (6.5), the plaquette operator becomes

$$P_{\mu\nu}(x) = e^{\frac{ie}{\hbar c} a_\mu a_\nu F_{\mu\nu}(x)}, \tag{6.10}$$

where $F_{\mu\nu}$ denotes the discretized field strength tensor

$$F_{\mu\nu}(x) := \Delta_\mu A_\nu(x) - \Delta_\nu A_\mu(x). \tag{6.11}$$

Moreover, expanding in lattice spacing, we have

$$1 - \frac{1}{2}\left(P_{\mu\nu} + P_{\mu\nu}^\dagger\right) \simeq \frac{1}{2}\frac{e^2}{\hbar^2 c^2} a_\mu^2 a_\nu^2 F_{\mu\nu} F_{\mu\nu}. \tag{6.12}$$

This allows us to write a lattice action for the free gauge field

$$\begin{aligned} S_{\text{Maxwell}} = \frac{\hbar^2 c^2}{2e^2} a_0 a_i^3 \sum_x \Bigg[& 2\alpha \frac{1}{a_0^2 a_i^2} \sum_i \left(1 - \frac{1}{2}\left(P_{0i} + P_{0i}^\dagger\right)\right) \\ & - \beta \frac{1}{a_i^4} \sum_{i,j} \left(1 - \frac{1}{2}\left(P_{ij} + P_{ij}^\dagger\right)\right) \Bigg], \end{aligned} \tag{6.13}$$

where the dimensionless parameters α, β have been introduced for later convenience. For $\alpha = \beta = 1$ this reduces, in the continuum limit $a \to 0$, to the usual Maxwell action. Using the identity $\cos x = \frac{1}{2}\left(e^{ix} + e^{-ix}\right)$ the action equals

$$\begin{aligned} S_{\text{Maxwell}} = \frac{\hbar^2 c^2}{2e^2} a_0 a_i^3 \sum_x \Bigg[& 2\alpha \frac{1}{a_0^2 a_i^2} \sum_i \left(1 - \cos\left(\frac{e}{\hbar c} a_0 a_i F_{0i}\right)\right) \\ & - \beta \frac{1}{a_i^4} \sum_{i,j} \left(1 - \cos\left(\frac{e}{\hbar c} a_i^2 F_{ij}\right)\right) \Bigg]. \end{aligned} \tag{6.14}$$

This has to be supplemented with a gauge-invariant action for the matter. Inspired by (6.7), let us define the covariant derivatives on the lattice by

$$D_0\phi(x) := \frac{i\hbar}{e}\frac{1}{\Delta t}\left(\phi(x + a\hat{t}) - U_0^\dagger(x)\phi(x)\right) \overset{a_\mu \to 0}{\longrightarrow} \left(\, i\frac{\hbar}{e}\partial_t - A_0 \,\right)\phi(x), \tag{6.15a}$$

$$D_i\phi(x) := \frac{i\hbar}{e}\frac{1}{a_i}\left(\phi(x + a\hat{i}) - U_i^\dagger(x)\phi(x)\right) \overset{a_\mu \to 0}{\longrightarrow} \left(\, i\frac{\hbar}{e}\vec{\nabla} + \vec{A} \,\right)\phi(x). \tag{6.15b}$$

This allows us to write a gauge-invariant action for the matter:

$$S_{\text{Matter}} = \frac{e}{\epsilon_0} a_0 a_i^3 \sum_x \left[\frac{1}{2}\left(\phi^* U_0 D_0\phi + D_0\phi^* U_0^\dagger \phi\right) - \frac{e}{2m}\sum_i D_i\phi^* D_i\phi\right], \tag{6.16}$$

where the parameter ϵ_0 can be identified with the permittivity of the vacuum.

Having derived the lattice equivalent of the action, we can deduce from it the discretized equations of motion. The variation of the total action $S_{\text{tot}} = S_{\text{Maxwell}} + S_{\text{Matter}}$ yields

$$\frac{i\hbar}{2\Delta t}\left[U_0\phi(x+a\hat{t}) - U_0^\dagger(x-a\hat{t})\phi(x-a\hat{t})\right] = -\frac{ie\hbar}{2m}\frac{1}{a_i}\sum_i\left[D_i\phi(x-a\hat{i}) - U_iD_i\phi\right],$$

$$\alpha\,\frac{\hbar c}{e}\,a_i^2\,\sum_i\overline{\Delta}_i\sin\left(\frac{e}{\hbar c}a_0a_iF_{0i}\right) = a_0a_i^3\frac{1}{\epsilon_0}\frac{e}{2}\left(\phi^*U_0\phi(x+a\hat{t}) + \phi^*(x+a\hat{t})U_0^\dagger\phi\right),$$

$$-\alpha\,\frac{\hbar c}{e}a_i^2\,\overline{\Delta}_0\sin\left(\frac{e}{\hbar c}a_0a_iF_{0i}\right) + \beta\frac{\hbar c}{e}a_0a_i\sum_j\overline{\Delta}_j\sin\left(\frac{e}{\hbar c}a_i^2F_{ji}\right)$$
$$= a_0a_i^3\frac{1}{\epsilon_0}\frac{e^2}{2mc}\left[U_i\phi^*D_i\phi + D_i\phi^*U_i^\dagger\phi\right].$$

For more details how the equations of motion are obtained, the interested reader is referred to the appendix C, where the derivation is given for the Schrödinger equation.

In contrast with the usual continuum Maxwell equations, the lattice equations of motion are non-linear. This illustrates how non-trivial it would have been to deduce gauge-invariant equations of motion by discretizing their continuum versions. It can be checked that all equations of motion are indeed gauge-invariant/covariant, as expected from the gauge symmetry of the action. Moreover, in the continuum limit $a \to 0$, they reduce to

$$i\hbar\partial_t\phi - eA_0\phi = \frac{1}{2m}\sum_i\left(-i\hbar\partial_i + \frac{e}{c}A_i\right)^2\phi,$$

$$\alpha\,\vec{\nabla}\cdot\vec{E} = \frac{1}{\epsilon_0}e|\phi|^2,$$

$$-\alpha\partial_0F_{0i} + \beta\sum_j\partial_jF_{ji} = \frac{1}{c\epsilon_0}\frac{-ie}{2m}\left[\phi^*\left(\hbar\partial_i + \frac{ie}{c}A_i\right)\phi - \left(\hbar\partial_i - \frac{ie}{c}A_i\right)\phi^*\phi\right],$$

which (for $\alpha = \beta = 1$) correspond to the standard Maxwell-Schrödinger equations

$$i\hbar\partial_t\phi - eA_0\phi = \frac{1}{2m}(-i\hbar\vec{\nabla} - e\vec{A})^2\phi, \tag{6.17a}$$

$$\vec{\nabla}\cdot\vec{E} = \frac{1}{\epsilon_0}e|\phi|^2, \tag{6.17b}$$

$$-\frac{1}{c}\partial_t\vec{E} + c\vec{\nabla}\times\vec{B} = \frac{1}{c\epsilon_0}\frac{-ie}{2m}\left[\phi^*(\hbar\vec{\nabla} - ie\vec{A})\phi - (\hbar\vec{\nabla} + ie\vec{A})\phi^*\phi\right]. \tag{6.17c}$$

Summarizing we have derived a fully gauge-invariant description of the Maxwell-Schrödinger theory on a lattice, which reduces to the correct continuum limit as the lattice spacing is sent to zero.

6.2 Lattice theory for our dimensionless formulation

In section 5.3 we derived the adimensional form of the Schrödinger-Maxwell equations corresponding to the cosmological Vlasov-Poisson system. As already discussed we want to use the lattice gauge theory approach to integrate the equations numerically. Having seen how to write a manifestly gauge-invariant action on the lattice, we can now use this knowledge, to find the lattice theory describing our Schrödinger-Maxwell equations (5.18).

By complete analogy with the previous section, the gauge-invariant theory on the lattice can be described by the Lagrangian (summation over i, j):

$$\mathscr{L}_{\text{Maxwell}} = \frac{\alpha}{\Delta\theta^2\Delta y^2}\left[1-\cos\left(\Delta\theta\Delta y F_{0i}\right)\right] - \frac{\beta C^2}{2\Delta y^4}\left[1-\cos\left(\Delta y^2 F_{ij}\right)\right], \quad (6.18a)$$

$$\mathscr{L}_{\text{Matter}} = \Lambda\sum_n \lambda_n\left[\frac{1}{2}\left(\chi_n^* U_0 D_0\chi_n + D_0\chi_n^* U_0^\dagger\chi_n\right) - \frac{1}{2a}\vec{D}\chi_n^*\cdot\vec{D}\chi_n\right], \quad (6.18b)$$

$$\mathscr{L}_{\text{background}} = \Lambda\, b^0, \quad (6.18c)$$

where the link variables are now given by

$$U_0 = e^{i\frac{\Delta\theta}{\lambda}b^0}, \quad U_i = e^{-i\frac{\Delta y}{\lambda}b^i}, \quad (6.19)$$

whereas the interaction with the matter fields is described by the covariant derivatives

$$D_0\chi_n(y) = \frac{i\lambda}{\Delta\theta}\left(\chi_n(y+a\hat{\theta}) - U_0^\dagger(y)\chi_n(y)\right), \quad (6.20a)$$

$$D_i\chi_n(y) = \frac{i\lambda}{\Delta y}\left(\chi_n(y+a\hat{i}) - U_i^\dagger(y)\chi_n(y)\right). \quad (6.20b)$$

The adimensional gauge transformations on the lattice are given by:

$$U_\mu(x)\mapsto G(x)U_\mu(x)G^{-1}(x+a\hat{\mu}), \quad \chi_n(x)\mapsto G(x)\chi_n(x), \quad (6.21)$$

where $G(x) = e^{i\frac{1}{\lambda}\vartheta(x)}$. We also make use of the discretized field strength $F_{0i} = -\Delta_0 b^i - \Delta_i b^0$, $F_{ij} = -\Delta_i b^j + \Delta_j b^i$. Furthermore note that the term yielding the background density in Poisson's equation is written in a form, where it is only gauge-invariant in the continuum limit. Alternatively one could construct this term using an auxiliary, non-dynamical scalar field, for which we could write a fully gauge-invariant action on the lattice. Both approaches result in the same equations of motion that are perfectly gauge-invariant on the lattice.

Finally, the equations of motion on the lattice in the $b^0 = 0$ gauge, reducing to (5.18) in the continuum limit, are found to be:

$$\frac{1}{2}\frac{i\lambda}{\Delta\theta}\Big(\chi_n(y+a\hat{\theta}) - \chi_n(y-a\hat{\theta})\Big) = -\frac{1}{2a}\frac{i\lambda}{\Delta y}\sum_i \Big[D_i\chi_n(y-a\hat{i}) - U_i D_i\chi_n\Big], \quad (6.22a)$$

$$-\alpha\frac{1}{\Delta y\Delta\theta}\sum_i \bar{\Delta}_i \sin\left(\Delta\theta\Delta y\ \Delta_0 b^i\right) = \Lambda\left(\sum_n \lambda_n \mathrm{Re}\left[\chi_n^*(y)\chi_n(y+a\hat{\theta})\right] - 1\right), \quad (6.22b)$$

$$-\alpha\frac{1}{\Delta y\Delta\theta}\bar{\Delta}_0 \sin\left(\Delta\theta\Delta y\ \Delta_0 b^i\right) + \beta C^2\frac{1}{\Delta y^2}\sum_j \bar{\Delta}_j \sin\left(\Delta y^2 F_{ji}\right) = \Lambda\frac{1}{2a}\sum_n \lambda_n\left[U_i\chi_n^* D_i\chi_n + D_i\chi_n^* U_i^\dagger\chi_n\right]. \quad (6.22c)$$

6.3 Iterative solution of the equations of motion

We now show how one can rearrange the equations of motion (6.22) to give formulas for the fields at the next timestep $y + a\hat{\theta}$. This is an example of an *explicit* scheme, where the fields at $\theta + \Delta\theta$ (for each y) can be calculated explicitly from the quantities already known. Moreover, in this case, the algorithm describes a *two-level* scheme where two time steps have to be stored to compute the next one. In terms of memory, this is the most efficient way, as it corresponds to the minimal number of time slices required to solve a second order difference equation.

Suppose we know all the fields at two initial time slices $y - a\hat{\theta}$ and y. We can then use the equations of motion to deduce the fields at the next time step $y + a\hat{\theta}$. First, the current appearing in Maxwell equations (6.22c) can be rewritten as follows:

$$\begin{aligned} J_i &:= \Lambda\frac{1}{2a}\sum_n \lambda_n\left[U_i\chi_n^* D_i\chi_n + D_i\chi_n^* U_i^\dagger\chi_n\right] \\ &= \Lambda\frac{1}{2a}\frac{i\lambda}{\Delta y}\sum_n \lambda_n\left[U_i\chi_n^*\chi_n(y+a\hat{i}) - \chi_n^*(y+a\hat{i})U_i^\dagger\chi_n\right] \\ &= \Lambda\frac{1}{a}\frac{\lambda}{\Delta y}\sum_n \lambda_n\ \mathrm{Im}\left(\chi_n^*(y+a\hat{i})U_i^\dagger\chi_n\right). \end{aligned}$$

The iterative solution of the equations (6.22a) and (6.22c) finally reads:

$$\chi_n(y + a\hat{\theta}) = \chi_n(y - a\hat{\theta}) + i\frac{1}{a}\frac{\lambda\Delta\theta}{\Delta y^2}\sum_i \Big[\, U_i(y)\chi_n(y + a\hat{i}) - 2\chi_n(y) + U_i^\dagger(y - a\hat{i})\chi_n(y - a\hat{i}) \,\Big], \quad (6.23a)$$

$$b^i(y + a\hat{\theta}) = b^i(y) + \frac{\lambda}{\Delta y}\arcsin\Bigg[\sin\left(\frac{\Delta y}{\lambda}\left(b^i(y) - b^i(y - a\hat{\theta})\right)\right) + \frac{\beta}{\alpha}C^2\frac{\Delta\theta^2}{\Delta y^2}\sum_j\left(\sin\left(\frac{\Delta y^2}{\lambda}F_{ji}\right) - \sin\left(\frac{\Delta y^2}{\lambda}F_{ji}(y - a\hat{j})\right)\right) - \frac{1}{\alpha}\Lambda\,\Delta\theta^2\frac{1}{a}\sum_n \lambda_n\ \mathrm{Im}\left(\chi_n^*(y + a\hat{i})U_i^\dagger\chi_n\right)\Bigg]. \quad (6.23b)$$

These equations define the time evolution of the fields and form the core of our numerical simulations. Notice that we only used the equations of motion for the matter fields (6.22a) and the spatial components of the vector field (6.22c), not the one corresponding to the temporal component (6.22b), since that equation plays a special role, as shall be discussed in the next section.

When solving the Schrödinger equation numerically, it is important to use an integration scheme, that is unitary and preserves the normalization of the wavefunction. In our case, the unitarity is a direct consequence of gauge invariance, as the norm of the wavefunction can be identified with the Noether charge of the global $U(1)$ symmetry. Therefore the use of a gauge-invariant lattice formulation also ensures that the normalization of the wavefunction is conserved in time, as could be checked in our numerical simulations.

6.4 Gauss constraint

The equation of motion for the temporal component of the gauge field, also known as Poisson's equation or Gauss constraint, plays a special role, as it is not a dynamical equation but merely a constraint on the initial data (Dirac 1964; Weinberg 1995). Let us illustrate this, for the sake of simplicity, in the continuous case. Using the equations of motion, it's straightforward to show that the time-derivative of the Poisson equation is proportional to the divergence of the current:

$$\partial_0(\text{Poisson eq.}) \propto \partial_\mu J^\mu. \quad (6.24)$$

In a gauge-invariant theory, the current is conserved $\partial_\mu J^\mu = 0$, implying that the Gauss constraint is conserved in time. So, if the theory is gauge-invariant, and the initial configuration of the fields satisfies Gauss constraint,

then it remains fulfilled at all later times. It is in this sense that Poisson's equation can be seen as nothing but a constraint on the initial data. Therefore, since we used Wilson's approach to insist on the gauge invariance of the theory, we only have to solve the other equations of motion.

One can show the lattice equivalent of (6.24) using the full non-linear equations of motion (6.22). Indeed, making use of the Schrödinger and Maxwell equations on the lattice one can show that

$$\overline{\Delta}_0(\text{Poisson eq.}) = 0, \tag{6.25}$$

where the discretized Poisson equation (6.22b) is understood. This result is a direct consequence of the gauge-invariant equations of motion. No approximations have to be made: it holds for any lattice spacing, not only in the continuum limit.

To fulfill the Gauss constraint on the initial data we use a minimization procedure: given the initial matter distribution, find a gauge field configuration that minimizes the Gauss constraint. The minimization relies on the *gradient descent* method which is based on the observation that a function $f(x)$ decreases fastest if one goes from an initial point x_n in the direction of the negative gradient of f at x_n. This prescription provides an iterative method to search for the minimum of f:

$$x_{n+1} = x_n - \epsilon_n \nabla f(x_n), \tag{6.26}$$

where ϵ_n is a small stepsize that is allowed to change at every iteration. The iteration hopefully converges to a local minimum of f.

Let's now describe how this is applied to our case. Let $\mathcal{G} = 0$ denote the Gauss constraint (6.22b). We want to determine a gauge field configuration $\vec{b}(y)$ minimizing the Gauss constraint to zero with a given accuracy. Since the constraint has to be satisfied at every point y, we minimize the squared deviation summed over the whole lattice

$$f(b^i) := \sum_y \mathcal{G}^2(b^i(y)). \tag{6.27}$$

Along the lines of the gradient descent method, this can be done solving the equations

$$\partial_\xi b^i = -\frac{\partial f}{\partial b^i}, \tag{6.28}$$

where ξ denotes an unphysical minimization time. If we solve this differential equation numerically using a first-order finite-differences scheme (Euler method), we recover the usual gradient descent algorithm (6.26). To improve the convergence and accuracy of the minimization, we instead use a second-order Runge-Kutta method (Numerical Recipes 2007):

$$b^i\big|_{\xi+1} = b^i\big|_\xi + \epsilon\, F^i\left(b^i\big|_\xi + \frac{1}{2}\epsilon\, F^i(b^i\big|_\xi)\right), \tag{6.29}$$

where we introduced the notation $F^i := -\frac{\partial f}{\partial b^i}$. In practice the stepsize ϵ is chosen small enough to make the iteration converge.

This minimization procedure allows us to find an initial field configuration satisfying Gauss constraint. In principle, the gauge invariance ensures that the constraint remains satisfied for all later times. Unfortunately, the numerical errors due to the limited precision of the simulation can lead to a violation of gauge invariance and thus of Gauss constraint. For this reason one should monitor the evolution of the Gauss constraint during the numerical simulations. When doing very long runs, the violation of Gauss constraint can become too large. In such a situation one can implement a *cooling procedure* to make the system come back to a state satisfying the constraint with the desired accuracy (Grigoriev, Rubakov, and Shaposhnikov 1989). The implementation of the cooling can be done using a gradient descent method, like we did to generate the initial conditions.

6.5 Complexity and memory requirements

Having presented the algorithm of the time evolution, let us estimate its computational complexity and memory requirements.

Consider a three-dimensional spatial grid made of L_x^3 lattice points. Let N_ψ be the number of wavefunctions we evolve. Adding the 3 spatial components of the gauge field, $N_f = N_\psi + 3$ is the total number of fields we evolve in time. At each timestep, we need to compute each of the fields at every lattice point, making the algorithm of complexity

$$\mathcal{O}\left(L_x^3 \cdot N_f\right). \tag{6.30}$$

This has to be compared with N-body simulations, which have a naive complexity of $\mathcal{O}(N^2)$, that can be reduced to $\mathcal{O}(N \log N)$ using optimized algorithms. The more particles are tracked, the better becomes the spatial resolution. Roughly, for a total of N particles, $\Delta x_{\text{resol}} \sim L_{\text{box}}/N^{1/3}$. In our case, the spatial resolution is defined by the lattice spacing $\Delta x_{\text{resol}} \sim L_{\text{box}}/L_x$. Thus, for comparable spatial resolution, we would need $L_x \sim N^{1/3}$. From this we conclude that the complexity of our algorithm scales as $\mathcal{O}(N \cdot N_f)$. In the ideal situation where we only need a few wavefunctions, $N_f \sim \mathcal{O}(1)$, our approach provides an $\mathcal{O}(N)$ algorithm to study structure formation. It seems that in the worst case we would need as many wavefunctions as there are Fourier modes on the lattice, $N_f \sim \mathcal{O}(L_x^3)$, implying a complexity of $\mathcal{O}(N^2)$, which is the same as the naive force summation in N-body simulations.

These estimates illustrate that our algorithm can indeed compete with the complexity of N-body simulations. It also shows how crucial it is to reduce the number of wavefunctions as much as possible.

Let us next have a look at the memory requirements of our approach. Given that our time evolution relies on a two-level explicit scheme, we need to keep the field configurations at two timesteps in memory. For N_ψ complex wavefunctions and 3 real gauge field components on the whole lattice, we need $2 \cdot L_x^3 \, [2N_\psi + 3]$ variables. Assuming that each is stored as a `double` of 8 byte, we can estimate the minimal memory needed by our numerical simulation

$$\text{Memory} \gtrsim 2 \cdot L_x^3 \, [2N_\psi + 3] \cdot 8 \text{ byte}. \tag{6.31}$$

Let's look once more at the worst case scenario $N_\psi \sim \mathcal{O}(L_x^3) \sim \mathcal{O}(N)$. Hence

$$\text{Memory} \gtrsim 32N^2 \text{ byte}. \tag{6.32}$$

This has to be compared with N-body simulations, which have to store at least the position and velocity of each particle at every timestep

$$\text{Memory}_{\text{N-body}} \gtrsim 2 \cdot 6N \cdot 8 \text{ byte}. \tag{6.33}$$

As an example we may give the Millennium simulation (see section 2.2.2), which needed about 400 GB to store the information of their 2160^3 particles, in agreement with the above estimate.

We have to conclude that our approach can be strongly constrained by its memory requirements. The gain in computational complexity seems to have come at a considerable cost in memory. If we consider the 1 TB of memory available to the Millennium simulation, we could only have $\sim 56^3$ lattice points!

To avoid this intolerable limitation, the number of wavefunctions must be much less than the number of lattice points. In this case our memory requirements also scale proportionally to N as for N-body simulations. It is conceivable that some situations of physical interest only need a relatively small number of wavefunctions. We also have already mentioned some possibilities to reduce the number of wavefunctions in section 4.7. Another direction for a solution could be to consider an adaptive mesh to increase the spatial resolution for a constant number of lattice points.

7. Discussion and Examples

7.1 Comparison with previous approaches

Let us now briefly review previous works using the Schrödinger equation to model structure formation in the universe and compare them to our approach.

7.1.1 Coles et al.

Let us first mention the works of Peter Coles and collaborators (Coles 2002a; b; Coles and Spencer 2003; Short and Coles 2006a; b) who use the relation between the hydrodynamic equations and quantum mechanics. In particular, starting from the Euler and continuity equations of a self-gravitating fluid with a curl-free flow $\vec{v} = \vec{\nabla}\phi$, one can make the Ansatz $\psi = \alpha e^{\frac{i}{\nu}\phi}$ and rewrite the fluid equations as a non-linear Schrödinger equation

$$i\nu\partial_t\psi = -\frac{\nu^2}{2}\nabla^2\psi + V\psi + P\psi, \tag{7.1}$$

where the potential V satisfies Poisson's equation and $P = \frac{\nu^2}{2}\frac{\nabla^2|\psi|}{|\psi|}$ is the quantum pressure term. Using the semi-classical Ansatz $\psi(x) = \sqrt{\rho(x)}e^{\frac{i}{\hbar}\theta(x)}$, where $\vec{\nabla}\theta(x) = \vec{p}(x)$ is the local momentum flow, they study cosmological structure formation (in the fluid limit) by solving the above Schrödinger equation.

Being based on the hydrodynamic formulation, their method shares the same limitations. In particular they cannot work with a completely general phase space distribution function.

7.1.2 Widrow et al.

A different approach, which is closer to ours, was proposed by Lawrence Widrow and collaborators (Davies and Widrow 1997; Widrow and Kaiser 1993). They model the collisionless dark matter particles by a single wave-function satisfying the Schrödinger-Poisson equations. As a possible motivation for this, they consider the Schrödinger equation as the non-relativistic limit of the Klein-Gordon equation for some scalar field describing the dark matter.

The general procedure is very similar to ours: sample the wavefunction from the initial phase space distribution, evolve in time using the Schrödinger-Poisson equations, recover the final phase space distribution from the wavefunction:

$$f(x,p,t_{\rm ini}) \overset{\text{sampling}}{\longmapsto} \psi(x,t_{\rm ini}) \overset{\text{Schröd.-Poiss.}}{\longmapsto} \psi(x,t_{\rm fin}) \overset{\text{distr.}}{\longmapsto} f(x,p,t_{\rm fin}). \quad (7.2)$$

But there are also a number of differences which we shall describe. The first is that they use a single wave-function, whereas we use several to have a better accuracy in reproducing the initial phase space distribution. Also the details of how the initial wavefunction is obtained are very different. They start from the N-body sampled phase space distribution and build Gaussians centered on each of these points, with a certain width η

$$|\eta(x_j,p_j)\rangle \propto e^{-\frac{(x-x_j)^2}{2\eta^2}-\frac{i}{\hbar}\vec{p}_j\cdot\vec{x}}. \quad (7.3)$$

The wavefunction is then obtained from the incoherent superposition of these wavepackets for each "particle"

$$|\psi\rangle := \frac{1}{\sqrt{N}}\sum_{j=1}^{N} e^{i\phi_j}|\eta(x_j,p_j)\rangle, \quad (7.4)$$

where $e^{i\phi_j}$ is a random phase. In particular, this sampling procedure relies on the assumption that each "particle" has a well-defined momentum. It is unclear how it could be generalized to the case of warm dark matter, where the velocity dispersion is important. We remove the need for this assumption by allowing for several wavefunctions. At the same time this allows us to represent any initial phase space distribution without relying on N-body sampling.

Time evolution of the non-local Schrödinger-Poisson system is done using an explicit finite-differences scheme for the wavefunction and a FFT algorithm to solve the Poisson equation. We try to improve the algorithm for the time evolution by introducing the gauge fields to work with a purely local interaction.

Widrow et al. use the Husimi representation to recover the phase space information from the wavefunction. The Husimi distribution is essentially equal to the Wigner distribution with an additional Gaussian smoothing of width η

$$\mathscr{F}_H(x,p) := \frac{1}{(2\pi\hbar)^3}\frac{1}{(\pi\eta^2)^{3/2}}\left|\int d^3x'\, e^{-\frac{(x-x')^2}{2\eta^2}-\frac{i}{\hbar}px'}\psi(x')\right|^2. \quad (7.5)$$

Compared to the WDF it has the advantage of yielding a phase space distribution that is positive-definite at every point. This comes at the price of the

marginal distributions not being equal to the usual position and momentum distributions, but rather Gaussian broadened versions of it

$$\rho_H(x) = \int d^3p \, \mathscr{F}_H(x,p) = \frac{1}{(\pi\eta^2)^{3/2}} \int d^3x' \; e^{-\frac{(x-x')^2}{\eta^2}} |\psi(x')|^2. \qquad (7.6)$$

Only in the limit $\eta \to 0$ does it reduce to the usual probability distribution. Similarly one can show that the other marginal distribution reduces to the standard momentum distribution only when $\eta \to \infty$. This complementarity is of course related to Heisenberg's uncertainty principle.

Note that it is in principle this smoothed distribution (7.6) that enters Poisson equation instead of $|\psi(x)|^2$. Since this would requiring an additional space integration at each timestep, Widrow and Davies approximate it with the usual distribution $|\psi(x)|^2$ in the Poisson equation.

When computing the Husimi distribution of the sampled wavefunction (7.4) one gets a first term with a summation over equal "particles", and a second "interference" term, which they claim to be small:

$$\mathscr{F}_H = \frac{1}{N} \sum_{j=1}^{N} e^{-\frac{(x-x_j)^2}{2\eta^2}} e^{-\frac{2\eta^2}{\hbar^2}(p-p_j)^2} + \text{ interference terms.} \qquad (7.7)$$

The first term represents a Gaussian-smoothed version of the usual δ representation $\frac{1}{N}\sum_j \delta(x-x_j)\delta(p-p_j)$ for N particles. The presence of the interference term implies that $\mathscr{F}_H$ is in general not a good point-by-point approximation of the real phase space distribution. Actually $\langle \mathscr{F}_H \rangle \simeq f$ only when averaged on scales $\Delta x \gtrsim \eta$, $\Delta p \gtrsim \frac{\hbar}{\eta}$. Note that there is no a priori reason why the non-linear time evolution should yield an answer that is again, in average, close to the real distribution function. Let us recall that we allow for several wavefunctions to have an initial phase space representation that is arbitrary close the to the classical distribution function at every point, not only when averaged.

The authors have made several simulations using this Schrödinger method obtaining results in agreement with usual N-body simulations. They also claim that their method is computationally comparable to N-body simulations making it a promising tool for cosmological purposes.

7.2 Implementation

Let us give a brief description of how we put our method into practice to run numerical simulations. The time evolution of the Maxwell-Schrödinger system is dictated by the iterative solution (6.23). This numerical scheme requires two time-slices of initial data. The initial configuration of the wavefunctions is related to the initial phase space distribution (see chapter 4). For better usability and larger flexibility, we used the symbolic language of

MATHEMATICA to generate the initial conditions for the wavefunctions. The core of the numerical simulation was implemented in C++. Such a high-level programming language has the clear advantage of being very readable and easily extensible, while producing portable and usually relatively efficient programs. To make use of nowadays multicore processors, the central parts of the code were parallelized using `OpenMP`. All our simulations were run on a quadcore desktop computer.

Given the initial wavefunctions, we make use of the gradient descent algorithm (6.29) to obtain the initial gauge field configuration. Now that all the fields are known at the initial time slices, we use our explicit scheme (6.23) to compute the next timestep. Since the iterative solution contains the fields at neighbouring lattice sites, care has to be taken that the boundary conditions are implemented correctly. This is most easily done by augmenting the arrays containing the values of the fields on the lattice by so-called ghost points to store the periodic boundary conditions.

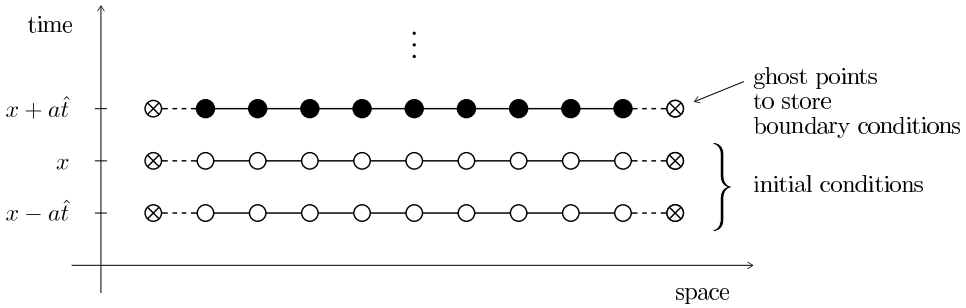

Fig. 7.2.1: Illustration of the arrays on the lattice, for simplicity taken to be one dimensional. Two time slices are given as initial conditions. An explicit scheme is used for the time evolution. We add ghost points to the array in order to store the boundary conditions.

At regular intervals, the configuration of the fields was written to a file for later analysis. The same was done with all simulation parameters and the quantities we monitored to check the accuracy of the simulation (like conservation of the total probability and total energy and the deviation from Gauss constraint). The data analysis was done using MATHEMATICA. Whenever the output files of the simulation were too large, they were preprocessed by PYTHON scripts before being analyzed.

7.3 Numerical tests of the tachyonic instability

Modelling the gravitational interaction by means of an Abelian gauge field comes at the price of introducing a tachyonic instability. Having estimated in section 5.4 under which conditions this instability is expected to occur, we now want to run some testbed simulations in which we can observe this exponentially growing mode and explicitly show that we can suppress it by the correct choice of parameters.

The instability occurs in Maxwell's equation independently of what happens in the matter sector. So let's consider the simplest case of a single background wavefunction χ that is constant in time and space. Let's furthermore consider a purely transverse gauge field $\vec{\nabla}\cdot\vec{b}_T = 0$ and a non-expanding universe $a(\theta) = 1$. In the continuum limit, the equation of motion for the gauge field reduces to

$$\alpha\,\ddot{\vec{b}}_T - \beta C^2\nabla^2\vec{b}_T + \Lambda|\chi|^2\vec{b}_T = 0. \tag{7.8}$$

7.3.1 Stable mode

For $\alpha = \beta = 1$ we recognize the standard Proca equation for a massive vector field of mass $m_b^2 = \Lambda|\chi|^2$. This system is free of instabilities for any choice of parameters. Let us have a closer look at the corresponding equations on the lattice. The current appearing in Maxwell equations (6.22c) can be rewritten as follows:

$$J_i = \Lambda\frac{1}{2}\left[\chi^* U_i D_i\chi + D_i\chi^* U_i^\dagger\chi\right] = \Lambda\frac{\lambda}{\Delta y}\,\mathrm{Im}\left(\chi^*(y+a\hat{i})U_i^\dagger\chi\right),$$

which, in the case of a constant matter distribution, becomes:

$$\begin{aligned}\Lambda\frac{\lambda}{\Delta y}\,\mathrm{Im}\left(\chi^*(y+a\hat{i})U_i^\dagger\chi\right) &= \Lambda\frac{\lambda}{\Delta y}|\chi|^2\,\mathrm{Im}U_i^\dagger \\ &= \Lambda\frac{\lambda}{\Delta y}|\chi|^2\sin\left(\frac{\Delta y}{\lambda}b^i\right).\end{aligned}$$

The full equation for the transverse component $b^x(y)$ then reads

$$\begin{aligned}\alpha\frac{1}{\Delta y\Delta\theta}\overline{\Delta}_0\sin\left(\Delta\theta\Delta y\;\Delta_0 b^x\right) - \beta C^2\frac{1}{\Delta y^2}\overline{\Delta}_y\sin\left(\Delta y^2\Delta_y b^x\right) \\ +\Lambda\frac{\lambda}{\Delta y}|\chi|^2\sin\left(\frac{\Delta y}{\lambda}b^x\right) = 0.\end{aligned} \tag{7.9}$$

In the continuum limit $\Delta\theta, \Delta y \to 0$ it indeed reduces to the Proca equation. For finite lattice spacing, however, the mass term is not directly proportional to the gauge field, but rather its sine. In order for this term to be in the linear regime, we need

$$\frac{\Delta y}{\lambda}b^x \ll 1. \tag{7.10}$$

In particular, this constraint depends on the parameter λ, which is arbitrary in the present case. If, for fixed lattice spacing Δy, λ is chosen too small, the above condition will not be satisfied, and the non-linearity of the mass term cannot be neglected. As a consequence, additional modes will be excited during the time evolution of the system. This effect can be seen nicely in figure 7.3.1a, which shows the gauge field b^x at different times. It compares the simulation data (blue dots) to the solution of the Proca equation with sine mass term (7.9) (full green line) and linear mass term (7.8) (dashed red line). Initially only one mode is present. The solution of the linear mass term Proca equation shows this single mode with oscillating amplitude. The solution of the sine mass term clearly shows that other modes get excited because of the non-linearity. The simulation data agrees nicely with this solution, but is very different from the solution of the linear Proca equation. The effect of the non-linearities becomes smaller if we reduce the lattice spacing. The figure 7.3.1b shows the result if we increase the number of lattice points from 30 to 90. The simulation data still agrees nicely with the non-linear Proca equation, and the difference with the linear equation is reduced considerably. For small enough lattice spacing, the two become indistinguishable, as expected from the continuum limit. For our later simulations, as usual when solving discretized equations, we need to pay attention to choose parameters to be close to the continuum limit.

7.3.2 Unstable mode

For $\alpha = \beta = -1$ the mass term of the gauge field becomes negative and the system contains a tachyonic instability for the modes with small enough wavenumber (5.29)

$$k^2_{\text{unstable}} \leq \frac{\Lambda|\chi|^2}{C^2}. \tag{7.11}$$

The amplitude of the unstable mode should increase exponentially with time. Figure 7.3.2 shows the time evolution of such an unstable mode in the simulation, and compares it to the solutions of the Proca equation with linear and sine mass term. Naively we would expect the amplitude to grow exponentially

$$A(\theta) = A_0 e^{\Omega\theta}, \quad \text{with } \Omega^2 = -C^2k^2 + \Lambda|\chi|^2. \tag{7.12}$$

The figure 7.3.3 shows the behaviour of the maximal amplitude of the gauge field as a function of time. As one can see, the slope of the solution of the linear Proca equation (dashed red line) agrees well with the expected exponential growth (dotted purple line). The solution of the non-linear Proca equation (full green line) however, reveals a saturation of the amplitude at late times. The value at which the amplitude saturates is roughly when the

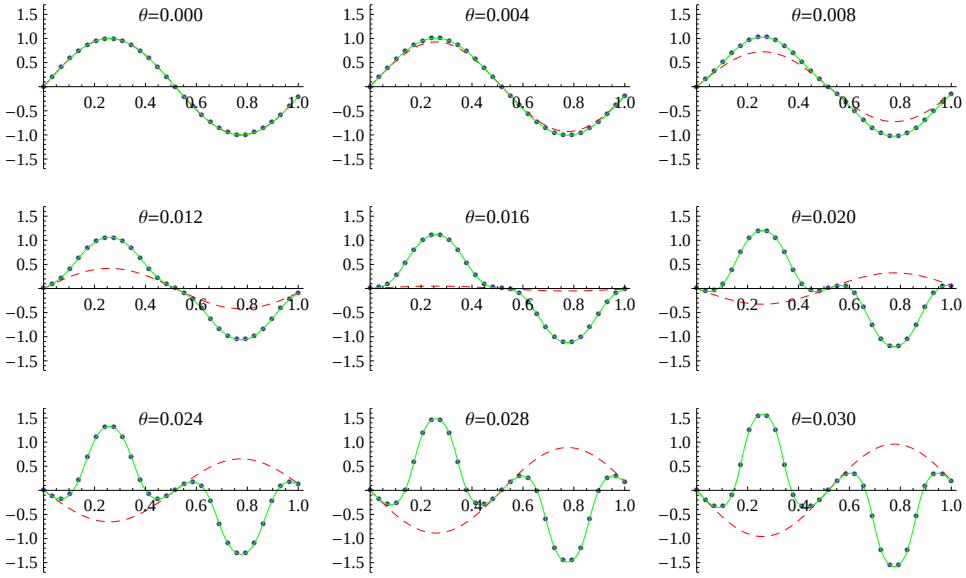

(a) 30 lattice points

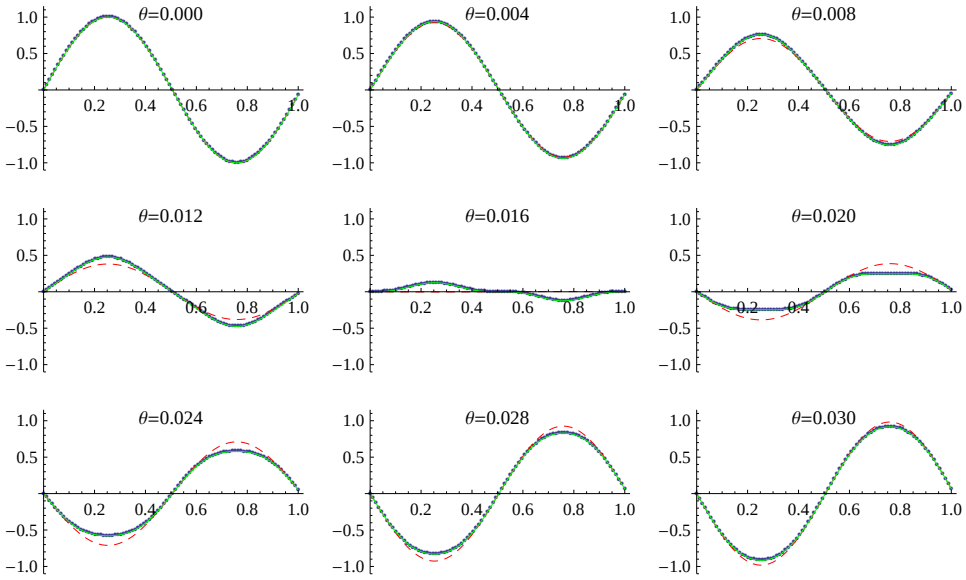

(b) 90 lattice points

Fig. 7.3.1: Gauge field $b^x(y)$ at different times. The plots correspond to the simulation data (blue dots) and the solutions of the Proca equation with sine mass term (full green line) and linear mass term (dashed red line). On the finer lattice the dots of the simulation data are almost indistinguishable from the green line.
[Parameters: $L_x = 30, 90, \lambda = 0.01, \Lambda = 10^4, C = 10\Delta y, |\chi|^2 = (\Delta y L_x)^{-3/2}$]

argument of the sine in the mass term is of order π. This shows that, if the non-linearity of the mass term cannot be neglected, it leads to a flattening effect in the growth of the amplitude. Interestingly, the non-linearity introduced because of the lattice formulation helps us in the sense that it suppresses the exponential growth of the instability.

7.3.3 Stable and unstable mode

As a next case study, we set up a numerical simulation with initial conditions containing two different modes with wavenumbers k_1, k_2 and amplitudes A_1, A_2 respectively

$$\vec{b}_T|_{\text{ini}} = [A_1 \sin(k_1 y) + A_2 \sin(k_2 y)]\, \vec{e}_x. \tag{7.13}$$

We can change the stability of the modes by tuning the parameters of the simulation. The most interesting situation is when one mode is stable and the second unstable. Let's consider the following setup:

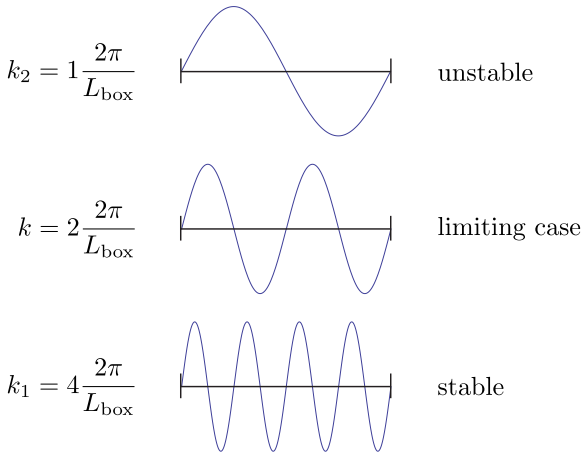

We choose the simulation parameters such that the intermediate mode $k = 2\frac{2\pi}{L_{\text{box}}}$ defines the limiting case of the stability condition:

$$2\frac{2\pi}{L_{\text{box}}} \equiv \frac{\Lambda|\chi|^2}{C^2}. \tag{7.14}$$

The propagation speed C is fixed by Courant's condition and the requirement that the timescale for the instability to develop

$$\tau_{\text{inst}} \sim \frac{1}{\sqrt{\Lambda|\chi|^2}} = \frac{4\pi}{L_{\text{box}} C^2} \tag{7.15}$$

is small compared to the time of the simulation. The figure 7.3.4 shows the outcome of such a simulation. The initial configuration contains the two

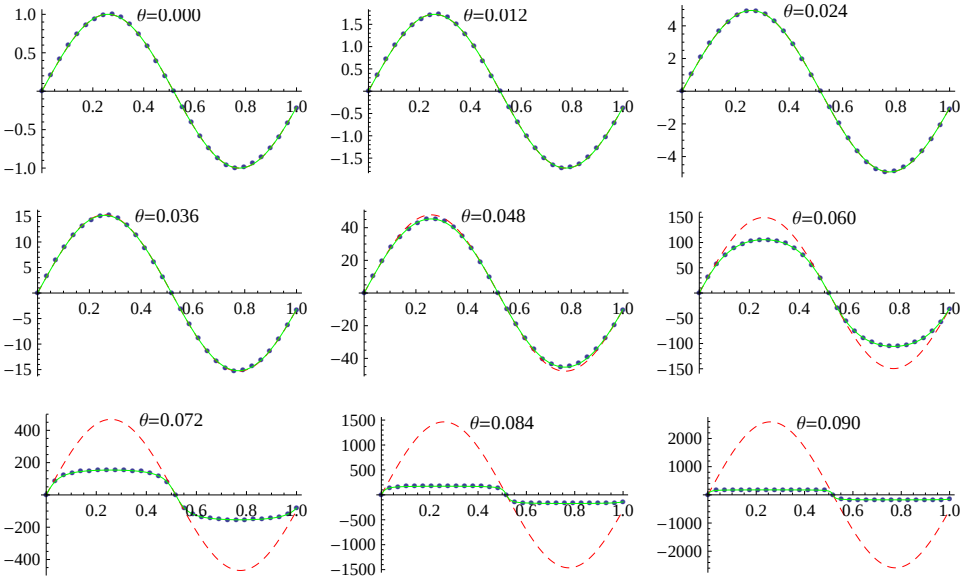

Fig. 7.3.2: Gauge field $b^x(y)$ at different times. The plots correspond to the simulation data (blue dots) and the solutions of the Proca equation with sine mass term (full green line) and linear mass term (dashed red line).
[Parameters: $L_x = 30, \lambda = 1, \Lambda = 10^4, C = 10\Delta y, |\chi|^2 = (\Delta y L_x)^{-3/2}$]

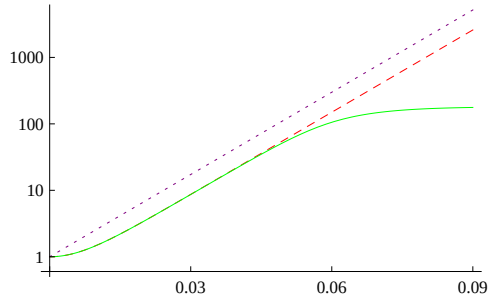

Fig. 7.3.3: Semi-Log plot of the maximal amplitude of the gauge field as a function of time. The dotted purple line shows the naive exponential behaviour, whereas the other correspond to the solutions of the Proca equation with linear (dashed red line) and sine (full green line) mass term.
[Parameters: $L_x = 30, \lambda = 1, \Lambda = 10^4, C = 10\Delta y, |\chi|^2 = (\Delta y L_x)^{-3/2}$]

modes with equal amplitudes $A_1 = A_2 = 0.01$. At later times, the instability develops only in the long wavelength mode, making its amplitude increase exponentially. Quickly, only that mode is visible, as the amplitude of the stable mode becomes negligible. One can see that the solution of the Proca equation fits nicely the data of the numerical simulation.

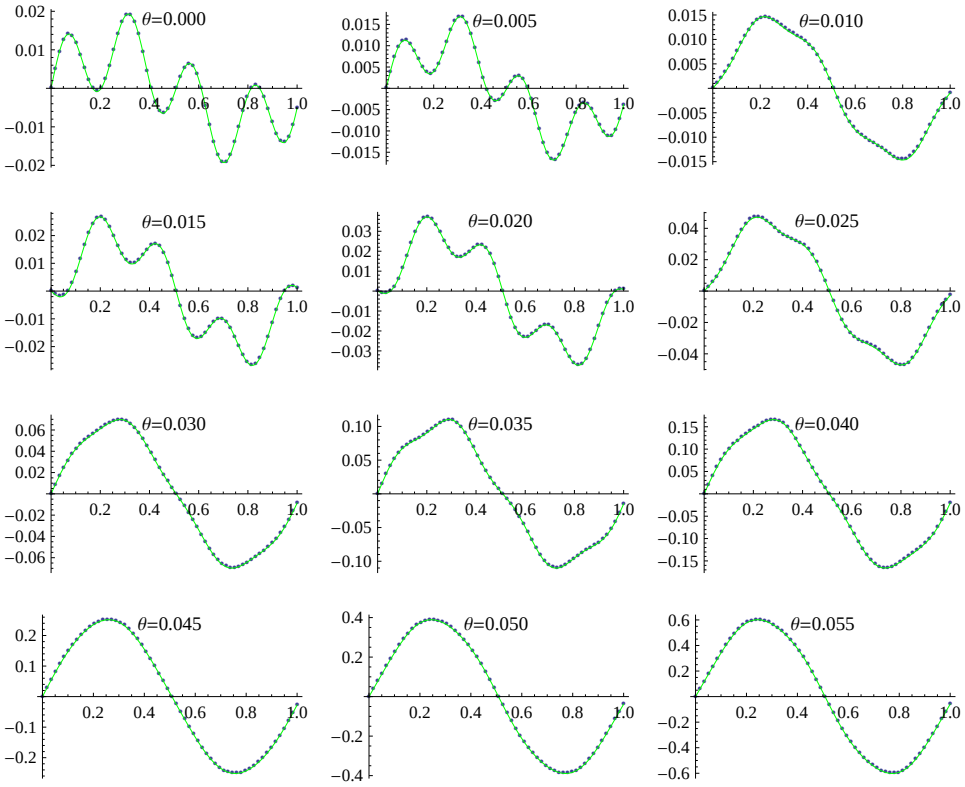

Fig. 7.3.4: Gauge field $b^x(y)$ at different times. The results from the simulation (blue dots) are almost indistinguishable from the solution of the Proca equation with linear mass term (green line).
[Parameters: $L_x = 60, \lambda = 1, \Lambda = 10517, C = 470\Delta y, |\chi|^2 = (\Delta y L_x)^{-3/2}$]

Conclusion

We can conclude that the exponentially growing mode is indeed present in the system, but that we know how to control it by choosing the parameters of our simulations. The examples show that the estimates we made for the instability in the continuous equations can also be trusted for the numerical simulations using the lattice gauge theory formalism. However, as usual when solving a system of equations via discretization, one has to be careful to be close to the continuum limit, in order to suppress undesired effects coming from the non-linearity of the lattice formulation.

7.4 Schrödinger-Newton system

As a next test of our approach, we consider the time evolution of the Schrödinger-Newton system

$$\begin{cases} i\lambda\partial_0\chi &= -\frac{\lambda^2}{2}\nabla^2\chi + U\chi\,, \\ \nabla^2 U &= \Lambda|\chi|^2, \end{cases} \tag{7.16}$$

with given initial conditions for the wavefunction. This system of equations has for instance been studied in the context of semi-classical gravity (Salzman 2005; Salzman and Carlip 2006, and references therein). The authors consider the spherically symmetric case and solve the radial equations numerically for a Gaussian initial state.

We use MATHEMATICA to solve the radial Schrödinger-Newton equations. Independently we run our full 3D code with dynamical gauge fields and spherically symmetric initial conditions. Finally we compare the solution of the radial equation to the result of our numerical simulation.

7.4.1 Numerical solution of the spherically symmetric case

We now consider the special case of the spherically symmetric Schrödinger-Newton system. Switching to spherical coordinates, and assuming that there is no angular dependence (i.e. zero angular momentum $\ell = 0$), the Laplacian reads $\nabla^2\chi = \frac{1}{r^2}\partial_r^2(r\chi)$. We also define $F := r\chi$ and $G := rU$, for which the Schrödinger-Newton (7.16) system becomes

$$\begin{cases} i\lambda\partial_0 F &= -\frac{\lambda^2}{2}\partial_r^2 F + \frac{1}{r}GF, \\ \partial_r^2 G &= \Lambda\frac{1}{r}|F|^2. \end{cases} \tag{7.17}$$

We choose initial conditions corresponding to a Gaussian wavefunction:

$$F_0(r) = r\chi_0(r) = r\left(2\pi\sigma_0^2\right)^{-3/4} e^{\frac{-r^2}{4\sigma_0^2}}. \tag{7.18}$$

The equations were split into real and imaginary parts and solved numerically using MATHEMATICA. We discretized the equations on a spatial grid for the radial component and replaced the corresponding derivatives by their finite-differences approximations. The time derivative was integrated using the built-in `NDSolve` routine. As a cross-check we solved the Schrödinger-Newton system with the same initial conditions as Peter Salzman. The results were found to be in good agreement with his plots.

7.4.2 Comparison with the 3D simulation

Independently we ran our full 3D numerical simulation with the dynamical gauge fields for the same parameters and Gaussian initial conditions.

The results are in good agreement with the solution of the radial equations obtained with MATHEMATICA.

The figure 7.4.1 shows how a slice of the density $|\chi|^2$ evolves with time: under the effect of gravity, the distribution collapses and becomes more peaked. The dots are the result of the 3D numerical simulation, and agree well with the full lines showing the solution of the radial equations.

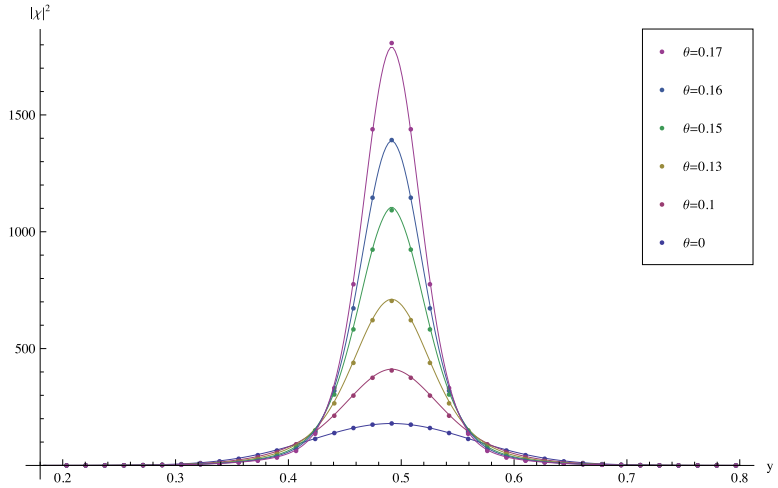

Fig. 7.4.1: Time evolution of the density $|\chi|^2$. Gravity makes the density collapse and become more peaked. The dots show the result of the full 3D numerical simulation. The lines were obtained from the MATHEMATICA code solving the spherically symmetric case. [Parameters: $L_x = 60, \lambda = 0.022866, \Lambda = 1, C = 30, \sigma_0 = 0.07071$]

In figure 7.4.2 we plot the maximum of the density as a function of time. Again, the results of the 3D simulation can be seen to match the spherically symmetric MATHEMATICA solution. The two curves start to deviate at late times, which can be related to the lattice resolution. At late times, the density is very peaked and only a few lattice points sample it in our simulation, which is not enough to resolve it with high precision.

Conclusion

To conclude we can say that our 3D numerical simulation with the gauge fields is able to reproduce the time evolution of the Schrödinger-Newton system. The results agree well with the solution of the spherically symmetric system obtained independently using MATHEMATICA.

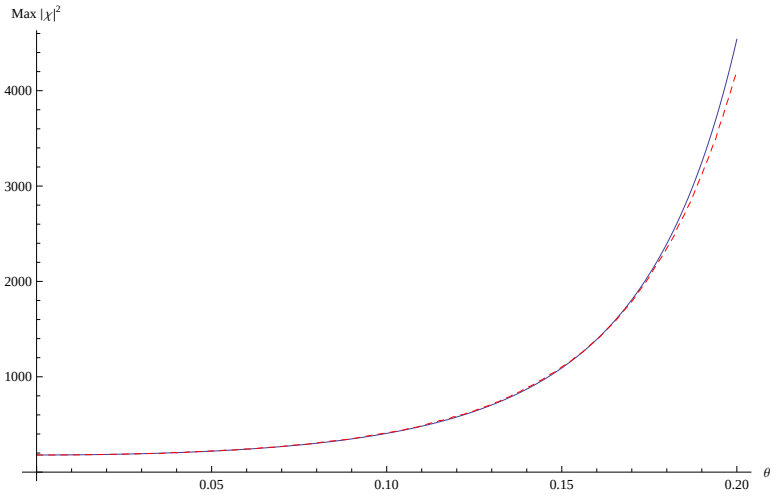

Fig. 7.4.2: Time evolution of the maximum of the density $|\chi|^2$. The blue line shows the result of the full 3D numerical simulation. The dashed red line was obtained from the MATHEMATICA code solving the spherically symmetric case.
[Parameters: $L_x = 60, \lambda = 0.022866, \Lambda = 1, C = 30, \sigma_0 = 0.07071$]

7.5 Growth of cosmic perturbations

We now apply our framework to a toy-example of cosmic perturbation growth. Let us consider the simplest possible case of a constant background $\bar{\rho}$ and a small perturbation ($\epsilon \ll 1$) with a single Fourier mode k_p taken along the x-direction

$$\rho(\vec{x}) = \bar{\rho} + \epsilon \left[\cos(k_p x) + \sin(k_p x)\right]. \tag{7.19}$$

Even such a simplified setup should be sufficient to study the qualitative features of the structure growth in both, a static and expanding universe.

Simulation setup

In chapter 4 we discussed the generation of the initial wavefunctions, in particular representing initial conditions for cosmological structure formation (section 4.5). The equations (4.24) define a possible representation of the density (7.19) in terms of wavefunctions. In this particular case we use three wavefunctions: one for the constant background, and two for the density perturbation.

The numerical simulation was performed on a 30^3 spatial grid corresponding to a physical box size of 60 Mpc (in comoving coordinates). To reduce unwanted effects of the limited size of the simulation, the scale of

the perturbation was chosen small compared to the box size and larger than the Nyquist mode defined by the lattice spacing. The background density is linked to the expansion of the universe through Friedmann's equation (2.1a)

$$H^2(\tau) = \frac{8\pi G}{3}\bar{\rho}_{\text{phys}}(\tau) = \frac{8\pi G}{3}\bar{\rho}_{\text{com}}\, a^{-3}(\tau), \tag{7.20}$$

where τ denotes the conformal time. In a purely matter dominated (Einstein-de Sitter) universe, the scale factor will grow as the square of the conformal time. Let us normalize it such that it is equal to one at the beginning of our simulation $a_{\text{ini}} \equiv 1$, implying

$$H^2_{\text{ini}} = \frac{8\pi G}{3}\bar{\rho}_{\text{com}} \equiv \frac{8\pi G}{3}|\Psi_0|^2, \tag{7.21}$$

where Ψ_0 denotes the constant wavefunction representing the background density. The above relation fixes the value of this wavefunction in terms of the initial Hubble parameter, which can be computed by rescaling today's value H_0 to the redshift corresponding to the beginning or our simulation

$$H_{\text{ini}} = H_0(1 + z_{\text{ini}})^{3/2}. \tag{7.22}$$

We ran our simulations for the choice $z_{\text{ini}} = 1000$ and using today's Hubble parameter $H_0 \simeq 70$ km s^{-1}Mpc^{-1}. The initial conditions with a density contrast of $\delta_{\text{ini}} \sim 10^{-6}$ where evolved up to a final redshift of $z_{\text{fin}} \sim 200$ using $3 \cdot 10^4$ timesteps. The same initial perturbations were evolved in a matter-dominated, expanding universe and in a static universe without expansion.

The free parameters of our simulation were determined as follows. The fiduciary propagation speed of the waves C was chosen to be compatible with the absence of the tachyonic instability and the numerical stability of our numerical scheme (as explained in section 5.4). The adimensional parameter λ related to $\hbar$ was chosen small enough for the quantum corrections to be negligible. More specifically, this means that the first quantum correction in the Wigner equation (3.26) has to be small compared to the contribution to the classical Vlasov equation:

$$\partial_x V \partial_p P_W > \frac{1}{24}\hbar^2 \partial_x^3 V \partial_p^3 P_W. \tag{7.23}$$

We checked that this condition was indeed satisfied in our simulation. Another condition of validity of our approach is to be close enough to the continuum limit, to suppress the non-linearities of the discretized equations (as illustrated in section 7.3). A sufficient condition for this to be the case, is that the exponent in the link variables

$$U_i = e^{-i\frac{\Delta y}{\lambda}b^i} \tag{7.24}$$

remains small[1]. The inverse dependence of the exponent on λ shows that we have to pay attention when reducing the value of λ not to spoil the continuum limit. In figure 7.5.1 we plot the maximal exponent in the link variable U_x to illustrate that it is indeed much smaller than 1. We can therefore neglect the non-linearities in the equations of motion because of the discretization.

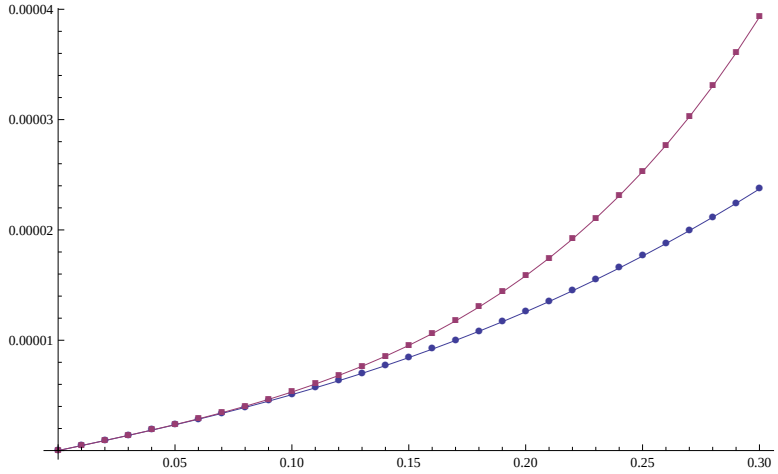

Fig. 7.5.1: Maximum of $\frac{\Delta y}{\lambda} b^x$ over all space as a function of the adimensional simulation time θ. The blue dots show the result in presence of expansion, whereas the purple squares correspond to a static universe.

Results

Figure 7.5.2 shows the time evolution of the density. The initial amplitude of the harmonic density increases with time, without distortion of the shape, as expected from the linear regime of structure formation.

To analyze the growth of the perturbation, we performed a Fourier transform on the density contrast to obtain $|\delta_k|^2$. In this way we could also check that no other Fourier modes than the initially present were excited during the simulation. This is a cross-check for the linearity of the evolution of the small density perturbation. The figure 7.5.3 compares the growth $|\delta_k(\theta)|^2/|\delta_k(\theta_{\text{ini}})|^2$ for our mode in the expanding and non-expanding universes. Clearly, the growth of the perturbation is suppressed in presence of expansion.

[1] Notice that this is actually not a *necessary* condition, as we could perform a gauge transformation (provided it exists) to make the exponent smaller.

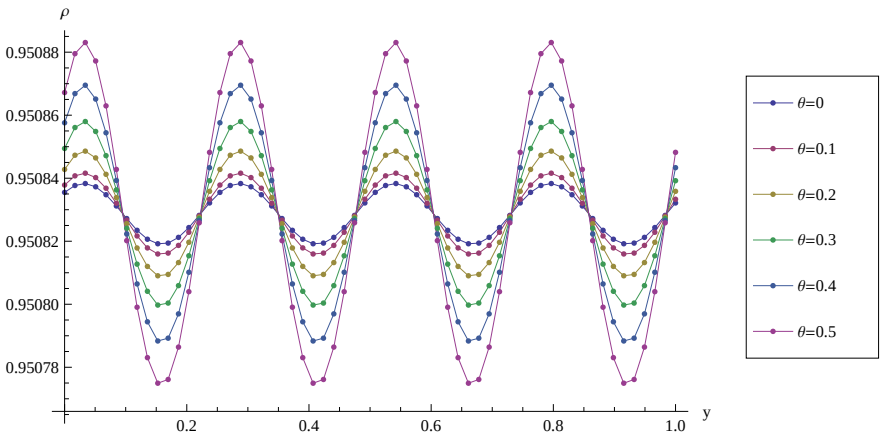

Fig. 7.5.2: Time evolution of the density field in an expanding universe. The initial amplitude of the harmonic density increases with time, without distortion of the shape, as expected from structure formation in the linear regime.
[Parameters: $L_x = 60, \lambda = 0.005, \Lambda = 114, C = 10, k_p = 2\pi\, 4/L$]

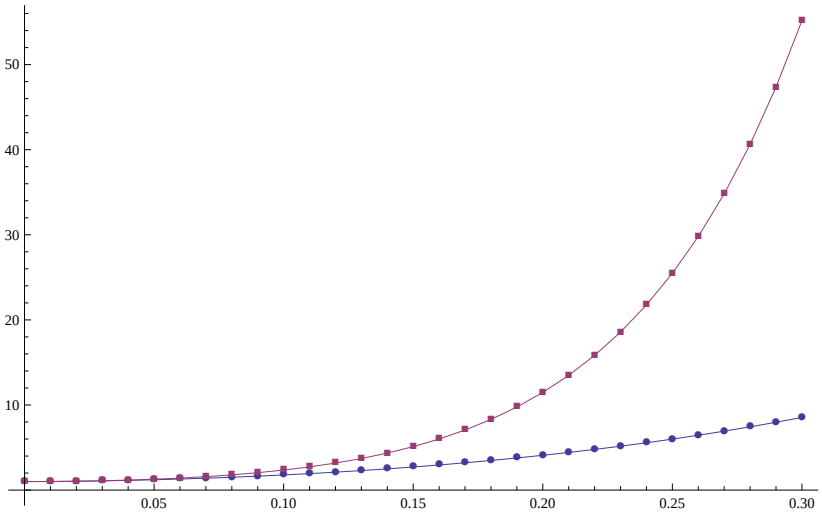

Fig. 7.5.3: Comparison of the growth of the perturbation $|\delta_k(\theta)|^2/|\delta_k(\theta_{\rm ini})|^2$ in a non-expanding universe (purple squares, upper line) and in a matter-dominated, expanding universe (blue dots, lower line) as a function of the conformal simulation time θ. The growth is clearly suppressed in the presence of expansion.
[Parameters: $L_x = 30, \lambda = 0.005, \Lambda = 114, C = 10, k_p = 2\pi\, 4/L$]

We also fitted the growth in the non-expanding universe with the expected superposition of an exponentially growing and decaying mode (see fig 7.5.4a). The presence of the decaying mode can be seen at early times, where it is essential to fit the growth. In the expanding Einstein-de Sitter universe, the density contrast is expected to be the superposition of a growing mode proportional to the scale factor a and a decaying mode proportional to $a^{-3/2}$ (see equation (2.20)). The results of our numerical simulations can be fitted with this expected behavior (see figure 7.5.4b).

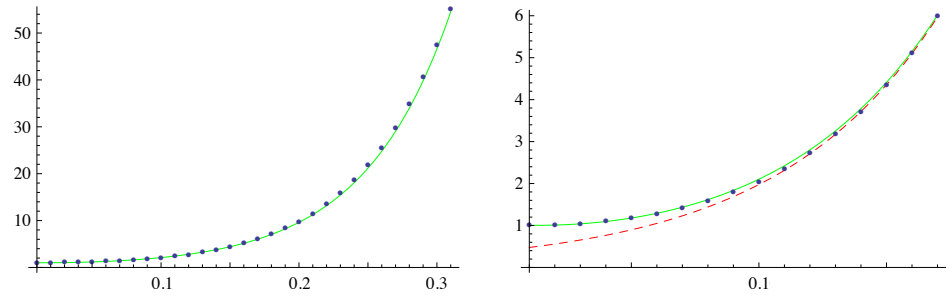

(a) non-expanding universe [Parameters: $L_x = 30, \lambda = 0.005, \Lambda = 114, C = 10, k_p = 2\pi\, 4/L$]

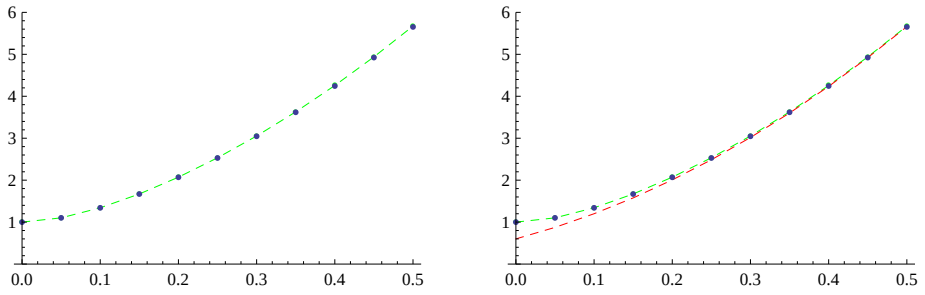

(b) expanding universe [Parameters: $L_x = 60, \lambda = 0.005, \Lambda = 108.3, C = 10, k_p = 2\pi\, 4/L$]

Fig. 7.5.4: Growth of the perturbation $|\delta_k(\theta)|^2/|\delta_k(\theta_{\text{ini}})|^2$ in a non-expanding and matter-dominated universe (blue dots) as a function of the simulation time θ. The green line represents a fit with a superposition of the growing and decaying modes. The dashed red line is a fit with the growing mode only. The figures on the right illustrate the importance of the decaying mode to fit the growth at early times.

Conclusion

We used our framework to study the growth of a single-mode density perturbation in a cosmological context, reproducing its main features.

8. Conclusion and Outlook

Concluding remarks

An alternative framework for numerical simulations of structure formation was presented. Inspired by the Wigner distribution function (WDF) in quantum mechanics and gauge field theories, we trade the classical Vlasov-Poisson equations for an equivalent system with a completely local interaction. Besides the hope that this might yield a faster algorithm for the simulations of structure formation, it could provide an alternative and independent approach to N-body simulations.

We derived the equation governing the dynamics of the WDF, showed its equivalence with the Schrödinger equation and summarized what is known about the semi-classical limit, in which it reduces to the classical Vlasov equation. We discussed several methods to obtain an initial set of wavefunctions having a WDF close to a given classical distribution function. We concluded that any classical distribution can be represented as the WDF of a set of wavefunctions, although no strict quantum mechanical interpretation should be given to the corresponding mixed state.

In one approach, the determination of the initial wavefunctions is shown to be equivalent to the solution of an eigenvalue problem for a hermitian operator. As a working example, we computed the wavefunctions representing the cold dark matter phase space distribution at early times. They were found to be related to the Fourier modes of the matter distribution. The computational efficiency depends crucially on the number of wavefunctions needed. We went through different techniques (minimization, weighted scalar product) which could help to find a minimal number of wavefunctions describing a given initial state. Fortunately such a procedure has only to be carried out once at the beginning of a numerical simulation to obtain the initial conditions. Moreover the quantum evolution will leave the number of wavefunctions fixed.

As a next essential step, we introduced dynamical gauge fields to obtain a purely local interaction. More specifically, the long-range gravitational force is mediated by an auxiliary Abelian gauge field. This simplest possible description comes at the price of introducing an exponentially growing mode into the system. We showed how a suitable choice of parameters can keep this tachyonic mode under control.

We proceeded by applying the techniques of lattice gauge theory to ob-

tain a fully gauge-invariant discretization of our system. This provided a numerical scheme for an iterative solution of the equations of motion. Insisting on a gauge-invariant formulation, the Poisson equation (Gauss constraint) plays a special role, and reduces to a constraint on the initial data. We described a minimization algorithm based on the gradient descent method that allows to compute the initial gauge field configuration satisfying the Gauss constraint.

The computational complexity of our approach was estimated and compared to N-body simulations. Depending on the number of wavefunctions being evolved, our complexity ranges from $\mathcal{O}(N)$ to $\mathcal{O}(N^2)$. Unfortunately our approach comes at a certain cost in memory, as it scales proportionally to N in the best case and N^2 in the worst. This emphasizes once more how crucial it is to have a minimal number of wavefunctions.

We discussed some previous works using the Schrödinger equation to model structure formation in the universe and outlined the improvements we made. We then described how we implemented the proposed framework into a fully three-dimensional numerical code which we used to perform different testbed simulations. First we applied it to the study of the tachyonic instability to show that the exponentially growing mode is indeed present, but that we know how to control it by an appropriate choice of parameters. As a second test of our framework we examined the time evolution of the Schrödinger-Newton system for an initial Gaussian wavefunction. We compared the results of our three-dimensional code to an independent numerical solution of the spherically symmetric Schrödinger-Newton system. The results were found to be in good agreement, giving us an additional confirmation of the validity of our local interaction framework using gauge fields.

Lastly we applied our approach to the study of cosmic perturbations. We considered the simplest case of the time evolution of a single Fourier mode in both a static and matter-dominated universe. The main features of the growth of perturbations in the cosmological context were reproduced.

Possible future work

Numerous open questions remain and many interesting routes have not been explored.

To reduce the complexity and memory requirements of our framework, it is crucial to reduce the number of wavefunctions needed as much as possible. One promising idea to investigate is how one should choose the weight function in the scalar product to obtain a minimal number of relevant eigenfunctions. A suitable choice of this weight function could also allow to solve the eigenvalue problem for more general phase space distributions. Yet another idea could be to look for inspiration in the domain of data compression and learn to encode the phase space information with a minimal number of

basis functions. Even lossy data compression could be useful, as we can allow for some error in the initial phase space representation provided that it reduces the number of wavefunctions considerably. Alternatively, it would also be interesting to identify physical problems that can be modelled with only a few wavefunctions. Another suggestion of possible future work is to analyze if one could describe the gravitational interaction using a scalar field instead of a vector field (refer to appendix E for more details). Besides having less fields to evolve, this would have the advantage of removing the exponentially growing thereby allowing us more freedom in the choice of simulation parameters.

In order to perform some additional tests of our framework, it could be instructive to first avoid the high memory requirements, and implement an effectively one-dimensional problem. The most straightforward procedure would be to run planar 1+1 dimensional simulations. Another setup of physical interest would be to study spherically symmetric systems. In particular we could compare our results with the analytical solution of the spherical infall model and the corresponding N-body simulations.

One possible application for three-dimensional simulations would be to thoroughly analyze the linear growth of cosmic perturbations. One could start in the deeply linear regime and compare the time evolution with Zel'dovich approximation and follow the generation of the Zel'dovich pancakes.

Since our main goal was to test the validity of the proposed framework, putting effort into optimizing the code was not one of our priorities. There is certainly a lot of potential for further optimization in different directions. Since we have a local interaction on a spatial grid, the parallelization of the algorithm using `MPI` is straightforward. As a result the code could be run with good efficiency on clusters. It would also be interesting to implement an adaptive mesh refinement. Any improvements along these lines would yield numerical simulations reaching significantly higher spatial resolutions and larger ranges of scales. Another advantage is that our approach scales very efficiently with the number of CPU's used as the time evolution is purely local.

Let us emphasize that our approach has a number of attractive features. Most importantly, the full phase space information is encoded in the wavefunctions. Working with many wavefunctions, we are in principle able to represent any given phase space distribution, including those where the velocity dispersion is important. Potentially, this would allow for numerical simulations of structure formation in presence of warm dark matter.

Acknowledgements

A number of people have contributed both directly and indirectly to the completion of this thesis. Firstly, I would like to express my gratitude to my supervisor Prof. Shaposhnikov for his guidance and providing many creative ideas to tackle encountered problems. Secondly, I am most grateful to Alexey Boyarsky and Oleg Ruchayskiy for their continual source of inspiration and help. They were an immeasurable source of scientific insight and advices. Their great efforts and patience made this thesis possible.

I am also very grateful to all my friends around me: Mathias, for exploring other worlds with me, Tamas for the rocking Cubotron sessions, Gøran for taking me to mind-blowing concerts and Martin, Daniel, Loic, Guillaume, Géraldine for the almost regular Tuesday meetings. Thanks also go to the friends on the 7th floor and everywhere else for many pleasant times together.

Last but not least, I wish to thank my parents and my family for having helped me to become who I am. A very special thank you goes to my dear wife Tessy for her endless love and constant support.

Appendix

A. Conventions

This appendix lists some of the conventions and units[1] used in this work.

4-vectors:

$$x^\mu = \begin{pmatrix} ct \\ \vec{x} \end{pmatrix}, \quad A^\mu = \begin{pmatrix} \Phi_{\text{el}} \\ c\vec{A} \end{pmatrix}, \quad J^\mu = \begin{pmatrix} c\rho \\ \vec{j} \end{pmatrix}, \quad \partial_\mu = \begin{pmatrix} \frac{1}{c}\partial_t \\ \vec{\nabla} \end{pmatrix}$$

$$x^\mu \,[\text{m}]\,,\ A^\mu \left[\frac{\text{J}}{\text{C}}\right],\ \vec{A}\left[\frac{\text{J s}}{\text{C m}}\right],\ J^\mu \left[\frac{\text{C}}{\text{s m}^2}\right],\ \partial_\mu \left[\frac{1}{\text{m}}\right]$$

Electromagnetic fields:

$$\vec{B} = \vec{\nabla} \times \vec{A}, \quad \left(\vec{E}\right)^i = F^{i0} = F_{0i} = \left(-\partial_t \vec{A} - \vec{\nabla}\Phi_{\text{el}}\right)^i$$

$$\vec{B}\left[\text{T} = \frac{\text{J s}}{\text{C m}^2}\right],\ \vec{E}\left[\frac{\text{V}}{\text{m}} = \frac{\text{J}}{\text{C m}}\right]$$

Field strength tensor:

$$F_{\mu\nu} = \begin{pmatrix} 0 & E_x & E_y & E_z \\ -E_x & 0 & -cB_z & cB_y \\ -E_y & cB_z & 0 & -cB_x \\ -E_z & -cB_y & cB_x & 0 \end{pmatrix} \quad F^{\mu\nu} = \begin{pmatrix} 0 & -E_x & -E_y & -E_z \\ E_x & 0 & -cB_z & cB_y \\ E_y & cB_z & 0 & -cB_x \\ E_z & -cB_y & cB_x & 0 \end{pmatrix}$$

Maxwell equations:

$$\begin{cases} \partial_\mu F^{\mu\nu} = \frac{1}{c\epsilon_0} J^\nu & \Longleftrightarrow \quad \begin{cases} \vec{\nabla}\cdot\vec{E} = \frac{1}{\epsilon_0}\rho \\ -\partial_t\vec{E} + c^2\vec{\nabla}\times\vec{B} = \frac{1}{\epsilon_0}\vec{j} \end{cases} \\ \varepsilon^{\mu\nu\rho\sigma}\partial_\nu F_{\rho\sigma} = 0 & \Longleftrightarrow \quad \begin{cases} \vec{\nabla}\cdot\vec{B} = 0 \\ \partial_t\vec{B} + \vec{\nabla}\times\vec{E} = \vec{0} \end{cases} \end{cases}$$

$$F^{\mu\nu}\left[\frac{\text{J}}{\text{C m}}\right],\ \frac{1}{\epsilon_0}\left[\frac{\text{J m}}{\text{C}^2}\right]$$

Vector identity:

$$\vec{\nabla}(\vec{\nabla}\cdot\vec{A}) - \nabla^2\vec{A} = \vec{\nabla}\times(\vec{\nabla}\times\vec{A})$$

[1] m=meter, s=seconds, C=Coulomb, J=Joule, T=Tesla, V=Volt

Gauge transformations:

$$\phi \mapsto e^{\frac{ie}{\hbar c}\vartheta}\phi, \quad A_\mu \mapsto A_\mu - \partial_\mu \vartheta \iff \Phi_{\text{el}} \mapsto \Phi_{\text{el}} - \frac{1}{c}\partial_t \vartheta, \quad c\vec{A} \mapsto c\vec{A} + \vec{\nabla}\vartheta$$

$$\vartheta \left[\frac{\text{J m}}{\text{C}}\right]$$

Covariant derivative:

$$D_\mu = \hbar\partial_\mu + i\frac{e}{c}A_\mu \iff D_0 = \hbar\frac{1}{c}\partial_t + \frac{ie}{c}\Phi_{\text{el}},\ D_i = \left(\hbar\vec{\nabla} - ie\vec{A}\right)^i$$

$$D_\mu \left[\frac{\text{J s}}{\text{m}}\right]$$

Fourier Transform:

$$\tilde{f}(\vec{k}) = \int d^3\vec{x}\, e^{-i\vec{k}\cdot\vec{x}} f(\vec{x})$$

$$f(\vec{x}) = \int \frac{d^3\vec{k}}{(2\pi)^3}\, e^{i\vec{k}\cdot\vec{x}} \tilde{f}(\vec{k})$$

$$\int \frac{d^3\vec{k}}{(2\pi)^3}\, e^{i\vec{k}\cdot\vec{x}} = \delta(\vec{x}), \quad \int d^3\vec{x}\, e^{-i\vec{k}\cdot\vec{x}} = (2\pi)^3\delta(\vec{k})$$

Green's function:

$$\nabla^2\Phi(\vec{x}) = -\rho(\vec{x}) \iff \Phi(\vec{x}) = \frac{1}{4\pi}\int d^3x' \frac{\rho(\vec{x}')}{|\vec{x} - \vec{x}'|}$$

Spherical coordinates without angular dependence:

$$\vec{\nabla} f = \partial_r f\ \vec{e}_r$$

$$\vec{\nabla}\cdot\vec{V} = \frac{1}{r^2}\partial_r\left(r^2 V_r\right)$$

$$\nabla^2 f = \frac{1}{r^2}\partial_r\left(r^2\partial_r f\right) = \frac{1}{r}\partial_r^2(rf) = \frac{2}{r}f' + f''$$

Numerical values:

$$1M_\odot \simeq 2\cdot 10^{30}\ \text{kg} \simeq 10^{57}\ \text{GeV}$$

$$1\ \text{Mpc} \simeq 3.086\cdot 10^{22}\ \text{m} \simeq 1.56\cdot 10^{38}\ \text{GeV}^{-1}$$

$$1\ \text{sec} \simeq 1.5\cdot 10^{24}\ \text{GeV}^{-1}$$

$$G_N \simeq 6.67428\cdot 10^{-11}\ \text{kg}^{-1}\text{m}^3\text{s}^{-2}$$

$$\simeq 4.5\cdot 10^{-48} M_\odot^{-1}\text{Mpc}^3\text{s}^{-2} \simeq 6.7\cdot 10^{-39}\ \text{GeV}^{-2}$$

$$c \simeq 3\cdot 10^5\ \text{km s}^{-1} \simeq 0.97\cdot 10^{-14}\ \text{Mpc s}^{-1}$$

$$H_0 \simeq 70\ \text{km s}^{-1}\ \text{Mpc}^{-1} \simeq 2.268\cdot 10^{-18}\ \text{sec}^{-1}$$

$$\hbar \simeq 6.626\cdot 10^{-34}\ \text{J s} \simeq 6.626\cdot 10^{-34}\ \text{kg m}^2\text{s}^{-1}$$

$$e \simeq 0.0854\ \text{GeV}^0\,, \quad \alpha = e^2 \simeq 0.00729 \simeq \frac{1}{137}$$

$$\rho_{\text{crit}} \simeq 2\cdot 10^{-47}\ \text{GeV}^4\,, \quad \rho_{\text{cluster}} \simeq 10^{-45}\ \text{GeV}^4$$

B. Numerical stability

A general problem when solving differential equations using finite differences is that of the propagation of numerical errors. A scheme is said to be *numerically stable* if the errors made at one timestep do not cause the errors to increase as the computations are continued. A numerically unstable scheme has exponentially growing errors and typically leads to divergences. The stability of a numerical scheme can be investigated by means of the *von Neumann stability analysis* (Numerical Recipes 2007).

Let us illustrate the stability analysis in the case of the Maxwell equation (5.24) with a single space dimension

$$\alpha \ddot{b}_T(\theta, y) - \beta C^2 \nabla^2 b_T(\theta, y) + \Lambda |\chi|^2 \, b_T(\theta, y) = 0. \tag{B.1}$$

Using the simplest finite differences prescription

$$\ddot{b}_T = \frac{1}{\Delta\theta^2} \left[b_t(y + a\hat{\theta}) - 2b_t(y) + b_t(y - a\hat{\theta}) \right], \tag{B.2a}$$

$$\nabla^2 b_T = \frac{1}{\Delta y^2} \left[b_t(y + a\hat{y}) - 2b_t(y) + b_t(y - a\hat{y}) \right], \tag{B.2b}$$

and a Fourier-like Ansatz

$$b_T(\theta = n\Delta\theta, y = r\Delta y) \equiv e^{i\omega n \Delta\theta - ikr\Delta y}, \tag{B.3}$$

the equation becomes for $\alpha = \beta = -1$

$$\sin^2\left(\frac{\omega\Delta\theta}{2}\right) = C^2 \frac{\Delta\theta^2}{\Delta y^2} \sin^2\left(\frac{k\Delta y}{2}\right) - \frac{\Lambda}{4}\Delta\theta^2 |\chi|^2. \tag{B.4}$$

This is the numerical dispersion relation for our method. We see that for the numerical solutions, ω is only approximately a linear function of k. Consequently the phase velocity $v_p = \omega/k$ will depend on k, and waves with different wavenumbers will propagate with different velocities. As a result, a wavepacket containing several k will change its shape as it propagates. This phenomenon, which is purely a result of the discretization, is called *numerical dispersion* (Bondeson, Rylander, and Ingelström 2005).

The method is numerically stable if the solution does not contain any exponentially growing modes, i.e. ω is real. Hence the stability condition

$$0 \leq \sin^2\left(\frac{\omega\Delta\theta}{2}\right) \leq 1. \tag{B.5}$$

Using the numerical dispersion relation, the lower bound becomes

$$C^2\frac{\Delta\theta^2}{\Delta y^2}\sin^2\left(\frac{k\Delta y}{2}\right) \geq \frac{\Lambda}{4}\Delta\theta^2|\chi|^2, \tag{B.6}$$

which, when expanded for small lattice spacing gives

$$C^2k^2 \geq \Lambda|\chi|^2, \tag{B.7}$$

which happens to coincide with the tachyon stability condition (5.29) derived before. The upper bound, however, produces a new condition, that can be seen as an upper bound on the timestep

$$\Delta\theta^2 \leq \frac{1}{\frac{C^2}{\Delta y^2}\sin^2\left(\frac{k\Delta y}{2}\right) - \frac{\Lambda}{4}|\chi|^2}. \tag{B.8}$$

In the special case without matter $\Lambda = 0$, and using the fact that the sine is bounded by 1, this reduces to

$$C\frac{\Delta\theta}{\Delta y} \leq 1, \tag{B.9}$$

which is commonly known as the *Courant condition*. As a result, the timestep should be small enough, that the wave doesn't propagate more than one gridspacing each integration step. In the cases of interest to us, it happens that the second term in the denominator of (B.8) is negligible compared to the first, so that we can work with the usual Courant condition.

In simulations of electrodynamics for instance, where the value of C has a physical origin, the Courant condition dictates the timestep to be small enough to avoid any numerical instabilities. In our case, however, the propagation speed C is purely fiduciary and we can reinterpret the stability condition as a lower bound on C. Combined with the upper bound from the tachyon stability, this defines the acceptable values for this parameter. Given that the range was always large enough in our simulations, we took the very conservative point of view to require

$$C\frac{\Delta\theta}{\Delta y} \lesssim (10^{-2} - 10^{-3}),$$

to avoid any numerical instabilities.

C. Derivation of the lattice Schrödinger equation from the action

In this appendix we give a more detailed derivation of the Schrödinger equation from the lattice action.

The matter action on the lattice is given by (6.16):

$$S_{\text{Matter}} = \frac{e}{\epsilon_0} a_0 a_i^3 \sum_x \left[\frac{1}{2} \left(\phi^* U_0 D_0 \phi + D_0 \phi^* U_0^\dagger \phi \right) - \frac{e}{2m} \sum_i D_i \phi^* D_i \phi \right],$$

Using the definition (6.15) of the covariant derivatives, we can expand the action as follows:

$$\begin{aligned} S_{\text{Matter}} = \frac{1}{\epsilon_0} a_0 a_i^3 \sum_x \Bigg[& \frac{1}{2} \frac{i\hbar}{\Delta t} \left(\phi^* U_0 \phi(x + a\hat{t}) - \phi^\dagger(x + a\hat{t}) U_0^\dagger \phi \right) \\ & - \frac{\hbar^2}{2m} \frac{1}{a_i^2} \sum_i \left(\phi^*(x + a\hat{i}) - U_i \phi^* \right) \left(\phi(x + a\hat{i}) - U_i^\dagger \phi \right) \Bigg]. \end{aligned}$$

The equations of motion are obtained by varying the action with respect to the fields. On the lattice, the functional derivative reduces to a normal derivative with respect to the field at a given lattice site:

$$\begin{aligned} \frac{\epsilon_0}{a_0 a_i^3} \frac{\partial S_{\text{Matter}}}{\partial \phi^*(z)} = & \frac{1}{2} \frac{i\hbar}{\Delta t} \sum_x \left(\delta_{x,z} U_0 \phi(x + a\hat{t}) - \delta_{x+a\hat{t},z} U_0^\dagger \phi \right) \\ & - \frac{\hbar^2}{2m} \frac{1}{a_i^2} \sum_x \sum_i \left[\delta_{x+a\hat{i},z} \left(\phi(x + a\hat{i}) - U_i^\dagger \phi \right) - U_i \delta_{x,z} \left(\phi(x + a\hat{i}) - U_i^\dagger \phi \right) \right] \\ = & \frac{1}{2} \frac{i\hbar}{\Delta t} \left(U_0(z) \phi(z + a\hat{t}) - U_0^\dagger(z - a\hat{t}) \phi(z - a\hat{t}) \right) \\ & + \frac{\hbar^2}{2m} \frac{1}{a_i^2} \sum_i \left[U_i(z) \phi(z + a\hat{i}) - 2\phi(z) + U_i^\dagger(z - a\hat{i}) \phi(z - a\hat{i}) \right], \end{aligned}$$

implying the equation of motion

$$\begin{aligned} & \frac{i\hbar}{2\Delta t} \left(U_0 \phi(x + a\hat{t}) - U_0^\dagger(x - a\hat{t}) \phi(x - a\hat{t}) \right) \\ & \qquad = -\frac{\hbar^2}{2m} \frac{1}{a_i^2} \sum_i \left[U_i \phi(z + a\hat{i}) - 2\phi + U_i^\dagger(z - a\hat{i}) \phi(z - a\hat{i}) \right]. \end{aligned}$$

The RHS can be rewritten in terms of covariant derivatives. Using

$$\begin{aligned} D_i\phi(x-a\hat{i}) - U_i D_i\phi(x) &= \frac{i\hbar}{ea_i}\left(\phi(x) - U_i^\dagger(x-a\hat{i})\phi(x-a\hat{i})\right) \\ &\quad - U_i(x)\frac{i\hbar}{ea_i}\left(\phi(x+a\hat{i}) - U_i^\dagger(x)\phi(x)\right) \\ &= \frac{i\hbar}{ea_i}\left[2\phi(x) - U_i^\dagger(x-a\hat{i})\phi(x-a\hat{i}) - U_i(x)\phi(x+a\hat{i})\right], \end{aligned}$$

the equation of motion equals

$$\frac{i\hbar}{2\Delta t}\left(U_0\phi(x+a\hat{t}) - U_0^\dagger(x-a\hat{t})\phi(x-a\hat{t})\right) = -\frac{ie\hbar}{2m}\frac{1}{a_i}\sum_i\left[D_i\phi(x-a\hat{i}) - U_i D_i\phi\right].$$

This is the equivalent of the Schrödinger equation on the lattice.

Let us check that it yields indeed the usual Schrödinger equation in the continuum limit. Expanding the link variables to first order in lattice spacing, we find

$$\begin{aligned} &i\hbar\frac{1}{2\Delta t}\left(\phi(x+a\hat{t}) - \phi(x-a\hat{t})\right) - \frac{e}{2}\left(A_0(x)\phi(x+a\hat{t}) + A_0(x-a\hat{t})\phi(x-a\hat{t})\right) \\ &\qquad = -\frac{ie\hbar}{2m}\frac{1}{a_i}\sum_i\left[D_i\phi(x-a\hat{i}) - D_i\phi + \frac{ie}{\hbar}a_i\vec{A}^i D_i\phi(x)\right] \\ &\qquad = -\frac{ie\hbar}{2m}\sum_i\left[-\bar{\Delta}_i D_i\phi + \frac{ie}{\hbar}\vec{A}^i D_i\phi(x)\right]. \end{aligned}$$

Taking the continuum limit $\Delta t, a_i \to 0$, we obtain

$$i\hbar\partial_t\phi - eA_0\phi = \frac{1}{2m}\sum_i\left(-i\hbar\vec{\nabla} - e\vec{A}\right)^2\phi,$$

which is indeed the Schrödinger equation in a background gauge field.

D. Unitarity of the discretized Schrödinger equation

A feature of the continuous Schrödinger equation is that it conserves the normalization of the wavefunction. One commonly refers to this property as *unitarity*, as it corresponds to the conservation of the total probability. From the field theoretic perspective, this is a consequence of the symmetry under global phase transformations of the wavefunction, the total probability being the associated Noether charge. When discretizing the Schrödinger equation to do numerical simulations one has to take care not to spoil the unitarity. Since our approach is fully gauge-invariant, we expect that it should also be unitary, given that the global symmetry is a trivial consequence of the gauge symmetry. Moreover, since we can perform a different global transformation on each wavefunction χ_n, the norm of the individual wavefunctions is preserved. We now propose to show explicitly how our discretized equations of motion imply the conservation of the normalization of the different wavefunctions.

From Noether's theorem we know that to every symmetry is associated a conserved current $\partial_\mu J^\mu = 0$ and a corresponding charge that is conserved in time $\partial_0 \int d^3y J^0 = 0$. Looking at the discretized Poisson equation (6.22b) we infer that the lattice version of J^0_n corresponding to the global phase transformation $\chi_n(y) \mapsto e^{i\vartheta}\chi_n(y)$ is given by

$$J^0_n = \mathrm{Re}\left[\chi^*_n(y)\chi_n(y + a\hat{\theta})\right]. \tag{D.1}$$

In the continuum limit $a \to 0$ it reduces to the standard probability density $|\chi_n(y)|^2$. We want to make use of the discretized Schrödinger equation (6.22a) to show explicitly that the norm is conserved at every timestep:

$$\begin{aligned} &\sum_x J^0_n(y) = \sum_x J^0_n(y - a\hat{\theta}) \\ \iff &\sum_x \mathrm{Re}\left[\chi^*_n(y)\chi_n(y + a\hat{\theta})\right] = \sum_x \mathrm{Re}\left[\chi^*_n(y - a\hat{\theta})\chi_n(y)\right] \end{aligned} \tag{D.2}$$

Replacing $\chi_n(y + a\hat{\theta})$ using the Schrödinger equation in the rewritten form

as in (6.23a), we obtain

$$\sum_x \mathrm{Re}\left[\chi_n^*(y)\chi_n(y+a\hat{\theta})\right] = \sum_x \mathrm{Re}\left[\chi_n^*(y)\chi_n(y-a\hat{\theta})\right] + \sum_x \mathrm{Re}\left[\chi_n^*(y)\frac{i\lambda\Delta\theta}{a\Delta y^2}\sum_i \left[U_i\chi_n(y+a\hat{i}) - 2\chi_n + U_i^\dagger(y-a\hat{i})\chi_n(y-a\hat{i})\right]\right].$$

The first term of the right-hand side corresponds to the total probability at the previous timestep. For the total probability to be conserved, we expect the second term to vanish. As it equals

$$\frac{\lambda\Delta\theta}{a\Delta y^2}\sum_x\sum_i \mathrm{Re}\left[i\left(-2\chi_n^*\chi_n + \chi_n^*U_i\chi_n(y+a\hat{i}) + \chi_n^*U_i^\dagger(y-a\hat{i})\chi_n(y-a\hat{i})\right)\right],$$

a sufficient condition for it to be zero is that we take the real part of a purely imaginary quantity, thus it is enough to show that

$$\sum_x \left[\chi_n^*U_i\chi_n(y+a\hat{i}) + \chi_n^*U_i^\dagger(y-a\hat{i})\chi_n(y-a\hat{i})\right] \in \mathbb{R}. \tag{D.3}$$

Since $\sum_x$ corresponds to the sum over all lattice points, we may relabel the coordinates as $y \mapsto y - a\hat{i}$ in the first term and use the periodic boundary conditions to obtain

$$\sum_x \left[\chi_n^*(y-a\hat{i})U_i(y-a\hat{i})\chi_n(y) + \chi_n^*U_i^\dagger(y-a\hat{i})\chi_n(y-a\hat{i})\right], \tag{D.4}$$

which is clearly in the form of a term plus its complex conjugate, and therefore real. Hence

$$\sum_x \mathrm{Re}\left[\chi_n^*(y)\chi_n(y+a\hat{\theta})\right] = \sum_x \mathrm{Re}\left[\chi_n^*(y)\chi_n(y-a\hat{\theta})\right] \tag{D.5}$$

We therefore conclude that the conservation of the norm of each wavefunction is an immediate consequence of our discretized equations of motion and the boundary conditions.

E. Scalar field mediated gravitation

Our framework for numerical simulations of structure formation is based on the introduction of an Abelian gauge field to have a local interaction. This comes at the price of having an exponentially growing mode in the system which has to be suppressed by a suitable choice of parameters. Alternatively, one may try to make use of a scalar field to mediate the gravitational interaction. Besides having less fields to evolve, this would have the advantage of not introducing any instability, thereby allowing us more freedom in the choice of simulation parameters. This section is devoted to investigating the scalar field description in more detail.

Consider the following Lagrangian for a real scalar field U interacting with the complex scalar matter fields χ_n

$$\begin{aligned}\mathscr{L} = &\frac{1}{2C^2}\dot{U}^2 - \frac{1}{2}(\vec{\nabla}U)^2 + \Lambda\bar{\rho}\,U \\ &+ \Lambda\sum_n \lambda_n\left[\frac{i\lambda}{2}\left(\chi_n^*\dot{\chi}_n - \dot{\chi}_n^*\chi_n\right) - \frac{\lambda^2}{2a}\vec{\nabla}\chi_n^*\cdot\vec{\nabla}\chi_n - |\chi_n|^2 U\right]. \end{aligned} \tag{E.1}$$

The equations of motion are found to be

$$i\lambda\dot{\chi}_n = -\frac{\lambda^2}{2a}\nabla^2\chi_n + U\chi_n, \tag{E.2a}$$

$$-\frac{1}{C^2}\ddot{U} + \nabla^2 U = \Lambda\left(\sum_n \lambda_n|\chi_n|^2 - \bar{\rho}\right). \tag{E.2b}$$

The first is Schrödinger equation and the second reduces to the Poisson equation sourced by the density contrast $\delta\rho$ when the additional $-\frac{1}{C^2}\ddot{U}$ term is negligible. In particular this happens in the non-relativistic limit $C \to \infty$. The associated Hamiltonian density is given by

$$\begin{aligned}\mathscr{H} = &\frac{1}{2C^2}\dot{U}^2 + \frac{1}{2}(\vec{\nabla}U)^2 \\ &+ \Lambda\sum_n \lambda_n\frac{\lambda^2}{2a}|\vec{\nabla}\chi_n|^2 + \Lambda\Big(\sum_n \lambda_n|\chi_n|^2 - \bar{\rho}\Big)U, \end{aligned} \tag{E.3}$$

which has a positive definite kinetic energy term for the scalar potential. This implies that there is no tachyonic instability in the system. This shows that one can use a scalar field to mediate the attractive gravitational interaction, without introducing any exponentially growing modes.

The next step in order to do numerical simulations is to rewrite a discretized version of the equations of motion (E.2). We opted again for an explicit scheme as it is computationally more efficient than an implicit algorithm. Our discretization of the equations of motion (E.2) is given by

$$\chi_n(y + a\hat{\theta}) = \chi_n(y - a\hat{\theta}) + i\,\frac{\lambda\Delta\theta}{a}\nabla^2_{\mathrm{dis}}\chi_n(y) - i\,\frac{2\Delta\theta}{\lambda}U(y)\chi_n(y), \tag{E.4a}$$

$$\begin{aligned} U(y + a\hat{\theta}) = {} & 2U(y) - U(y - a\hat{\theta}) \\ & + C^2\Delta\theta^2\nabla^2_{\mathrm{dis}}U(y) - C^2\Delta\theta^2\Lambda\left(\sum_n \lambda_n|\chi_n|^2 - \bar{\rho}\right), \end{aligned} \tag{E.4b}$$

where ∇^2_{dis} denotes the discretized Laplacian

$$\begin{aligned} \nabla^2_{\mathrm{dis}}U(y) = \frac{1}{12\Delta y^2}\sum_i \Big(& -U(x + 2a\hat{i}) + 16U(x + a\hat{i}) \\ & - 30U(y) + 16U(x - a\hat{i}) - U(x - 2a\hat{i})\Big)\,. \end{aligned} \tag{E.5}$$

In particular, one can show along the lines of appendix D that this numerical scheme is unitary and conserves the norm of each wavefunction. Several numerical simulations where performed with this method and the results agree with the ones obtained with the gauge fields.

Curriculum Vitæ

Personal information

Name	Claude Becker
Address	Chemin du Bochet, 20 1024 Ecublens VD
Email	claude.becker@epfl.ch
Birthdate	13 June 1982
Nationality	Luxembourgish

Education

2006–2010	PhD in Physics Under the direction of Prof. Shaposhnikov Laboratoire de physique des particules et de cosmologie Ecole Polytechnique Fédérale Lausanne
2001–2006	Master of Science MSc in Physics Titre d'ingénieur physicien Ecole Polytechnique Fédérale Lausanne
2001	Diplôme de fin d'études secondaires Lycée Robert Schuman, Luxembourg

Work experience

2004–2010	Teaching: Assistant for various lectures of theoretical physics: Quantum Field Theory, General Relativity, Classical Electrodynamics
2006–2010	Assistant computer administrator at Cubotron, EPFL
2005	Internship Paul Wurth SA, Luxembourg

Language skills

Luxembourgish (mother tongue)
English, French, German (fluent)
Italian, Spanish (basics)

Bibliography

Cosmology

Albrecht, Andreas et al. (2006). "Report of the dark energy task force". In: arXiv:astro-ph/0609591.

Avila-Reese, Vladimir et al. (2001). "Formation and structure of halos in a warm dark matter cosmology". In: *ApJ* 559 pp. 516–530.

Bode, Paul, Jeremiah P. Ostriker, and Neil Turok (2001). "Halo formation in warm dark matter models". In: *ApJ* 556 pp. 93–107.

Boyarsky, Alexey et al. (2009). "Lyman-alpha constraints on warm and on warm-plus-cold dark matter models". In: *JCAP* 05.012, arXiv:0812.0010 [astro-ph].

Dodelson, Scott (2003). *Modern Cosmology*. Academic Press.

Hannestad, Steen et al. (2010). "Neutrino and axion hot dark matter bounds after WMAP-7". In: *JCAP* 08 p. 1, arXiv:1004.0695 [astro-ph.CO].

Komatsu, Eiichiro et al. (2010). "Seven-year WMAP observations: Cosmological interpretation". In: arXiv:1001.4538 [astro-ph.CO].

Peebles, Phillip J. E. and Bharat Ratra (2003). "The cosmological constant and dark energy". In: *Rev. Mod. Phys.* 75 pp. 559–606, arXiv:astro-ph/0207347.

Riess, Adam G. et al. (1998). "Observational evidence from supernovae for an accelerating universe and a cosmological constant". In: *Astron. J.* 116 pp. 1009–1038, arXiv:astro-ph/9805201.

Roos, Matts (2010). "Dark Matter: the evidence from astronomy, astrophysics and cosmology". In: arXiv:1001.0316 [astro-ph.CO].

Seljak, Usos and Matias Zaldarriaga (1996). "A line-of-sight integration approach to cosmic microwave background anisotropies". In: *ApJ* 469 pp. 437–444.

Taoso, Marco, Gianfranco Bertone, and Antonio Masiero (2008). "Dark matter candidates: a ten-point test". In: *JCAP* 0803.022, arXiv:0711.4996 [astro-ph].

Weinberg, Steven (2008). *Cosmology*. Oxford University Press.

Zeldovich, Ya B. (1970). "Gravitational instability: an approximate theory for large density perturbations". In: *Astron. & Astrophys.* 5 pp. 84–89.

Structure Formation

Bernardeau, Francis et al. (2002). "Large-scale structure of the universe and cosmological perturbation theory". In: *Phys. Rep.* 367 pp. 1–248, arXiv:astro-ph/0112551.

Bertschinger, Edmund (1995). "Cosmological dynamics". In: arXiv:astro-ph/9503125.

Binney, James and Scott Tremaine (1987). *Galactic dynamics*. Princeton University Press.

Ma, Chung-Pei and Edmund Bertschinger (1995). "Cosmological perturbation theory in the synchronous and conformal newonian gauges". In: *ApJ* 455 pp. 7–25, arXiv:astro-ph/9506072.

Mukhanov, V.F., H.A. Feldman, and R.H. Brandenberger (1992). "Theory of cosmological perturbations". In: *Phys. Rep.* 215 pp. 203–333.

White, Simon D. M., Carlos S. Frenk, and Marc Davis (1983). "Clustering in a neutrino-dominated universe". In: *ApJ* 274 pp. L1–L5.

N-Body Simulations

Bagla, Jasjeet Singh (2005). "Cosmological N-body simulation: Techniques, scope and status". In: *Current Science* 88.7 pp. 1088–1100, arXiv:astro-ph/0411043.

Bertschinger, Edmund (1998). "Simulations of structure formation in the universe". In: *Annu. Rev. Astr. Astroph.* 36 pp. 599–654.

Boylan-Kolchin, Michael et al. (2009). "Resolving cosmic structure formation with the Millennium-II simulation". In: *MNRAS* 398 p. 1150, arXiv:0903.3041 [astro-ph.CO].

Dehnen, Walter (2000). "A very fast and momentum-conserving tree code". In: *ApJ* 536 pp. L39–L42.

— (2001). "Towards optimal softening in 3D N-body codes: Minimizing the force error". In: *MNRAS* 324 pp. 273–291, arXiv:astro-ph/0011568.

— (2002). "A hierarchical O(N) force calculation algorithm". In: *J. Comp. Phys.* 179 pp. 27–42.

Diemand, J. et al. (2008). "Clumps and streams in the local dark matter distribution". In: *Nature* 454 pp. 735–738, arXiv:0805.1244 [astro-ph].

Hockney, Roger W. and James W. Eastwood (1988). *Computer Simulation using particles*. Adam Hilger.

Joyce, Michael (2008). "Cosmological simulations of structure formation and the Vlasov equation". In: *Comm.Nonlin.Sc.Num.Sim* 13 p. 100, arXiv:0805.1453 [cond-mat/stat-mech].

Klypin, Anatoly, Sebastian Trujillo-Gomez, and Joel Primack (2010). "Halos and galaxies in the standard cosmological model: results from the Bolshoi simulation". In: arXiv:1002.3660 [astro-ph.CO].

Navarro, Julio F. et al. (2010). "The diversity and similarity of cold dark matter halos". In: *MNRAS* 402 pp. 21–34, arXiv:0810.1522 [astro-ph].

Springel, Volker (2005). "The cosmological simulation code GADGET-2". In: *MNRAS* 364 pp. 1105–1134.

Springel, Volker et al. (2005). "Simulating the joint evolution of quasars, galaxies and their large-scale distribution". In: *Nature* 435 pp. 629–636, arXiv:astro-ph/0504097.

Stadel, Joachim et al. (2008). "Quantifying the heart of darkness with GHALO - a multi-billion particle simulation of our galactic halo". In: arXiv:0808.2981[astro-ph].

Wang, Jie and Simon D. M. White (2007). "Discreteness effects in simulations of hot/warm dark matter". In: *MNRAS* 380 pp. 93–103, arXiv:astro-ph/0702575.

Wigner distribution function

Ballentine, Leslie E. (2000). *Quantum mechanics – A modern development.* World Scientific Publishing.

Bastiaans, Martin J. (1997). "Application of the Wigner distribution function in optics". In: *The Wigner distribution – Theory and applications in signal processing, ed. Mecklenbräuker & Hlawatsch* pp. 375–426, Pdf.

Ercolessi, Elisa et al. (2007). "Wigner distributions in quantum mechanics". In: *J.Phys.: Conf. Ser.* 87.

Hillery, M. et al. (1984). "Distribution functions in physics: Fundamentals". In: *Phys. Rep.* 106.3 pp. 121–167.

Hirshfeld, Allen C. and Peter Henselder (2002). "Deformation quantization in the teaching of quantum mechanics". In: *Am. J. Phys.* 70 pp. 537–547.

Hudson, R.L. (1974). "When is the Wigner quasi-probability density non-negative?" In: *Rep. Math. Phys.* 6 pp. 249–252.

Lee, Hai-Woong (1995). "Theory and application of the quantum phase-space distribution functions". In: *Phys. Rep.* 259 pp. 147–211.

Moyal, José Enrique (1949). "Quantum mechanics as a statistical theory". In: *Proc. Cam. Phil. Soc.* 45 pp. 99–124.

Wigner, Eugene Paul (1932). "On the quantum correction for thermodynamic equilibrium". In: *Phys.Rev.* 40 pp. 749–759.

Semiclassical limit

Fröhlich, Jürg, Sandro Graffi, and Simon Schwarz (2007). "Mean-field- and classical limit of many-body Schrödinger dynamics for bosons". In: *Commun. Math. Phys.* 271 pp. 681–697.

Jin, Shi, Xiaomei Liao, and Xu Yang (2007). "The Vlasov-Poisson equations as the semiclassical limit of the Schrödinger-Poisson equations: A numerical study". In: Pdf.

Lions, Pierre Louis and Thierry Paul (1993). "Sur les mesures de Wigner". In: *Rev. Mat. Iber.* 9.3 pp. 553–618.

Majda, Andrew J., George Majda, and Yuxi Zheng (1994). "Concentrations in the one-dimensional Vlasov-Poisson equations – Temporal development and non-unique weak solutions in the single component case". In: *Physica D* 74 pp. 268–300.

Markowich, Peter A. and Norbert J. Mauser (1993). "The classical limit of a self-consistent quantum-Vlasov equation in 3D". In: *Math. Mod. Meth. Appl. Sc.* 3.1 pp. 109–124.

Mauser, Norbert J. (2002). "(Semi)classical limits of Schrödinger-Poisson systems via Wigner transform". In: *Journées équations aux derivées partielles (Jeadp)* 11.

Zhang, Ping, Yuxi Zheng, and Norbert J. Mauser (2002). "The limit from the Schrödinger-Poisson to the Vlasov-Poisson equations with general data in one dimension". In: *Comm. on Pure and Appl. Math.* 55 pp. 582–632.

Field theory

Dirac, Paul A. M. (1964). *Lectures on quantum mechanics.* Belfer graduate school of science Yeshiva university.

Vlasov, Viktor V. et al. (1987). "Canonical quantization of gauge theories with a scalar condensate and the problem of spontaneous symmetry breaking". In: *Sov. J. Part. Nucl.* 18.

Weinberg, Steven (1995). *The quantum theory of fields, Vol 1.* Cambridge University Press.

Lattice field theory

Grigoriev, D. Yu, Valery A. Rubakov, and Mikhail Shaposhnikov (1989). "Topological transitions at finite temperatures: a real-time numerical approach". In: *Nucl. Phys.* B 326 pp. 737–757.

Montvay, István and Gernot Münster (1994). *Quantum fields on a lattice.* Cambridge University Press.

Rothe, Heinz J. (2005). *Lattice gauge theories.* World Scientific Lecture Notes.

Smit, Jan (2002). *Introduction to quantum fields on a lattice.* Cambridge University Press.

Wilson, Kenneth G. (1974). "Confinement of quarks". In: *Phys. Rev.* D 10.8 pp. 2445–2459.

Schrödinger equation in structure formation

Coles, Peter (2002a). "The origin of spatial intermittency in the galaxy distribution". In: *MNRAS* 330 pp. 421–424.

— (2002b). "The wave mechanics of large-scale structure". In: arXiv:astro-ph/0209576.

Coles, Peter and Kate Spencer (2003). "A wave-mechanical approach to cosmic structure formation". In: *MNRAS* 342 pp. 176–184, arXiv:astro-ph/0212433.

Davies, George and Lawrence M. Widrow (1997). "Test-bed simulations of collisionless, self-gravitating systems using the Schrödinger method". In: *ApJ* 485 pp. 484–495, arXiv:astro-ph/9607133.

Short, Chris J. and Peter Coles (2006a). "Gravitational instability via the Schrödinger equation". In: *JCAP* 12 p. 012, arXiv:astro-ph/0605012.

— (2006b). "Wave-mechanics and the adhesion approximation". In: *JCAP* 12 p. 016, arXiv:astro-ph/0605013.

Widrow, Lawrence M. and Nick Kaiser (1993). "Using the Schrödinger equation to simulate collisionless matter". In: *ApJ* 416.

Schrödinger-Newton system

Salzman, Peter J. (2005). "Investigation of the time dependent Schrödinger-Newton equation". Pdf. PhD thesis. University of California.

Salzman, Peter J. and Steven Carlip (2006). "A possible experimental test of quantized gravity". In: arXiv:gr-qc/0606120.

Miscellanea

Bondeson, Anders, Thomas Rylander, and Pär Ingelström (2005). *Computational Electromagnetics*. Springer.

Plewa, Tomasz, Timur Linde, and V. Gregory Weirs, eds. (2005). *Adaptive Mesh Refinement – Theory and Applications*. Springer.

Press, William H. et al. (2007). *Numerical recipes – The art of scientific computing*. 3rd edition. Cambridge University Press.

Zwillinger, Daniel (1997). *Handbook of differential equations*. 3rd edition. Academic Press.